FROM THE EVALUATION OF PrP PEPTIDES CONFORMATIONAL PROPERTIES TO THE DEVELOPMENT OF NEW ANTI-PRION COMPOUNDS

LUISA RONGA

UNIVERSITÉ MONTPELLIER 2
SCIENCES ET TECHNIQUES

FROM THE EVALUATION OF PrP PEPTIDES CONFORMATIONAL PROPERTIES TO THE DEVELOPMENT OF NEW ANTI-PRION COMPOUNDS

LUISA RONGA

DOTTORANDA: Luisa Ronga

RELATORI: Prof. Ettore Benedetti

                              Prof. Jean Martinez

COORDINATORE: Prof. Giovanni Sannia

<p style="text-align:center">INDEX</p>

ABBREVIATIONS

Amino Acids: singol and 3 letters code

A	Ala	Alanine		L	Leu	Leucine
βA	β-Ala	β-Alanine		K	Lys	Lysine
N	Asn	Asparagine		M	Met	Methionine
R	Arg	Arginine		F	Phe	Phenylalanine
D	Asp	Aspartic Acid		P	Pro	Proline
C	Cys	Cysteine		S	Ser	Serine
Q	Gln	Glutamine		T	Thr	Threonine
G	Gly	Glycine		W	Trp	Tryptophan
E	Glu	Glutamic Acid		Y	Tyr	Tyrosine
H	His	Histidine		V	Val	Valine
I	Ile	Isoleucine				

BSE	Bovine Spongiform Encephalopathy
Boc	*Tert*-butoxycarbonyl
BOP	Benzotriazole-1-yl-oxy-tris-(dimethylamino)-phosphonium hexafluorophosphate
CD	Circular Dichroism
CJD	Creutzfeldt-Jakob Disease
DCM	Dichloromethane
DIEA	N,N-diisopropylethylamine
DMF	Dimethylformamide
DRM	Detergent Resistant Microdomains
ER	Endoplasmic Reticulum
FC	Fatal Concentration
GPI	Glycosyl Phosphatidyl Inositol
GSS	Gerstmann-Straussler-Scheinker
HBTU	2-(1H-Benzotriazole-1-yl)-1,1,3,3-tetramethyluronium hexafluorophosphate
HCl	Chlorhydric acid
hPrP	human Prion Protein
LC	Liquid Chromatography
MTT	3-(4,5-Dimethylthiazol-2-yl)-2,5-diphenyltetrazolium bromide
NaOH	Sodium hydroxide
PrP	Prion Protein
PrP^C	Cellular form of Prion Protein
PrP^{Sc}	Scrapie form of Prion Protein
MD	Molecular Modelling
MeOH	Methanol
mPrP	murin Prion Protein
MS	Mass Spectroscopy
nd	not detected
NMR	Nuclear Magnetic Resonance
Pbf	2,2,4,6,7-Pentamethyldihydro-benzofuran-5-sulfonyl
SDS	Sodium dodecyl sulfate

SPPS   Solid Phase Peptide Synthesis
sPrP   sheep Prion Protein
tBu   *Tert*-Butyl
TC   Tetracycline
TFA   Trifluoroacetic acid
TFE   Trifluoroethanol
TIS   Tri-isopropyl-silane
Trt   Trityl
TSE   Transmissible Spongiform Encephalopathies

SUMMARY

A large number of human disorders, ranging from type II diabetes to Parkinson's and Alzheimer's diseases, are associated with protein aggregation resulting from aberrant folding or processing events. Despite its fundamental biological importance, little is known about the molecular basis or specificity of the general phenomenon of protein aggregation. Transmissible spongiform encephalopathies, also known as prion diseases, belong to this class. They are all characterized by progressive neuronal degeneration. In almost all cases there is a marked extracellular accumulation of an amyloidogenic conformer of the normal cellular prion protein (PrP^C), referred to as the scrapie isoform (PrP^{Sc}), which is thought to be responsible for the disease symptoms.

PrP is an ubiquitous 231-amino acid glycoprotein whose physiological role is still elusive. Its structure exhibits an N-terminal unfolded region and a C-terminal globular domain characterized by the presence of three α-helices (α1, α2 and α3), two short β-strands and an interhelical disulfide bridge between the α2 Cys179 and the α3 Cys214, which confers structural stability. Particularly fascinating is the notion that the protein possesses one or several 'spots' of intrinsic conformational weakness, which may lead the whole secondary and tertiary structure to succumb in favour of more stable, but aggregation-prone conformations, depending on pH, redox condition or glycosylation. The C-terminal side of helix 2, containing four adjacent threonines, is decidedly suspected to be one of such spots and, in this regard, has recently gained the attention of several investigations. As the α-helix 2 possesses chameleon conformational behaviour, gathers several disease-associated point mutations, can be toxic to neuronal cells and strongly fibrillogenic, it is a suitable model to investigate both structural determinants of PrP^C misfolding and rational structure-based drug design of compounds able to block or prevent prion diseases. The intriguing structural properties of this protein domain prompted us to investigate the conformational landscape of the α-helix 2 domain. The α-helix 2 of hPrP was used as a template for designing α2-helix-derived peptides, which were synthesized by SPPS and characterized by CD and NMR in aqueous buffer at different pH, in structuring media (SDS and TFE) and in presence of anions and bivalent metal cations. Finally, the neurotoxicity of these peptides was also assayed on B104 neuroblastoma cells. Overall, these studies strongly suggest that the role played by the α-helix 2 domain is not to be considered neutral in the misfolding mechanism of the PrP^C to the scrapie isoform. In addition, the affinity of the α-helix 2-derived peptides for potential PrP-binding molecules was investigated by integrated spectroscopical (CD and steady-state fluorimetry) and computational studies (molecular dynamic simulations and docking calculations).

In particular, we have shown that the antibiotic tetracycline can strongly interact with the α-helix 2 and that interaction concerns residues within its C-terminal half, previously suggested as a good candidate to promote a local α→β transition.

Finally, preliminary results on the interaction between the α-helix 2 and peptide constructs, designed on a Fab-ovPrP crystallographic complex, could open interesting perspectives for the diagnostic or therapeutic use of these molecules in PrP-associated diseases and give useful hints on the region/residues potentially important for the PrP^C→PrP^{Sc} conversion and on the conformational rearrangements involved in prion misfolding.

RIASSUNTO

Un numero crescente di malattie neurodegenerative quali i morbi di Alzheimer, di Parkinson e di Huntington, il diabete di tipo II e la fibrosi cistica, sono attualmente identificati come "malattie conformazionali", nelle quali le normali funzioni cellulari risultano compromesse da *misfolding* e aggregazione proteica [1]. Il *folding* anomalo della proteina prionica (PrP^C), in particolare, costituisce l'evento chiave alla base di patologie note come "encefalopatie spongiformi trasmissibili" (TSE) [2].

Il riarrangiamento strutturale di PrP^C nella forma patologica *scrapie* (PrP^{Sc}) e la conseguente formazione di fibrille amiloidi accomuna le TSE alle altre malattie conformazionali [3]. Pertanto, lo studio delle preferenze conformazionali della PrP potrebbe fornire un valido modello per la comprensione dei meccanismi del *misfolding* proteico.

La PrP è una glicoproteina di 231 amminoacidi presente nel sistema nervoso e linfatico, il cui ruolo fisiologico rimane ancora da chiarire, sebbene numerose ipotesi siano state avanzate riguardo a un suo coinvolgimento nel trasporto del rame e dello zinco, nell'apoptosi, e nella protezione da stress ossidativi [4]. Essa è caratterizzata da una zona N-terminale disordinata e flessibile e da un dominio C-terminale costituito da 3 α eliche (α1, α2 e α3), 2 β-*strands* ed un ponte disolfurico fra Cys179 e Cys214, che collega l'elica α2 con l'elica α3 conferendo stabilità strutturale all'intero dominio [5]. Particolarmente suggestiva è l'ipotesi che la proteina possegga uno o più siti di intrinseca fragilità strutturale che potrebbero costituire il punto di partenza della transizione PrP^C→PrP^{Sc} e, quindi, di nucleazione per la formazione di strutture β-*sheet*. A tale proposito, di particolare interesse risulta lo studio del frammento C-terminale dell'elica α2 che, per la presenza di 4 treonine consecutive nella sua sequenza [6], potrebbe costituire uno dei tratti di PrP caratterizzati da una propensione ad assumere una conformazione di tipo β.

In particolare, lo studio dell'elica α2, la cui sequenza peptidica è caratterizzata da ambivalenza conformazionale [7], dalla presenza di mutazioni amminoacidiche associate a patologie [8] e da neurotossicità [9], risulta particolarmente utile non solo per indagare i determinanti strutturali del *misfolding* prionico ma anche per il *de novo design* di composti in grado di prevenire o bloccare le malattie da prione.

A partire dalle particolari caratteristiche strutturali di questo sotto-dominio proteico, nel corso del lavoro di tesi, sono state analizzate le proprietà conformazionali della sequenza peptidica 173-195 corrispondente all'elica α2 della proteina prionica umana ed è stata inoltre valutata la sua affinità nei confronti di molecole peptidomimetiche ed organiche con potenziale attività anti-prionica.

A tale scopo, sono state sintetizzati, mediante metodiche in fase solida, i peptidi riportati in **Tabella 1(A)**, nella forma N- e C-terminale protetta, e quelli riportati in **Tabella 1(B)**, funzionalizzati mediante fluoresceina. In particolare, i peptidi **PrP[173-195]** e **PrP[173-195]D178N**, corrispondenti all'intera sequenza dell'elica α2 della proteina prionica umana, rappresentano, rispettivamente, il *wild type* ed il suo analogo D178N recante la mutazione amminoacidica associata alla sindrome di Creutzfeldt-Jakob (CJD) [10]. Il peptide **PrP[180-195]** costituisce il frammento più corto dell'elica α2, comprendente la sua zona C-terminale, ricca di treonine e caratterizzata da una forte propensione a formare strutture di tipo β, ed il peptide **PrP[173-179]** è il suo segmento complementare.

Il peptide **PrP[180-195]H187A** è stato infine scelto allo scopo di analizzare il ruolo del residuo di His187 nell'arrangiamento strutturale del frammento 180-195.

Tabella 1 Abbreviazione e sequenza dei peptidi sintetizzati.

	Abbreviazione	Sequenza peptidica
A	PrP[173-195]	Ac-NNFVHDCVNITIKQHTVTTTTKG-NH$_2$
	PrP[173-195]D178N	Ac-NNFVHNCV**N**ITIKQHTVTTTTKG-NH$_2$
	PrP[180-195]	Ac-VNITIKQHTVTTTTKG-NH$_2$
	PrP[180-195]H187A	Ac-VNITIKQ**A**TVTTTTKG-NH$_2$
	PrP[173-179]	Ac-NNFVHDC-NH$_2$
B	Fluo-PrP[173-195]	Fluo-βANNFVHDC(Met)VNITIKQHTVTTTTKG-NH$_2$
	Fluo-PrP[180-195]	Fluo-βAVNITIKQHTVTTTTKG-NH$_2$
	Fluo-PrP[106-126]	Fluo-βAKTNMKHMAGAAAAGAVVGGLG-NH$_2$
	Fluo-βA[25-35]	Fluo-βAGSNKGAIIGLM-NH$_2$

Nel corso del lavoro sperimentale, sono stati quindi condotti:

1) Studi comparativi mediante CD, NMR e *test* di tossicità cellulare sul peptide **PrP[173-195]**, sull'analogo **PrP[173-195]D178N** e sui frammenti **PrP[180-195]** e **PrP[173-179]**, allo scopo di chiarire il ruolo strutturale che l'intero dominio dell'elica α2, ed in particolare la sua parte C-terminale, riveste nel *misfolding* della proteina prionica ed inoltre l'influenza che mutazioni amminoacidiche legate alle TSE possono avere sulla sua stabilità e tossicità.

Dall'analisi mediante CD emerge che i peptidi PrP[173-195], PrP[173-195]D178N e PrP[173-179] assumono in acqua una conformazione di tipo *random*. Al contrario, il frammento PrP[180-195] mostra nelle stesse condizioni una conformazione di tipo β, che rimane sostanzialmente invariata in presenza dell'agente α-strutturante TFE. È quindi ragionevole ricondurre la conformazione *random* dell'intero frammento 173-195 al suo segmento N-terminale che è probabilmente in grado di attenuare la forte propensione β della parte C-terminale.

Inoltre, la sostituzione del residuo di Asp178 carico negativamente con uno neutro di Asn che è associata alla sindrome CJD, conferisce al peptide PrP[173-195]D178N una maggiore propensione ad assumere una conformazione di tipo β in SDS rispetto al peptide *wild type* nelle stesse condizioni.

L'analisi mediante NMR dimostra che la conformazione α-elicoidale, mostrata dal peptide *wild type* in TFE, riarrangia nel peptide mutato in due piccole α eliche separate da un ripiegamento centrato sulla Lys185 e la Gln186.

Test di tossicità condotti su cellule B104 di neuroblastoma di ratto hanno infine dimostrato che il peptide PrP[173-195]D178N esibisce una tossicità più alta (FC$_{50}$=12 μM) rispetto al peptide *wild type* (FC$_{50}$=68 μM), probabilmente a causa della destabilizzazione strutturale legata alla sostituzione Asp178 con Asn.

2) Analisi mediante CD sull'influenza del pH e della forza ionica sulla conformazione del peptide **PrP[180-195]** ed del suo analogo **PrP[180-195]H187A**.

Abbiamo dimostrato che anioni caotropici, quali Cl$^-$, ClO$_4^-$, e H$_2$PO$_4^-$, debolmente idratati a causa della loro bassa densità di carica, favoriscono l'accessibilità del solvente alla superficie peptidica e, quindi, una conformazione scarsamente strutturata dei peptidi, mentre anioni cosmotropici, quali SO$_4^{2-}$ e HPO$_4^{2-}$, fortemente idratati grazie alla loro alta densità di carica, sfavoriscono l'accessibilità del solvente alla superficie peptidica e inducono una organizzazione strutturale, che è di tipo α

elicoidale, nel caso del peptide PrP[180-195]H187A, o di tipo β, nel caso del peptide PrP[180-195].

3) Titolazioni CD ed NMR dei peptidi **PrP[173-195]** e **PrP[173-195]D178N** in presenza di cationi metallici bivalenti.

L'indagine strutturale dei frammenti *wild type* e dell'analogo D178N in presenza di Zn^{2+} e Cu^{2+} non ha evidenziato alcuna interazione specifica fra i cationi metallici ed i peptidi prionici. I nostri risultati dimostrano che i domini C- ed N-terminale giocano ruoli differenti nella conversione della proteina prionica e forniscono ulteriore supporto ai dati di letteratura preesistenti che individuando in quello N-terminale il *target* naturale dell'interazione di PrP con i metalli [11, 12].

4) Studio integrato spettroscopico e computazionale sull'interazione fra l'antibiotico **tetraciclina** (TC) e i peptidi dell'elica α2, allo scopo di verificare l'ipotesi che la tetraciclina possa interagire con la parte N-terminale di PrP, come è stato in precedenza dimostrato [13], e contemporaneamente con il tratto C-terminale dell'elica α2, intercalandosi fra queste due regioni strutturalmente instabili della proteina (**Figura 1**). Si è infatti ipotizzato che, nel contesto della struttura tridimensionale della proteina, l'elica α2 sia spazialmente adiacente al frammento 106-126 della parte N-terminale di PrP, precedentemente indicato come capace di interagire con la TC. I nostri risultati sono stati validati estendendo l'analisi anche al frammento PrP[106-126] ed al peptide βA[25-35], derivante dal β-Amiloide[1-42], opportunamente scelto per le caratteristiche amiloidi che lo accomunano ai peptidi prionici.

Abbiamo dimostrato quindi che l'antibiotico ha una forte affinità nei confronti di peptidi derivati dell'elica α2 e che l'interazione interessa soprattutto la sua parte C-terminale, della quale era stata precedentemente ipotizzato un possibile coinvolgimento nella formazione di strutture di tipo β [14]. TC potrebbe quindi stabilizzare tale tratto di PrP prevenendo la sua conversione strutturale e la conseguente aggregazione.
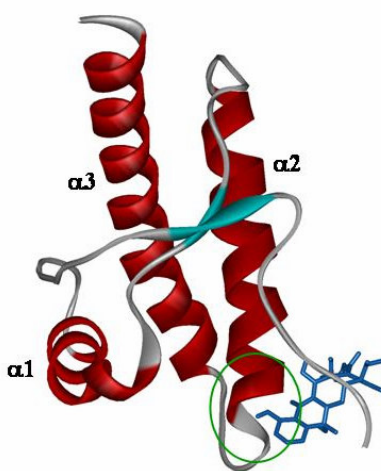
Figura 1 Modello molecolare ottenuto per simulazione dell'interazione della tetraciclina (blu) con l'estremità N-terminale della PrP e la parte C-terminale dell'elica α2 (evidenziata in verde).
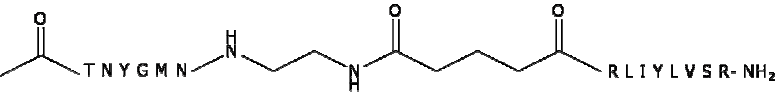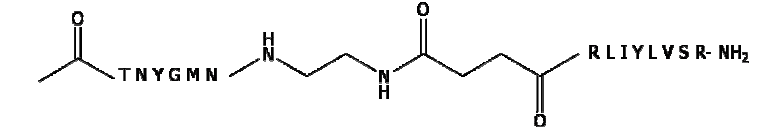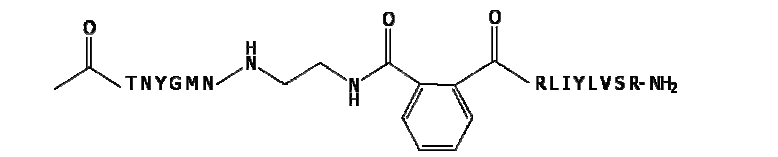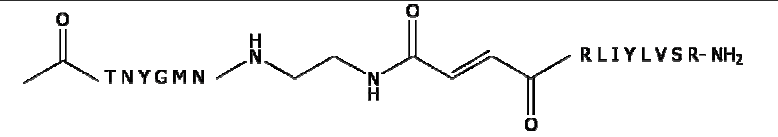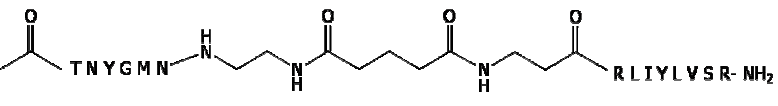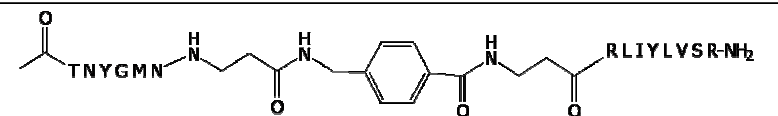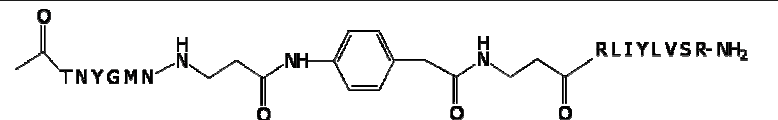
5) Analisi dell'affinità dell'elica α2 nei confronti di costrutti peptidici disegnati a partire dalla struttura a raggi X del complesso fra ovPrP ed un anticorpo Fab (**Figura 2**) [15]. I costrutti peptidici (composti **JMV** riportati in **Tabella 2**) sono stati sintetizzati unendo con *spacers* di differente lunghezza, rigidità e natura chimica, i due frammenti peptidici Fab[30-35] e Fab[46-53] (TNYGMN e RLIYLVSR, rispettivamente) capaci di formare legami idrogeno con la parte C-terminale dell'elica α2 nel struttura cristallografica Fab-ovPrP. L'interazione dei composti JMV con il peptide PrP[173-195] funzionalizzato con fluoresceina è stata poi analizzata mediante spettroscopia di fluorescenza. Dall'analisi è emerso che tutti i costrutti peptidici JMV sono capaci di legare fortemente il tratto peptidico 173-195 suggerendo che la loro affinità per tale tratto sia scarsamente correlata alle dimensioni, alla rigidità ed alla natura chimica degli *spacers*.
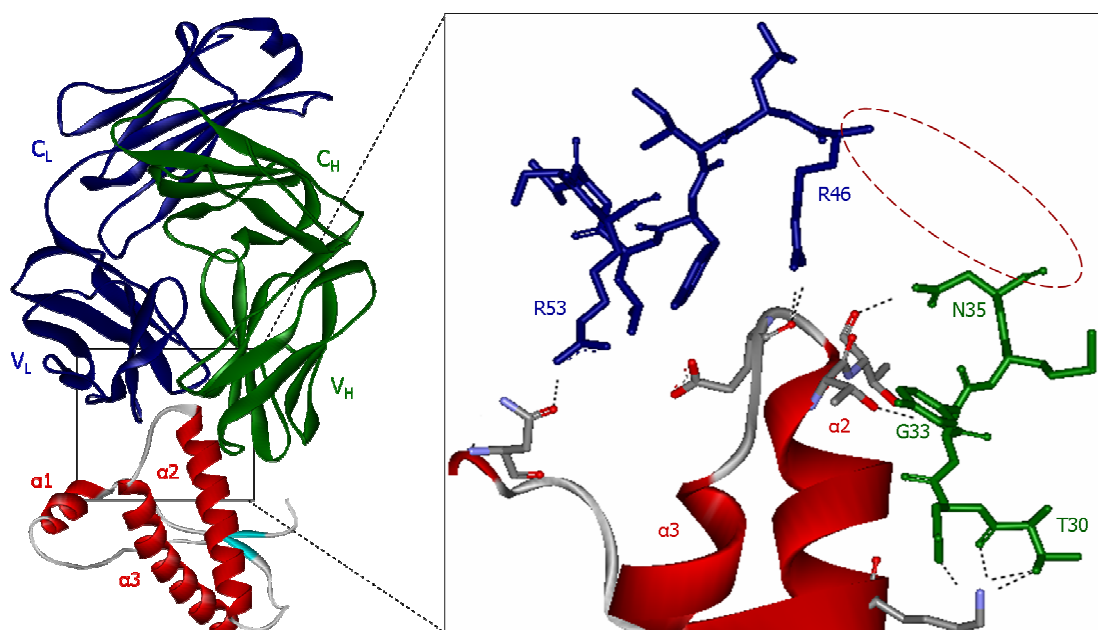
Figura 2 (Sinistra) Overview del complesso. **(Destra)** Ingrandimento della regione di interazione. Per chiarezza, solo gli atomi che interagiscono attraverso legami idrogeno (linee tratteggiate) sono rappresentati nel formato "stick" [15].

L'insieme dei risultati ottenuti sul panorama conformazionale dell'elica α2 dimostra che questo dominio gioca un ruolo di fondamentale importanza nel meccanismo di *misfolding* della proteina prionica. La forte sensibilità dell'elica α2 a modifiche dell'intorno chimico ed a singole mutazioni amminoacidiche conferma infatti il carattere ambivalente di tale tratto peptidico, rendendolo un importante bersaglio per nuove strategie terapeutiche e diagnostiche. Inoltre, riguardo allo studio di molecole capaci d'interagire con l'elica α2, i nostri risultati aprono importanti prospettive per l'uso diagnostico e farmacologico della TC e dei costrutti sintetici JMV nelle TSE.

Tabella 2 Abbreviazione e struttura dei costrutti peptidici JMV.

Abbreviazione	Struttura
JMV3302	
JMV3307	
JMV3388	
JMV3308	
JMV3389	
JMV3390	
JMV3391	

[1]   Carrel, R.W. and Lomas, D.A. (1997) Lancet, 350, 134-138.
[2]   Prusiner, S.B. (1998) Proc. Natl. Acad. Sci. USA, 95, 13363-13383.
[3]   Temussi, P.A., Masino, L. and Pastore, A. (2003) EMBO J., 22, 355-361.
[4]   Campana, V., Sarnataro, D. and Zurzolo, C. (2005) Trends Cell Biol., 15, 102-111.
[5]   Zahn, R., Liu, A., Lührs, T., Riek, R., von Schroetter, C., Garcia, F.L., Billeter, M., Calzolai, L., Wider, G. and Wüthrich, K. (2000) Proc. Natl. Acad. Sci. USA, 97, 145-150.
[6]   Minor, D.L. Jr. and Kim, P.S. (1994) Nature, 367, 660-663.
[7]   Tizzano, B., Palladino, P., De Capua, A., Marasco, D., Rossi, F., Benedetti, E., Pedone, C., Ragone, R. and Ruvo, M. (2005) Proteins, 59, 72-79.
[8]   Kuznetsov, I.B. and Rackovsky, S. (2004) Protein Sci., 13, 3230-3244.
[9]   Thompson, A., White, A.R., McLean, C., Masters, C.L., Cappai, R. and Barrow, C.J. (2000) J. Neurosci. Res., 62, 293-301.
[10] Gsponer, J., Ferrara, P. and Caflisch, A. (2001) J. Mol. Graph. Model., 20, 169-182.
[11] Millhauser, G.L. (2004) Acc. Chem. Res., 37, 79-85.
[12] Millhauser, G.L. (2007) Annual Review of Physical Chemistry, 58, 299–320.
[13] Tagliavini, F., Forloni, G., Colombo, L., Rossi, G., Girala, L., Canciani, B., Angeretti, N., Giampaolo, L., Peressini, E., Awan, T., De Gioia, L., Ragg, E., Bugiani, O. and Salmona, M. (2000) J. Mol. Biol., 300, 1309–1322.
[14] Haire, L.F., Whyte, S.M., Vasisht, N., Gill, A.C., Verma, C., Dodson, E.J., Dodson, G.G. and Bayley, P.M. (2004) J. Mol. Biol., 336,1175-1183.
[15] Eghiaian, F., Grosclaude, J., Lesceu, S., Debey P., Doublet, B., Tréguer, E., Rezaei, H. and Knossow, M. (2004) Proc. Natl. Acad. Sci. USA, 101, 10254-10259.

RESUME

Un grand nombre de pathologies humaines, du diabète de type II à la maladie de Parkinson et la maladie d'Alzheimer, est associé à l'agrégation de protéines résultant d'un repliement anormal. Malgré son importance biologique fondamentale, peu de choses sont connues sur les processus physiologiques qui conduisent à l'accumulation de ces protéines. Les encéphalopathies spongiformes transmissibles (TSE), plus connues sous le nom de maladies du prion, appartient à cette classe. Elles sont toutes caractérisées par une dégénération neuronale progressive. Dans presque tous les cas, il y a une forte accumulation extracellulaire d'un conformère amyloïdogénique de la forme cellulaire normale de la protéine prion (PrP^C), appelé *scrapie isoform* (PrP^{Sc}). Cette forme est probablement responsable de la maladie. PrP est une glycoprotéine ubiquitaire de 231-aminoacides acide dont le rôle physiologique n'est pas encore connu. Les structures montrent une région N-terminale non-structurée et un domaine globulaire C-terminal caractérisé par la présence de trois hélices α (α1, α2 et α3), de deux brins β courts et d'un pont disulfure entre Cys179 et Cys214, qui relie les deux hélices α2 à α3 et confère la stabilité structurale. Aujourd'hui, est acceptée l'hypothèse que la protéine possède une ou plusieurs régions de fragilité conformationelle qui entraine une déstabilisation totale de la structure secondaire et tertiaire de la protéine en fonction du changement de pH, des propriétés rédox du milieu et de l'état de glycosylation. La partie C-terminale de l'hélice 2, contenant quatre thréonines adjacentes est soupçonnée d'être une de ces régions et, à cet égard, elle fait l'objet de nombreuses études. Comme l'hélice α2 possède un comportement conformationnel ambivalent et plusieurs points de mutation associés aux pathologies TSE, elle constitue un modèle de choix pour étudier les déterminants structuraux du *misfolding* de PrP^C et pour concevoir de façon rationnelle de nouveaux composés à visée thérapeutique. Les propriétés structurales particulièrement intéressante de ce domaine de la protéine PrP, nous a incité à étudier ses caractéristiques conformationnelles. Pour cela, nous avons synthétisé par SPPS l'hélice α2 de hPrP et divers fragments peptides de cette hélice. Nous les avons ensuite caractérisé par CD et par RMN en solution aqueuse à différents pH, dans des milieux structurants (SDS et TFE) et en présence d'anions et de cations métalliques bivalents. La neurotoxicité de ces peptides a également été testée sur des cellules de neuroblastomes B104. L'ensemble des résultats suggère fortement que l'hélice α2 joue un rôle important dans la conversion de la PrP^C en PrP^{Sc}. De plus, l'affinité de l'hélice α2 et de certains de ces dérivés pour des molécules organiques et des pseudopeptiques que nous avons synthétisés a été étudié par analyse spectroscopique (CD et fluorescence) et par analyse computationnelle (dynamique moléculaire et docking). En particulier, nous avons montré que l'antibiotique tétracycline peut fortement interagir avec l'hélice α2 et que l'interaction concerne des résidus dans sa partie C-terminale, précédemment suggéré comme un bon candidat pour étudier la transition locale α→β. Enfin, les résultats concernant l'interaction entre l'hélice α2 et les composés synthétisés, conçus à partir de la structure cristallographique d'un complexe Fab-ovPrP offrent des outils pour localiser les régions/résidus potentiellement importantes pour la conversion PrP^C→PrP^{Sc} et les réarrangements conformationels impliqués dans la la forme spongiforme de la protéine prion.
De plus, ils ouvrent des perspectives intéressantes pour l'utilisation de ce type de molécules dans le diagnostic ou le traitement des maladies associées à la PrP.

INTRODUCTION

I.1. *Conformational diseases*

An increasing family of neurodegenerative disorders such as Alzheimer's, Parkinson's and Huntington's diseases, transmissible spongiform encephalopathies (TSE) and cystic fibrosis are currently classified as conformational diseases, which is a family of disorders where cellular functions are compromised because of protein misfolding and aggregation [1].

Since all members of this family of diseases are linked to a mechanism of aberrant protein folding, knowledge of the three-dimensional structure of the proteins implicated, both in their healthy and in their pathological forms, is the prerequisite for understanding the mechanism of aggregate formation and, eventually, preventing it. Yet, only relatively limited structural information is currently available. It is believed that the pathogenesis of these diseases is to be ascribed to reduced or lacking efficiency of physiological quality control systems, which leads to the formation of toxic protein aggregates, possibly affecting cellular function and eventually causing neuronal death [2]. Evidence has been accumulated that these aggregates possess various supramolecular architectures and, in most cases, form insoluble fibrillar deposits with well-defined structure, called amyloids [3]. A causative link between aggregation and disease is not, however, universally acknowledged, because amyloid fibril formation might be simply the consequence of a pathogenetic mechanism that could reside in causes to be identified [2]. The most widely accepted explanation for aggregation and amyloid formation is that the native fold of a protein isomerizes to an improperly folded conformation prior to a structural reorganization resulting in protein aggregation and deposition. Fibrils are not toxic in themselves, but the quick β-strand-bonding-driven autolinkage of polypeptide chains may easily cause further linkage that leads to insoluble macrostructures with inflammatory or, more in general, toxic properties [4, 5].

The term amyloidosis applies when deposition of such macrostructures in the tissue is a dominant, histologically apparent feature [6]. Amyloidosis is characterized by the accumulation of abnormal proteinaceous deposits in cell compartments and/or within the extra-cellular matrix, in which amyloid fibrils share a cross-β core structure [3, 7]. Amyloid formation can also occur when the plasma concentration of normal proteins is persistently increased, as with acute-phase proteins and immunoglobulins in chronic inflammation [5].

Such structural rearrangements likely take place in a class of degenerative neurological disorders involving the host-encoded prion protein (PrP), which are usually identified as TSE [8-10]. The general features of prion diseases are common to other amyloid disorders [2], underlining the interest for the prion protein as useful model to provide the bases for a comprehensive evaluation of protein misfolding mechanism.

I.2. *Prion protein structure*

The mammalian PrP gene encodes the PrP^C protein as a 253 aminoacid polypeptide chain from which the first 22 aminoacids (signal peptide) are cleaved shortly after translation commences (**Figure I.2.1**). Post-translational processing adds a C-terminal glycosylphosphatidylinositol (GPI)-anchor at residue 230, which facilitates glycolipid linkage of PrP^C to the cell membrane [11]. Recent studies on an anchorless, secreted version of PrP^C, expressed in transgenic mice, have clarified that membrane anchoring is a crucial prerequisite for prion toxicity resulting in clinical TSE [12]. Two N-linked glycosylation sites are located at residues 181 and 197. A nonapeptide followed by four identical octapeptide repeats are normally located between residues 51 and 91.

PHGGGWGQ PHGGGWGQ PHGGGWGQ PHGGGWGQ
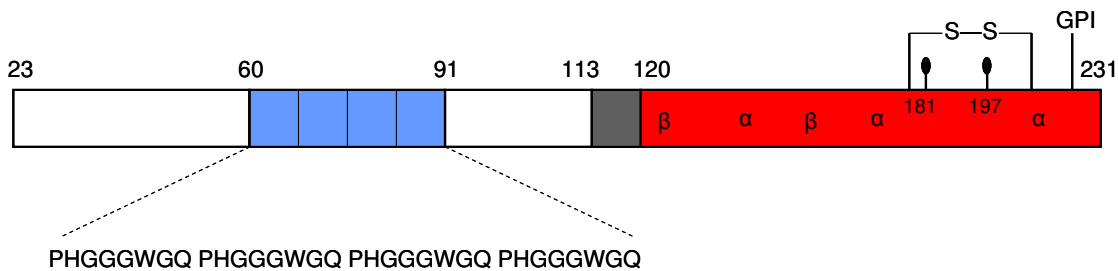
Figure I.2.1 Diagram indicating secondary structure and other features of the prion protein (PrP). The C-terminal domain (red) contains three α-helical segments, two short β-strands, a disulfide bond, and a glycosylphosphatidylinositol (GPI) anchor that tethers PrP to the membrane surface. The N-terminal segment, up to approximately residue 120, is largely unstructured and contains the octarepeat domain (blue) and a hydrophobic region (green).

As schematically depicted in **Figure I.2.2**, the structure of ubiquitous benign cellular form of PrP consists of an unstructured tail encompassing residues 23–125 and a globular domain, stabilized by an intramolecular disulfide bond (Cys179-Cys214) [13] and comprising residues 126–231, with a structure made of three α-helices and a short β-sheet.

In a series of studies Wüthrich and co-authors have reported the NMR structure of the globular C-terminal domain of recombinant human PrP^C ($hPrP^C$), also investigating several recombinant prion proteins from other species [14-20]. The overall structural organization of these PrPs is very similar, with residues 128-131, 144-154, 161-164, 173-195 and 200-228 forming the β-strand 1, the α-helix 1, the β-strand 2, the α-helix 2 and the α-helix 3, respectively. Crystallographic studies lend support to this monomeric structure, but in the dimeric form, an unusual domain swapping of α-helix 3 is apparent, with creation of a novel short anti-parallel β-sheet segment at the molecular interface [21].

As a consequence of a post-translational process, PrP^C is converted into the aberrantly folded and disease-specific scrapie isomer, PrP^{Sc}, through a process whereby a portion of its predominantly α-helical structure is refolded into β-sheet [8]. PrP^{Sc} exhibits resistance to proteinase K digestion [22, 23]. It is also known that the conversion of PrP^C into PrP^{Sc}, whose high β-sheet content is an essential constituent of putatively infectious prions [8, 24, 25], can also intrinsically occur as a result of a

genetic mutation, as in rare familial encephalopathies. More disturbingly, however, transgenetic studies argue that inoculated PrP^{Sc} can impart conformational variability to normal prions, thus triggering PrP^{C} refolding into a nascent PrP^{Sc} [8]. It can be concluded that mechanisms that underlie pathological transitions remain unclear, despite attention paid to their understanding, because the highly aggregated state has hampered elucidation of the PrP^{Sc} structure at the atomic level.
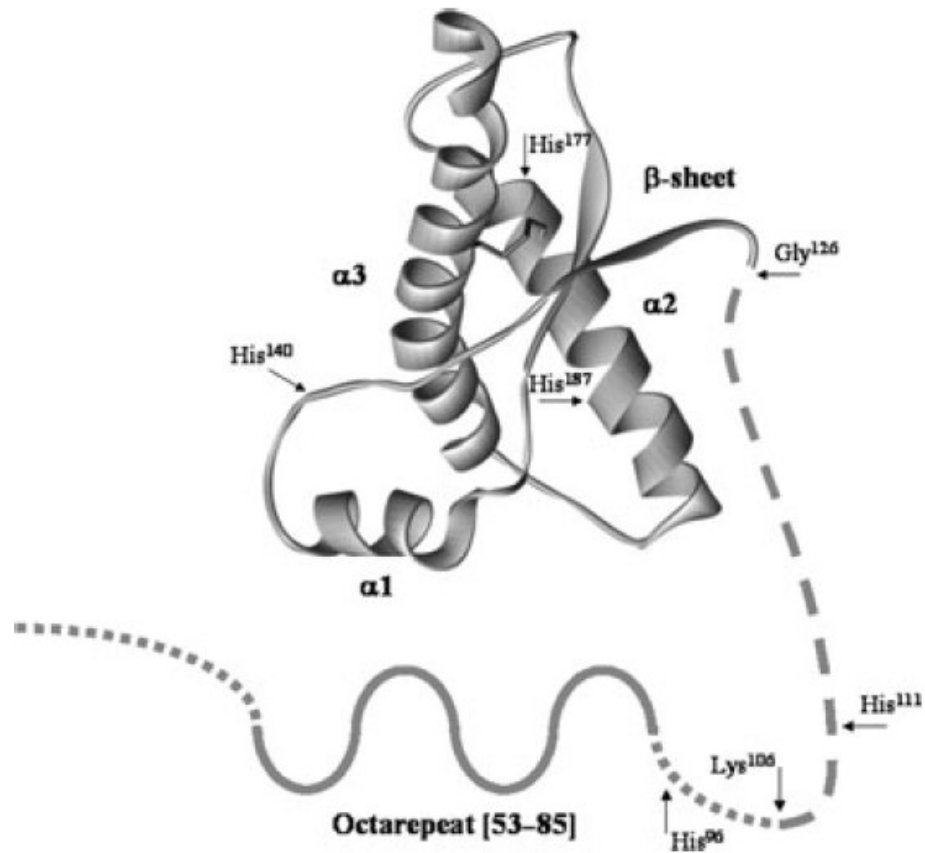
Figure I.2.2 Cartoon of the hPrP structure. The sketch was drawn according to current information [13]. Most salient residues are indicated by arrows.

I.3. *Determinants of PrP^C conversion: the N-terminal region*

The neurodegeneration observed in spongiform encephalopathies is believed to be mediated by partially protease-resistant forms of PrP. In fact, the neuropathological changes observed in prion disease are caused, at least in part, by the accumulation of proteinase K-resistant PrP^{Sc} [21-23]. This view is supported by the observation that the partially protease-resistant core of PrP^{Sc} displays a variety of pathogenic effects *in vitro*, including neurotoxicity and the ability to interact with plasma membrane, conferring an increased microviscosity. PrP^{Sc} accumulates in the central nervous system of affected individuals, and its partially protease-resistant core aggregates extracellularly into amyloid fibrils. The process is accompanied by nerve cell loss, whose pathogenesis and molecular basis are not well understood. Frankenfield and co-workers [26] compared the *in vitro* aggregation of a truncated portion of the prion protein (PrP[90–231]) and a full-length version (PrP[23–231]), which can be distinguished from the truncated protein because it contains the largely unstructured N-terminal region in addition to the α-helical C-terminal one. They found that the full-length protein forms larger aggregates than the truncated protein, which indicates that the N-terminal region may mediate higher-order aggregation processes, possibly influencing the assembly state of PrP before aggregation begins. Other studies [27] have confirmed that the N-terminal region has a pivotal role in the development of prion misfolding and aggregation. In fact, by using N-terminal deletion mutations of recombinant murine PrP, mPrP[51–90] and mPrP[32–121], it has been shown that the stability against pressure of the protein is dramatically reduced with decreasing N-domain length and the process is not reversible for mPrP[51–90] and mPrP[32–121], whereas it is completely reversible for the wild-type form. Moreover, the temperature-induced transition was found to lead to aggregation of all forms, but the deletion mutants showed higher thermal lability. Similar effects have been observed with a short synthetic peptide fragment encompassing residues 106–126 of hPrP, which is toxic to cultured neurons depending on the expression of endogenous PrP. This synthetic peptide recapitulates several properties of PrP^{Sc}, including the propensity to form β-sheet-rich, insoluble and protease-resistant fibrils similar to those found in prion diseased brains [28]. Experimental data indicate that PrP[106–126] does not induce the formation of abnormal PrP species, suggesting, as an alternative explanation, that peptide toxicity depends on triggering alteration of a physiological function of PrP^C [29]. In fact, the N-terminal truncated PrP is toxic only to neurons that lack endogenous PrP, while PrP[106–126] is toxic only to neurons that express the endogenous protein. The structure of PrP[106–126] is modulated by pH, and its β-sheet content is higher at pH 5 than at pH 7. Furthermore, in the presence of lipids it acquires a predominantly β-sheet conformation. Extensive studies were performed to understand the relationships between toxicity and physicochemical properties of amyloid peptides. To determine the role of the hydrophobic palindromic sequence in PrP[106–126] toxicity, Jobling et al. [30] have generated a series of mutant PrP[106–126] peptides with hydrophilic substitutions in the hydrophobic core. The results of these studies correlate the neurotoxic action of PrP[106–126] to its secondary structure and subsequent fibril-forming propensity. The data suggest that the hydrophobic C-terminal valines and the palindromic region from Ala113 to Ala120 of PrP[106–126] are involved in the folding and/or stabilization of a β-sheet aggregate. These findings are similar to those described for amyloid β-

peptide aggregates and strengthen the view of a common structure-function mechanism of amyloid generation in spongiform encephalopathies and Alzheimer's disease [2]. On the other hand, on consideration that, in infectious and familial prion disorders, neurodegeneration is often seen without deposits of PrP^{Sc}, Gu and co-workers [31] have shown that exposure of neuroblastoma cells to PrP[106–126] catalyzes the aggregation of cellular prion protein to a weakly proteinase K-resistant form and induces the synthesis of transmembrane prion protein, suggesting that neurotoxicity is mediated by a complex pathway involving transmembrane prion protein and not not only by deposits of aggregated and proteinase K-resistant PrP.

I.4. *Determinants of PrP^C conversion: the C-globular domain*

In the X-ray structure of monomeric sheep PrP^C (sPrP^C) were identified two potential loci of β-structure propagation [32]. The former locus (residues 129-131) is involved in an intramolecular β-sheet with residues 161-163 and in lattice contacts about a crystal dyad to generate a four-stranded intermolecular β-sheet between neighboring molecules. Modeling on the latter locus (residues 188-204) suggests that it is able to act as an α→β switch within the monomer. The α→β isomerization of PrP is most frequently observed *in vitro* in the pH range from 4 to 7 [33-37] and has been postulated to be induced *in vivo* by the low pH of endosomal compartments [38]. A comparison between the C-*terminus* crystal structures of monomeric sPrP^C and dimeric hPrP^C showed that the dimer results from the swapping of the C-terminal α-helix 3 and rearrangement of the Cys179-Cys214 disulfide bond. An interchain two-stranded antiparallel β-sheet is formed at the dimer interface between the corresponding crystal-symmetry-related residues 190-194, which are located in α-helix 2 in the monomeric NMR structures [21]. The segment 188-201 (TVTTTTKGENFTET) is invariant across a wide variety of species [39] and, on the basis of its primary structure, several features emerge that might drive PrP^C reorganization. In particular, the seven threonine residues could confer the necessary conformational plasticity. Moreover, residues 188-201 in hPrP adopt an architecture that appears to be of lower stability as compared to the rest of the structure. The high intrinsic β-propensity of four adjacent threonines [40] makes this segment a good candidate to promote a local α→β transition, which, under suitable conditions, could lead to PrP^{Sc} formation, even independently of disulfide bridge rearrangement, since PrP^{Sc} monomers are not linked by intermolecular disulfide bonds. Furthermore, PrP^{Sc} can induce the conversion of the disulfide-intact form of the monomeric cellular prion protein to its protease-resistant form without the temporary breakage and subsequent re-formation of the disulfide bonds in cell-free reactions [41]. From the above studies, it emerges that quite small conformational adjustments can convert the monomeric PrP^C into a potentially oligomeric nucleating unit. It is likely that some conformational weaknesses converging on the sequence 190-195 or a shorter surrounding region are able to affect the whole protein architecture and promote the non-covalent association of misfolded monomers. It has been also proposed [32] that the synergical propagation of β-sheet association involving the whole molecule mediates protein oligomerization. Recently, Thompson and co-authors [4] have investigated the conformational and aggregation behaviour of synthetic peptides corresponding to PrP^C helices in aqueous solutions. The fragment corresponding to α-helix 1 exhibited a random coil CD spectrum at any pH value from 3 to 12, whereas in 40% trifluoroethanol (TFE) the peptide was 20% helical and did not aggregate over time neither did it form amyloid fibrils. However, it has been also shown that α-helix 1 possesses a remarkably high instrinsic α-helical propensity [42] and retains significant helicity under a wide range of conditions, such as high salt, pH variation, and presence of organic co-solvents [43]. Because of its high stability against environmental changes, helix 1 is unlikely to be involved in the initial steps of the pathogenic conformational change and it could unfold in the late stage of the structural transition as a consequence of global conformational rearrangements occurring in other parts of the prion protein [43]. The fragment corresponding to α-helix 2 underwent a time dependent β-sheet rearrangement with formation of

aggregates over time. However, electron microscopy showed that aggregates taken from CD samples were organized in fibrils, which were small at pH 7.2, but longer and more distinct at higher pH values. The fragment corresponding to α-helix 3 also underwent pH dependent β-sheet formation. The CD curve exhibited random organization at pH 6.0 and 7.2, and β-sheet at pH 3, with an aggregation dependent intensity decrease after 24 hours. The precipitate did not show fibril formation indicating that this peptide is not truly amyloidogenic under the conditions studied. As can be concluded from these observations, the relationship between amyloidogenicity and neurotoxicity remains unclear, because the fact that a peptide is somehow prone to aggregate and readily form a β-sheet structure does not necessarily imply that it forms amyloid fibrils. Additional evidence indicates that an intermediate along the pathway to fibril formation could cause toxicity, whereas large fibrils may not be toxic in themselves. Gallo and coworkers [44] have recently reported that the conserved capping box (Thr199-Glu200-Thr201-Asp202) and, in part, the ionic bond formed between Glu200 and Lys204 render the PrP^C segment corresponding to the α-helix 3 structurally autonomous, in contrast to α-helix 1 and α-helix 2 peptides. In fact, the D202N capping mutation associated to the Gerstmann-Straussler-Scheinker (GSS) disease almost completely destabilizes the isolated α-helix 3 peptide, thus possibly initiating the PrP^C pathogenic process associated with this substitution. Moreover, cell culture data based on the NMR structure of mouse PrP^C suggest that the highly conserved hydrophobic side chain at residue 204 of α-helix 3 is required for folding and maturation of PrP^C, providing an essential stabilization of α-helix 1 structure by interacting with Phe140, Glu145, Tyr148, and Tyr149. Disruption of α-helix 1 prevented attachment of the GPI anchor and the formation of complex N-linked glycans. In the absence of a C-terminal membrane anchor, however, α-helix 1 induced the formation of unglycosylated and partially protease-resistant PrP aggregates [45]. This result is confirmed by molecular dynamic simulations, in which disturbances of the folding and maturation process of PrP^C have been interpreted as consequences of mutation-induced structural changes in PrP, involving α-helix 1 and its attachment to α-helix 3 [46]. A number of results on cellular toxicity [4], fibrillization capabilities [13], and metal binding properties [47] of synthetic variants of the α-helix 2 point to an important contribution of this region to the overall biological behaviour of the prion protein. In fact, perturbations leading to structural rearrangements that may strongly affect the stability of the α-helix 2 could involve deglycosylation of Asn181 [13] and/or copper binding to His187 [47]. Rearrangements of the α-helix 2 could promote β-sheet-mediated protein association leading to a further α→β transition and subsequently to aggregation. In a novel thermodynamic study, the α→β conversion of the N- and C-*termini* blocked fragment corresponding to the α-helix 2, PrP[173-195], has been characterized by measuring α-helical and β-structure formation propensities in the temperature interval from 280 K to 350 K [48]. The thermodynamic cycle reported in **Figure I.4.1** shows that the two ordered conformations were found to be separated by 5-8 kJ/mol, with an entropic advantage of 0.04 kJ mol^{-1} K^{-1} favoring the α-helical organization. This subtle free energy difference was interpreted as denoting the chameleon-like character of PrP[173-195], which could be governed, in the protein, by the cellular microenvironment, according to the finding that slight conditional changes may cause chameleon sequences to fold into either α- or β-structure [49]. In this context, it is worth noting that, in the whole PrP^C, the close packing of the first three turns of the α-helix 2 against the α-helix 3 generates a complementary interface [17, 21] that strongly stabilizes the helix up to around residue 188, with the glycosyl moiety bound

to Asn181 providing further stabilization [13]. Conversely, the region spanning residues 190-195 is rather apart from the α-helix 3, which is well characterized only up to Thr219 in the NMR structures of mouse PrP[C] [50] and found in β-conformation in the dimeric crystal structure of hPrP[C] [21], suggesting that this site is one of the most prone to structural rearrangements upon suitable perturbation. Thus, the short C-terminal end of the full length α-helix 2 could be involved in the nucleation process of prion misfolding and oligomerization, possibly in cooperation with the N-terminal fragment 82-146, whose intrinsic properties are dependent upon the integrity of the C-terminal region [51].
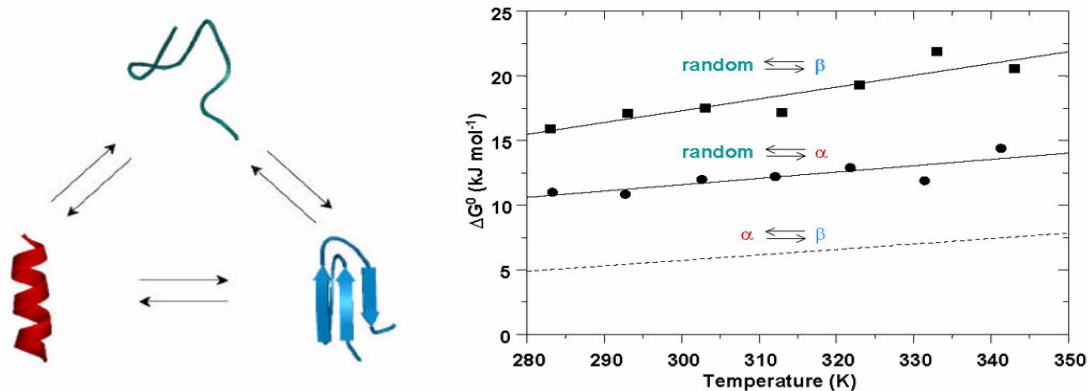
Figure I.4.1 Thermodynamic diagram of structural preferences of PrP[173–195] (α-helix 2). Extrapolated values of ΔG° for the random-to-α and random-to-β transitions are plotted as a function of temperature. The dashed line represents the thermodynamics of the α→β transition as obtained by difference between the ΔG°s of the two random-to-ordered structure transitions. All experimental data were fitted to straight lines because neither transition is accompanied by an appreciable heat capacity change, suggesting that enthalpy and entropy changes are independent of temperature [48].

I.5. *Binding by metal ions*

Research over the past few years clarified that PrP^C can exist in a Cu-metalloprotein form *in vivo* [52] and displays high selectivity for Cu^{2+} [53, 54]. Screens against other divalent cations, such as Ca^{2+}, Co^{2+}, Mg^{2+}, Mn^{2+} and Ni^{2+}, failed to find high-affinity interactions. In order to extract functional information, many efforts have been devoted to the structural characterization of Cu^{2+} binding sites [49, 52-66]. The emerging consensus is that most copper binds in the octarepeat domain, comprising the HGGGW segment as the fundamental unit involved in Cu^{2+} coordination [67, 68]. The crystal structure of the complex reveals equatorial coordination of Cu^{2+} by the histidine imidazole, two deprotonated glycine amides, and a glycine carbonyl, along with an axial water bridging to the Trp indole, consistently with companion experiments in solution [68]. This somewhat unusual copper binding site is by no means unprecedented. In most copper binding proteins, side chain moieties such as histidine imidazole or cysteine thiol enter into contact with the metal ion [69]. Previous studies showed that unstructured peptides containing histidines coordinate in a fashion similar to that now identified for PrP [70, 71]. The pKa of amide protons is typically 13–15, and consequently the amide nitrogen is not ionized at pH 7. However, nitrogen and Cu^{2+} are well matched on the hard-soft scale of Lewis acid–base interactions. Thus, with the histidine imidazole anchoring the metal ion close to the polypeptide backbone, Cu^{2+} may be uniquely able to displace a nearby amide proton at physiological pH [72]. Modeling, EPR and companion spectroscopic studies on peptides as well as full length protein provide however evidence that additional copper sites are located in the region connecting the unstructured N-terminal segment to the C-terminal globular portion of PrP [58, 59, 66]. Accordingly, it has been proposed that an additional copper-binding site compared with the four of the octarepeat domain binds around His 96 and/or His 111, a region of the PrP molecule known to be crucial for prion propagation [55, 73-75]. In fact, proteolytic cutting of PrP^{Sc} at approximately residue 90 does not result in loss of infectivity. This suggests that the octarepeat domain, and hence copper, do not play a role in TSEs and may not be necessary to PrP conversion and disease, but a modulating role in kinetics and pathology cannot be excluded. Indeed, the octarepeat domain and copper have been directly implicated in neurological disease [55]. Finally, recent studies show that binding of a single copper rapidly and reversibly induces PrP^C to become protease-resistant and detergent-insoluble [76]. There is experimental evidence that binding takes place at His96 in full-length PrP, that is outside both the octarepeat and the C-globular domains [53, 74, 75]. The amyloidogenicity and neurotoxicity of PrP[106-126] are common to the Alzheimer's disease amyloid β peptide. Given that the biophysical behaviour and activity of amyloid β peptide are governed by transition metals, the effect of metals has been also studied on PrP[106-126]. The fibrillization of this peptide is completely inhibited in a metal-depleted buffer, and Cu^{2+} and to a lesser extent Zn^{2+} have been found to restore its aggregation [64]. The metal binding site was found to comprise the N-terminal amino group, His111 and Met112. This supports the view of a common structure-function mechanism of amyloid generation in spongiform encephalopathies and Alzheimer's disease [43–45]. Most recently, the stimulatory potential of Cu^{2+}, Mn^{2+}, Zn^{2+}, and Al^{3+} in inducing defective conformational rearrangements which trigger aggregation and fibrillogenesis has been investigated in the recombinant hPrP fragment spanning residues 82-146 [77].

This region has been identified as a major component of the amyloid deposits in the brain of patients affected by GSS disease. Amino acid substitution in the neurotoxic core (sequence 106-126) reduced its amyloidogenic potential. However, alteration of the 127-146 sequence, which comprises a segment of the C-terminal globular domain, also caused strong inhibition of the fibrillogenesis, thus suggesting that integrity of this region was essential both to confer amyloidogenic properties on GSS peptides and to activate the stimulatory potential of the metal ions. Notably, only a few studies have been carried out on metal interaction with peptides derived from the C-*terminus* of PrP, which contains the histidine residues (H140, H177 and H187) and the helical region. Recent spectroscopic experiments [47, 78] exclude the involvement of H140 in Cu^{2+} binding, but the aggregation of model peptides hampered characterization of the metal interaction with H177 and caused uncertainty about Cu^{2+} binding to His 187 at physiological pH. Incidentally, it has been found [79, 80] that the only known histidine variant associated with familial encephalopathy could be associated with the H187R mutation in the PrP gene. Brown and co-authors [47] characterized Cu^{2+} complexes with two analogues of the peptide fragment 180-193 (VNITIKQHTVTTTT), which almost entirely encompasses the PrP^{C}'s α-helix 2, one with blocked and the other with free C- and N-*termini*. They analyzed the involvement of His in the interaction with Cu^{2+} at pH values close to neutrality. The different histidine side-chain anchoring in the two peptide forms and the formation of different Cu^{2+} complex species were attributed to the competition between the amino and imidazole nitrogens in their binding to the metal ion. However, the significant increase of toxicity of the N- and C-*termini* blocked peptide upon Cu^{2+} addition was unclear and interpreted as likely reflecting the effect of the different coordination environment on the conformation of the peptides. Other studies on α-helix 2-derived peptides [4] showed that PrP[178-193] and PrP[180-193] are the only ones able to form amyloid. Exposure to copper ions resulted in a significant increase of PrP[178-193] neurotoxicity as compared to the metal control. The peptide was also found to promote Cu(II)-induced lipid peroxidation and cytotoxicity in primary neuronal cultures. On the other hand, PrP[198-218], which can form β-sheet aggregates but does not form fibrils, showed no copper-induced neurotoxicity. In conclusion, most data suggest that copper ions may play a role in toxicity of amyloidogenic and/or fibrillogenic proteins, also indicating that a region of PrP^{C} other than PrP[106-126] may be involved in neurotoxicity.

I.6.   *PrP Biology*

In the most accredited model of prion formation and replication, a direct interaction between the pathogenic PrP^{Sc} template and the endogenous PrP^C substrate is proposed to drive the formation of nascent infectious prions in the case of infectious diseases [8]. Characterizing the exact intracellular localization of PrP^C and PrP^{Sc} is important for identifying the intracellular compartment and the mechanism that underlie prion formation. The possibility that misfolding and/or misfuction of PrP^C correlate with defects in its trafficking is supported by several studies in which the intracellular localization of some inherited pathological PrP mutants have been shown to be altered [81]. It is not yet clear, however, whether mislocalization is the cause or the effect of prion misfolding and/or misfunction [82]. Consequently, it is important to understand the relationships between the intracellular trafficking, proper protein misfolding and function of PrP^C (**Figure I.6.1**) [83].
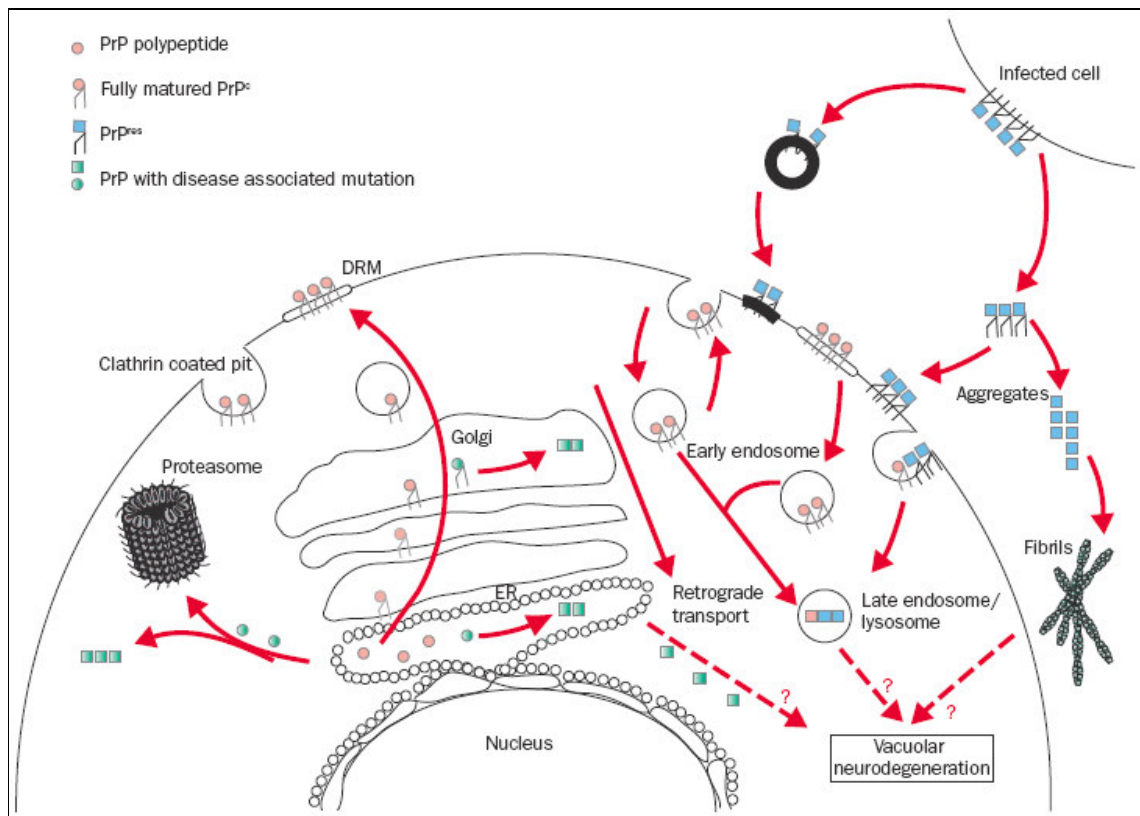
Figure I.6.1 Intracellular trafficking of PrP^C and PrP^{Sc} and possible patways of PrP^{Sc} formation [83].

PrP^C is synthetized in the rough endoplasmic reticulum (ER), where simple N-linked oligosaccharides and the GPI-anchor are added, and it arrives at the cell surface after transiting the Golgi apparatus where further oligosaccharide modifications take place. Most PrP^C is transported to the cell surface where it is predominantly located in specialised detergent-resistant microdomains (DRM) known as rafts or caveolae [84]. Findings of transfected-cell studies indicate that wild-type PrP cycles between the cell surface and an early endocytic compartment, via an association with clathrin-

coated pits [85], but also can migrate to late endosomes or lysosomes via non-classic, caveolae-containing endocytic structures, apparently completely bypassing clathrin-related endocytic mechanisms [84]. Such variations in PrP^C endocytic trafficking could indicate the cell type in which exogenous PrP was expressed [86]. Disturbances in normal intracellular trafficking of PrP^C can culminate in its retrograde transport through the Golgi apparatus, with heightened accumulation of PrP^{Sc} in the endoplasmic reticulum. The site of PrP^C→PrP^{Sc} conversion is uncertain. DRM [85] and the endosomal pathway [87] are possible sites for transformation. The endoplasmic reticulum may participate too, especially in familial TSE [88]. DRM could be important sites for initial PrP^{Sc} propagation during intercellular spread, because membrane-associated conversion seems to need insertion of PrP^{Sc} into the cell membrane, possibly by exchange of membrane particles or by GPI-anchor-dependent painting. Cell-free conversion models show the need for physical contiguity when different membrane components harbour PrP^C and PrP^{Sc} [89]. Other aspects of normal PrP^C cell biology may be closely related to pathogenesis. PrP^C has a half-life of only 5 h or so, and up to 10% of newly synthesised protein might be retrogradely transported from the endoplasmic reticulum to the cytosol, where it undergoes degradation [90], although conflicting results have been reported [91]. PrP^C synthesis followed by degradation and clearance of misfolded protein seem to be finely balanced functions, since incorrectly folded conformers are not detected under usual conditions. Manipulation of synthesis and degradation pathways has indicated possible mediators of PrP-related toxic effects and highlighted the complexity of the system. Perturbation of proteasome function results in wild-type PrP accumulation in the cytoplasm, which correlates with toxic effects in vulnerable cell lines and neurodegeneration in transgenic mice, without PrP^{Sc} formation [92]. However, findings of subsequent studies suggest that cytoplasmic accumulation of PrP^C may indicate an absence of translocation of the nascent PrP peptide to the endoplasmic reticulum under conditions of increased PrP expression rather than retrograde transport [91]. Nonetheless, PrP, harbouring mutations associated with familial TSE, accumulates in the endoplasmic reticulum [88] and cytoplasm in the absence of proteasomal inhibition. PrP accumulating in the cytosol forms aggregates, which acquire some properties of PrP^{Sc}, and, once present, persist despite only transient proteasome inhibition [93]. This occurrence suggests that PrP, by contrast with other proteasomaly degraded proteins, could have a unique innate ability to promote and sustain its own conformation change. Importantly, *in vitro* toxic effects did not correlate with appearance of PrP^{Sc} [93]. Data of this type suggest a generic mechanism underlying age-related neurodegenerative diseases, wherein compromise of quality control of endoplasmic reticulum protein synthesis from whatever cause allows harmful soluble conformers to accumulate. Once present, PrP^{Sc} seems to serve as a template for conversion of PrP^C to the abnormal disease-associated form, in a cyclic autocatalytic amplification, needing at least temporary dimerisation of the two isoforms. This template property of PrP^{Sc}, shown in a cell-free conversion assay [94], has replicated *in vitro* many of the species and strain characteristics noted in TSE. The precise *in vivo* mechanism by which PrP^C is converted to PrP^{Sc} remains to be clarified, but a stepwise transformation and acquisition of altered biophysical properties seems most likely, with folding intermediates, including molten globule forms [85, 22].

I.7. *Approaches to TSE therapy*

Anti-prion compounds

Devising approaches to the therapy of TSE, is beset by many difficulties. First of all, the nature of the infectious agent is understood only in outline, and its composition, structure, and mode of replication are still shrouded in mystery. In addition, the mechanism of pathogenesis is not well understood. And finally, because the disease is usually recognized only after onset of severe clinical symptoms, only the preclinical diagnosis of TSE would permit the prevention (or delay) of neurodegeneration.

On the basis of the present knowledge on prion diseases, potential therapeutic strategies are: to stabilize the structure of PrP^C via the formation of a PrP^C-drug complex; to prevent the formation or induce the degradation of amyloid aggregates; to hinder the conversion process or bind to PrP^{Sc}; to destabilize the PrP^{Sc} structure or interfere with the cellular uptake of PrP^C/PrP^{Sc}. Currently, no effective treatment exists, and the development of novel therapeutic strategies against prion diseases has become a priority. Various studies have shown that compounds with properties that interfere with fibrillogenesis may be of therapeutic and prophylactic interest. Thus, different classes of drugs have been described to interfere with the formation of PrP^{Sc} in scrapie–infected cell lines or animal models. All these compounds, including sulphated polyanions [95-97], acridine-based compounds [98, 99], tetrapyrroles (e.g., porphyrines, phtalocyanines) [100], the sulfonated azo-dye Congo red and some of its synthesized derivatives [97, 101, 102], antibiotics (e.g., amphotericin B derivatives) [103], branched polyamines [104, 105] and synthetic peptides [106], have been investigated for their ability to prevent the conformational change PrP^C→PrP^{Sc} or to interfere with the fibril formation of synthetic peptides. However, the therapeutic use of these compounds is restricted by their intrinsic cytotoxicity and pharmacokinetic properties, as well as by their limited ability to pass the blood/brain barrier.

Recently, the anti-prion and the anti-amyloidogenic ability of the tetracycline antibiotics (TCs) were shown by studies performed *in vitro* [28] and *in vivo* [107].

The TCs are a group of structurally-related antibiotics used to treat bacterial infections since the 1940s [108]. They have very similar chemical stuctures with twofold features: a hydrophobic interface derived from a common hydronaphthacene moiety containing four fused rings [109, 110] and an opposite H-bond donor-rich side that undergoes tautomerization depending on pH conditions [111].

The main features required for antibacterial activity are well established [108] and, according to these requirements, the clinically used TCs present various substitutions (**Figure I.7.1**).

These molecules have well characterized pharmacological and pharmacokinetic properties, relatively low toxicity, and some of them are efficient in crossing the blood/brain barrier if an appropriate treatment route is used [112]. Among the others, the anti-prion ability of the antibiotic tetracycline (TC) was shown by *in vitro* models [28] studying the interaction of TC with the PrP aggregates generated by synthetic peptides, homologues to the sequences spanning residues 82-146 and 106-126 of hPrP. TC has been described as able to prevent the PrP peptides aggregation, to reduce the protease resistance and the disruption of PrP peptide aggregates and to abolish the neurotoxicity and astroglial proliferation induced by PrP peptides. In an *in*

vivo study [107], TC significantly delayed the onset of clinical signs of disease and prolonged survival into Syrian hamsters infected with scrapie-infected brain homogenates.

Moreover, NMR experiments on the 106-126 fragment of hPrP suggest that the hydrophobic interface of TC can interact with several residues in the N-terminal part of hPrP, namely, Ala 117- 119, Val 121-122, Leu 125 [113]. These residues lie within the well known 106-126 region, which when isolated from the context of the entire protein, has a high propensity to adopt β-sheet secondary structure and to form amyloid fibrils [28]. Further, as already discussed, the 106-126 peptide is also neurotoxic and induces glial cell activation *in vitro* [28, 114-117]. All these properties are strongly suggestive of a heavy involvement of this region in the protein pathological mechanisms. On the ground of the earlier findings, the effects of TC on prion diseases have been ascribed to its interaction with 106-126 hPrP fragment.
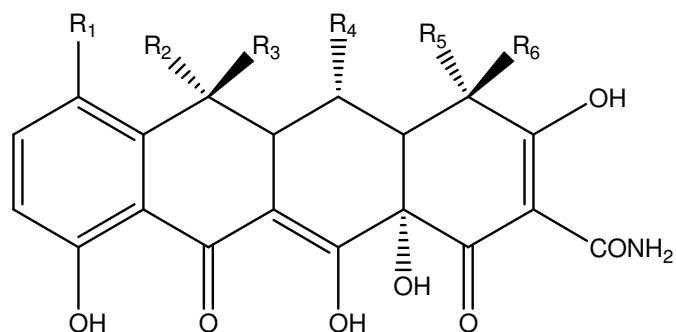
Compound	R_1	R_2	R_3	R_4	R_5	R_6
Tetracycline	H	CH_3	OH	H	$N(CH_3)_2$	H
Chlortetracycline	Cl	CH_3	OH	H	$N(CH_3)_2$	H
Demeclocycline	Cl	H	OH	H	$N(CH_3)_2$	H
Doxycycline	H	CH_3	H	OH	$N(CH_3)_2$	H
4-Epichlortetracycline	Cl	CH_3	OH	H	H	$N(CH_3)_2$
4-Epioxytetracycline	H	CH_3	OH	OH	H	$N(CH_3)_2$
4-Epitetracycline	H	CH_3	OH	H	H	$N(CH_3)_2$
Meclocycline	Cl	$=CH_2$	-	OH	$N(CH_3)_2$	H
Methacycline	H	$=CH_2$	-	OH	$N(CH_3)_2$	H
Minocycline	$N(CH_3)_2$	H	H	H	$N(CH_3)_2$	H
Oxytetracycline	H	CH_3	OH	OH	$N(CH_3)_2$	H

**Figure I.7.1** Chemical structure of tetracycline and its analogues.

Immune intervention

Given the few possibilities for therapeutic and/or prophylactic intervention to date, new therapeutic strategies are a major focus of research to identify new compounds able to block or prevent prion diseases. A promising therapy lies in the potential of active or passive immunization using anti-PrP antibodies. Although active immunization strategies are confronted with a problem of self-tolerance [118], polyclonal anti-PrP auto-antibodies can be induced with dimeric PrP in wild-type mice and interfere efficiently with PrP^{Sc} propagation in prion-infected cells [119]. In addition, vaccination with recombinant mouse prion protein delays the onset of prion disease in mice [120]. Another vaccination approach by passive immunization is also promising. Indeed, anti-PrP antibodies were not only shown to inhibit formation of protease-resistant PrP in a cell-free system [121] but were also shown to prevent scrapie infection of susceptible mouse neuroblastoma N2a cells [122] and inhibit prion replication in infected cells [123-125]. In addition, transgenic expression of the anti-PrP monoclonal antibody 6H4 in mice expressing PrP blocks pathogenesis of prion introduced by intraperitoneal inoculation [126]. The mechanism by which anti-PrP antibodies interfere with PrP^{Sc} replication is not clear, but the main hypothesis presented so far involves either a perturbation of PrP^{C} trafficking and degradation [124] or a disruption of the interaction between PrP^{C} and PrP^{Sc} [123] by the antibodies.

However, despite the abundance of data now available on anti-PrP monoclonal antibodies, their application in TSE therapy or diagnosis is limited by the poor knowledge on the infectious and pathological mechanisms of prion diseases and the exact roles of PrP^{C} and PrP^{Sc} in the brain dysfunctions caused by TSE. Therefore, progress in therapy is tightly linked to a better understanding of the basic science of TSE. A first step in such a understanding would be to identify and structurally define epitopes of antibodies that cross-react with PrP^{C} and PrP^{Sc}. This would provide structural information directly derived from the infectious agent and help understand the mechanisms of PrP^{Sc} formation and spreading in infected organisms.

Eghiaian and co-authors [127] determined the X-ray structures of the C-terminal domain of three scrapie-susceptible ovine PrP variants. They have cocrystalized this domain with a Fab fragment that cross-react with PrP^{C} and PrP^{Sc} and reported the 2.5-Å-resolution crystal structure of these complexes (**Figure I.7.2**). The ovPrP–Fab structure defines the epitope of the antibody that basically consists of the last two turns of ovPrP helix 2, structural invariant in the human domain. This epitope is conserved in PrP^{C} and PrP^{Sc} from brains of infected animals, which constitutes structural information on the pathological prion conformer directly derived from an infectious sample.

This characterization of the interaction of OvPrP^{C} and infectious OvPrP^{Sc} with an antibody have provided structural information on the PrP$^{C} \rightarrow$ PrP^{Sc} conversion; the availability of additional antibodies, Fab fragments and molecules that bind to PrP^{C} and/or PrP^{Sc} will allow further structural characterization of this transformation.
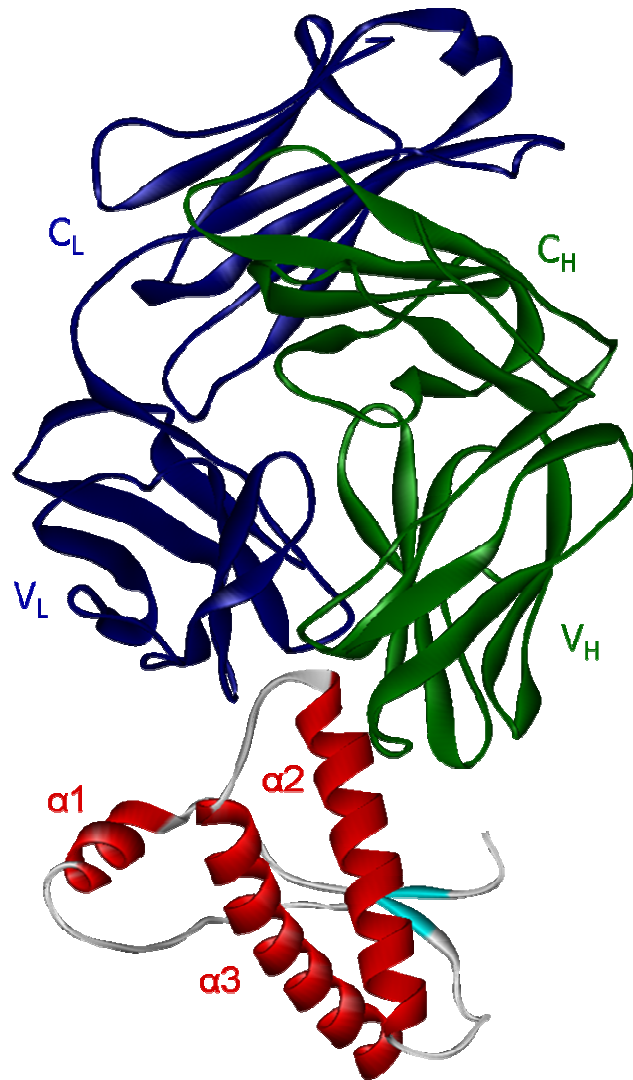
Figure I.7.2 Overview of the OvPrP–Fab complex. Fab heavy and light chains are shown in green and blue, respectively [127].

II.   AIM OF THESIS

A computational analysis illustrates that native PrP exhibits large regions of conformational ambivalence and suggest that it is only a marginally stable protein [46]. Other simulations also indicate that the conformational variability of the entire prion protein sequence is unusually high compared with other proteins of similar length [128]. Moreover, the tendency to increase the β-structure content is very likely an intrinsic characteristic of the prion protein fold, irrespective of thermodynamic or structural conditions [129]. In the C-globular domain, unusually low α-helical and β-sheet propensities feature the segment 173-195, corresponding to α-helix 2, in spite of the fact that this segment retains a helical conformation in the whole protein. In addition, the unusually high density of disease-promoting mutations in α-helix 2 also points to the particular importance of this helix for conformational transition of PrP. More specifically, it seems reasonable that a single amino acid replacement in the vicinity of the α-helix 2 may significantly affect the organization of the entire α2-α3 helical part, enhancing the propension of this region for the β-conformation and facilitating structural rearrangements.

Further support to this hypothesis comes from the finding that the hPrP^C mutants T183A and F198S, which are associated to inherited prion diseases, severely affect folding and maturation of PrP^C in the secretory pathway of neuronal cells *in vitro*, adopting misfolded and partially protease-resistant conformations [130]. These pathogenic mutations interfere with folding and attachment of the GPI anchor [130]. Indeed, based on a refined NMR structure, it was predicted that they would specifically destabilize the PrP C-terminal globular domain, because they involve key interactions in the hydrophobic core [50]. The resulting three-dimensional arrangement could account for the defect in maturation and the efficiency of the GPI anchor attachment. The hypothesis that the segment comprising the C-*terminus* of α-helix 2 and the adjacent loop may be partially unfolded and represent a potential oligomerization site is also supported by crystallographic data [21]. Furthermore, the α-helix 2 fragment, also depending on the glycosylation state and the presence of metals [13, 47, 131] can be toxic to neuronal cells and strongly fibrillogenic, adding a further clue to the working hypothesis that it is involved in the protein aggregation process and in the toxicity associated to the scrapie variant.

Following the thread of these arguments, we have investigated the structural behaviour of the α-helix 2 domain designing peptides corresponding to the α-helix 2 of hPrP (listed in **Table II.1(A)**) which were characterized in aqueous buffer, in structuring media, in presence of ions and assayed for their *in vitro* neurotoxicity.

The peptides reported in **Table II.1(A)**, obtained in the N- and C-*termini* blocked form by solid phase peptide synthesis (SPPS), were chosen as representative contributors to the conformational landscape of the human prion protein helix 2 domain. The first two peptides, **PrP[173-195]** and **PrP[173-195]D178N**, are related to the full length α-helical 2 region, and represent the wild type sequence and the D178N mutant, which is the most important mutation occurring in Creutzfeldt-Jakob Disease (CJD), respectively [132]. In addition, the shorter **PrP[180-195]** peptide and its complementary segment **PrP[173-179]** were also studied. The investigation into the PrP[180-195] peptide is justified by two reasons. First, it includes the threonine-rich region, which is characterized by strong β-sheet forming propensity [133]. Second, the absence of cysteine in the primary structure allowed us to exclude effects linked

to the reactivity of the thiol moiety. Moreover, the **PrP[180-195]H187A** analogue was chosen to investigate the role of the histidine 187 in the structural arrangement of the 180-195 fragment and the conformational dependence of this prion segment on pH change with respect to the H187 protonation.

In particular,

▪ we have undertaken a comparative CD, NMR and cellular toxicity study on peptides corresponding to the full length α-helix 2 of hPrP (**PrP[173-195]**), to the shorter C-terminal region (**PrP[180-195]**) and to the CJD-associated mutant (**PrP[173-195]D178N**), in order to shed further light on the structural properties of this intriguing protein domain and on the influence that a disease-associated mutation can have on its relative stability and toxicity;

▪ we have showed how ionic strength and pH influence the conformation of the hPrP α-helix 2 fragment **PrP[180-195]** and its analogue **PrP[180-195]H187A** according to a Hofmeister-series-type dependence [134, 135];

▪ we have performed CD and NMR titrations of **PrP[173-195]** and **PrP[173-195]D178N** in presence of metal cations.

Table II.1 Code and sequence of synthetic peptides

	Code	Peptide sequence
A	PrP[173-195]	Ac-NNFVHDCVNITIKQHTVTTTTKG-NH$_2$
	PrP[173-195]D178N	Ac-NNFVHNCV**N**ITIKQHTVTTTTKG-NH$_2$
	PrP[180-195]	Ac-VNITIKQHTVTTTTKG-NH$_2$
	PrP[180-195]H187A	Ac-VNITIKQ**A**TVTTTTKG-NH$_2$
	PrP[173-179]	Ac-NNFVHDC-NH$_2$
B	Fluo-PrP[173-195]	Fluo-βANNFVHDC(Met)VNITIKQHTVTTTTKG-NH$_2$
	Fluo-PrP[180-195]	Fluo-βAVNITIKQHTVTTTTKG-NH$_2$
	Fluo-PrP[106-126]	Fluo-βAKTNMKHMAGAAAAGAVVGGLG-NH$_2$
	Fluo-βA[25-35]	Fluo-βAGSNKGAIIGLM-NH$_2$

In a further set of experiments, three PrP fragments and another representative amyloidogenic peptide (see **Table II.1(B)**) were functionalized with fluorescein in order to investigate, by steady-state fluorimetry, their affinity for potential PrP-binding molecules.

In detail,

▪ we have performed an integrated spectroscopic and computational study of the interaction between **tetracycline** (TC) and these fluorescein derivatized α-helix 2 petides to check the reliability of the hypothesis that TC can interact with both the N-terminal 117-125 segment, as already demonstrated [113], and with the Thr-rich helix 2 portion, acting as a joining moiety between two structurally unstable PrP regions. It has intriguingly been hypothisezed that, within the context of the prion protein tridimensional structure, the α-helix 2 region is spatially adjacent to the 106-126 fragment and could be packed with this part. To increase the meaningfulness of our results, the same analysis has been applied to the study of PrP[106-126] and to another representative amyloidogenic peptide, βA[25-35], that is derived from the βA[1-42] [136].

▪ we have identified the Fab[30-35] and Fab[46-53] fragments which are able to form hydrogen bonds with the α-helix 2 C-terminal end in the Fab-ovPrP X-ray structure (**Figure I.7.2**) [127] and designed peptide constructs putatively suitable to model the ovPrP-Fab interaction. Finally, we have investigated the interaction of the helix 2-derived peptide with these compounds by steady-state fluorimetry.

III. RESULTS

III.1. *Comparative CD, NMR and cellular toxicity study on PrP[173-195], its D178N analogue and the shorter PrP[180-195] segment*

CD

The solution behaviour of the three hPrP peptides, **PrP[173-195]**, **PrP[173-195]D178N** and **PrP[180-195]**, was assayed in aqueous buffer at neutral pH and in presence of SDS and TFE.

As shown in **Figure III.1.1**, the shape of CD spectra at pH 7.0 gradually changes in going from PrP[173-195] to PrP[180-195]. In fact, the spectrum of the wild-type peptide is dominated by disordered structure, as suggested by the minimum around 198 nm. Similarly, disordered structure is still predominant in the D178N mutant, but the shoulder at about 220 nm suggests an increase of β-type organization as compared to the wild-type peptide. Finally, the main contribution to the spectrum of PrP[180-195] is β-type. Additional experiments performed on **PrP[173-179]** dissolved in water showed a random organization (**Figure III.1.2**). Thus, it seems reasonable to infer that, in the presence of this segment, peptides derived from the full length α-helix 2 (PrP[173-195] and PrP[173-195]D178N) are not able to display spectral characteristics that are otherwise prominent in PrP[180-195].
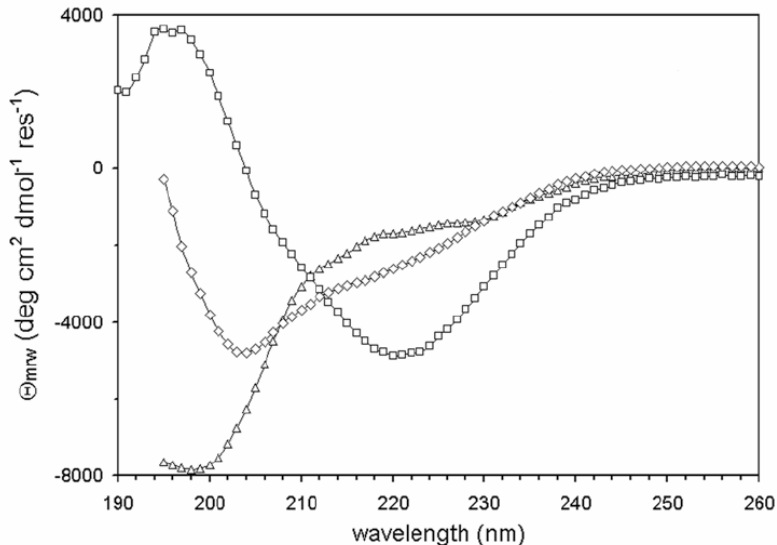
Figure III.1.1 CD spectra at neutral pH. (-△-) PrP[173-195]. (-◇-) PrP[173-195]D178N. (-□-) PrP[180-195].
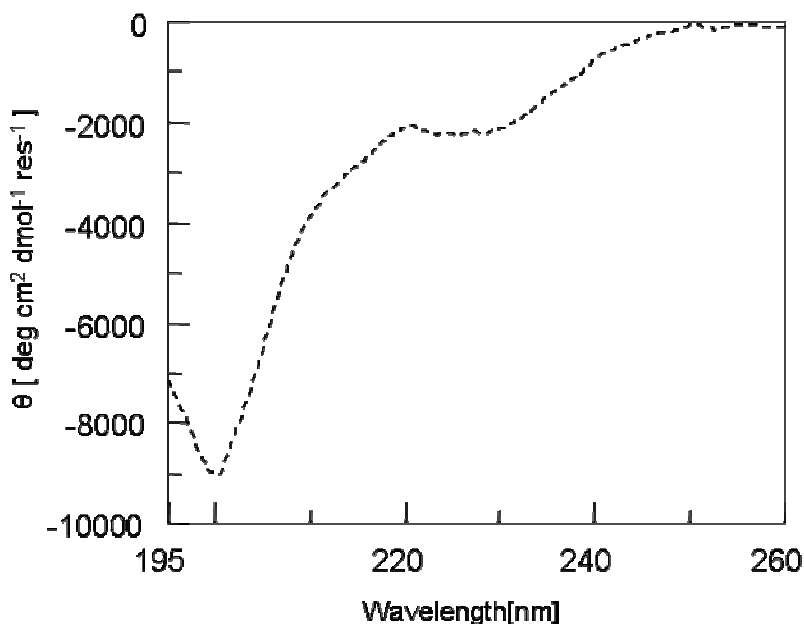
Figure III.1.2 CD spectra at neutral pH of PrP[173-179].

The first set of experiments was carried out using **SDS** as the structuring agent, based on the notion that peptides may be induced into a β-sheet structure at sub-micellar concentrations of this substance [137-139]. Actually, little is known about the nature of this solvent system, which has been described as a mimetic of protein interiors. It is presumed that the non-polar tails provide a template for the hydrophobic domains of peptides, mimicking the environment found in the interior of the parent protein, whereas the sulfate moiety keeps the β-structured peptide in solution.

The addition of SDS modified the shape of the spectra of the wild-type and the mutant peptides into that typical of a β-type profile, with positive and negative bands near 195-200 nm and 216-220 nm, respectively [140]. SDS-induced transitions, as monitored by the signal intensity at 200 nm, are shown in **Figure III.1.3**. It can be appreciated that intensities for PrP[173-195] and PrP[173-195]D178N increase to final positive values that reflect the different amounts of β-type structure. It is worth noting that this occurs in a very narrow range of SDS concentration for PrP[173-195]D178N.

A similar set of experiments was carried out monitoring **TFE**-induced modifications of the far UV CD spectrum of PrP[173-195], PrP[173-195]D178N and PrP[180-195]. TFE is a hydrophilic and hydrogen-bonding solvent that appears to stabilize peptides in the secondary structure for which a given sequence has propensity [139]. It belongs to a group of organic substances such as methanol, ethanol, acetonitrile, 1,1,1,3,3,3-hexafluoroisopropanol at low pH, octanol mixed with other alcoholic solvents, and SDS at high concentrations, which are known to induce α-helical organization in peptides [141-143]. TFE addition caused the spectra of wild-type and mutant peptide to change into an alpha-helical profile, although to a different extent, with pronounced minima at 208 and 222 nm and a strong positive maximum at 191-193 nm [140], whereas PrP[180-195] underwent less pronounced spectral modifications, with still predominant β-type features. TFE-induced transitions, as monitored by the signal intensity at 222 nm, are shown in **Figure III.1.4**.

30
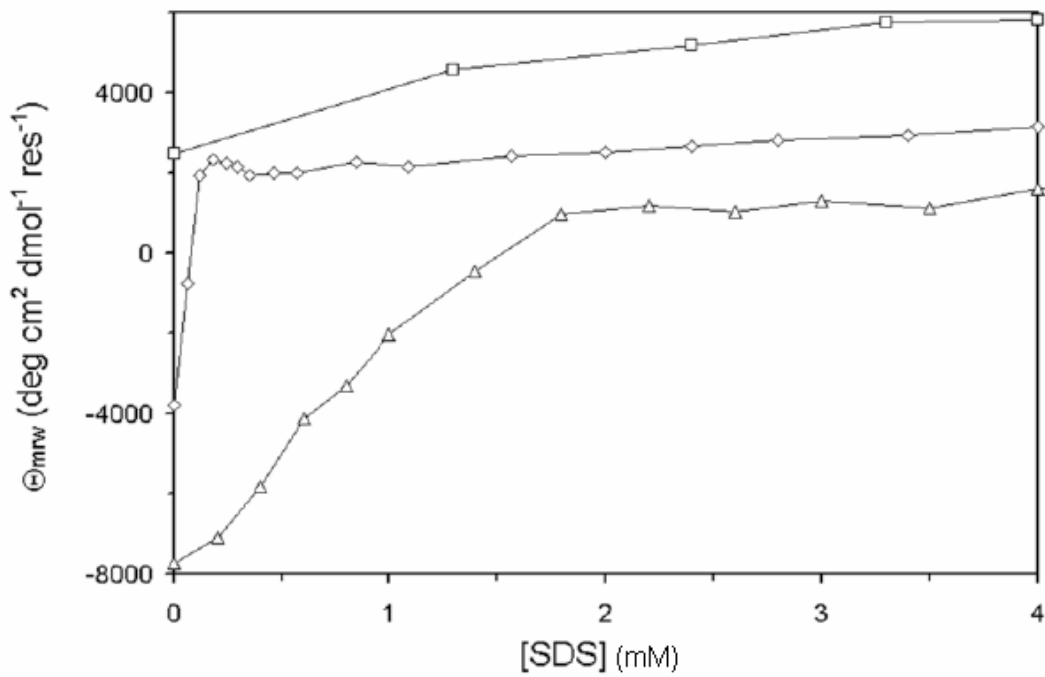
Figure III.1.3 SDS titrations. (-△-) PrP[173-195]. (-◇-) PrP[173-195]D178N. (-□-) PrP[180-195]. The intensity was monitored at 200 nm.
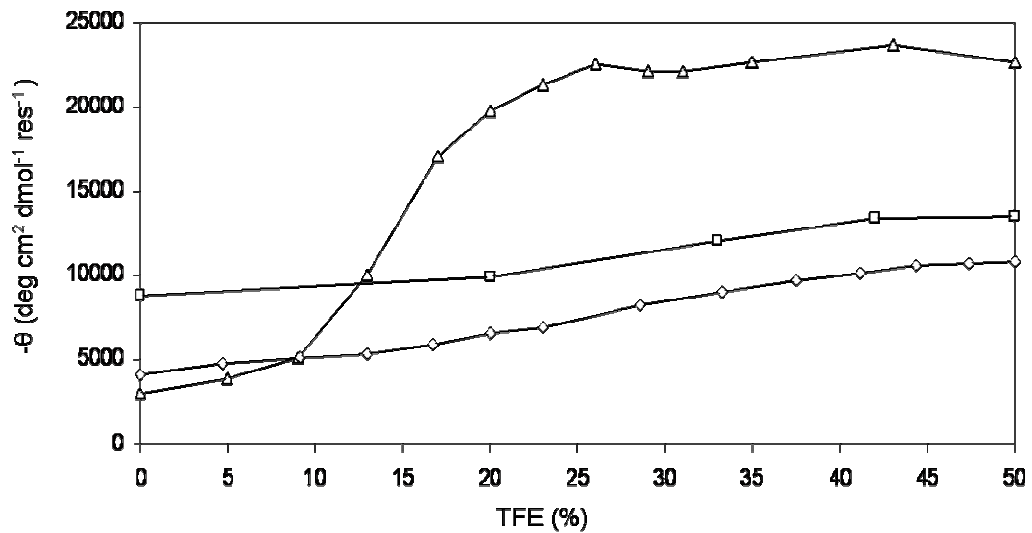

Figure III.1.4 TFE titrations. Symbols used for peptides are the same as reported in Figure III.1.3. The intensity was monitored at 222 nm.

The CD analysis has shown that these peptide fragments exhibit random or β-type organization in aqueous solution. This is likely to be ascribed to absence of mutual interactions with the other helical segments as well as of the interhelical disulphide bridge, which contribute to the integrity of the whole C-terminal globular domain in PrP[C]. To avoid experimental ambiguity due to the fact that the parent segment in the native protein assumes helical conformation, we have mimicked native-like conditions using the α-inducer TFE to force the peptides to assume a conformation as close as possible to that observed in the cellular prion protein.

PrP[173-195]. The bar diagram of diagnostic NOE effects, as derived from the NOESY spectrum in TFE at 300 ms mixing time, is reported in **Figure III.1.5** Any ambiguity caused by the signals of the four consecutive Thr residues was overcome by NOESY and $^1H^{15}N$-HSQC experiments. $^3J_{NH-CH}$ coupling constants assumed the very small values typical of α-helix. Weak $d_{\alpha N(i,i+3)}$ medium range, strong $d_{NN(i,i+1)}$ sequential as well as strong $d_{\alpha\beta(i,i+3)}$ medium range effects for almost all residues are consistent with α-helical conformation. The 175-193 bundle of the best thirty DYANA structures, as obtained by best fitting of the backbone (RMSD = 1.13 ± 0.50 Å), is also drawn in this **Figure III.1.5**.
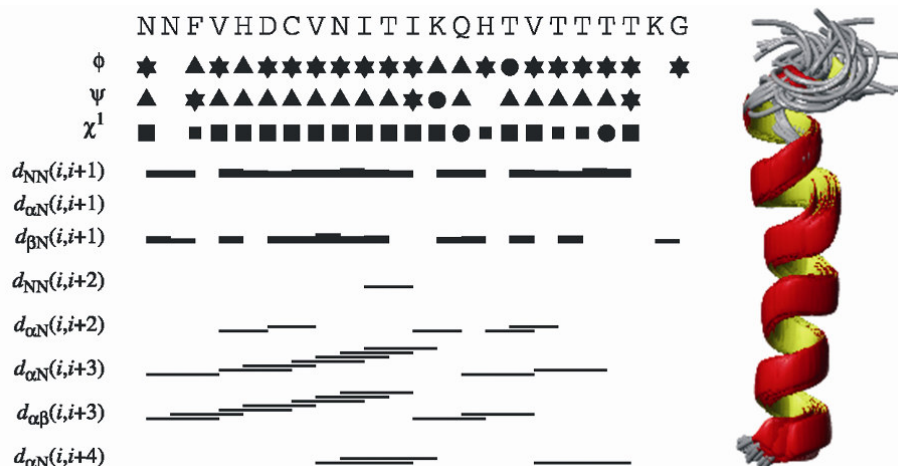
Figure III.1.5 NOE effects and DYANA backbone fitting of **PrP[173-195]**. Connectivities were derived from NOESY spectra at 300 ms mixing time. Backbone NOE connectivities are indicated by horizontal lines between residues, with thickness indicating their relative magnitude. The first three lines below the amino acid sequence represent torsion angle restraints for the backbone torsion angles Φ and Ψ, and for the side-chain torsion angle X[1]. For Φ and Ψ, a ✱ symbol encloses secondary-structure-type conformation; a ▲ symbol indicates compatibility with an ideal α-helix; and a ● symbol marks a restraint that excludes the torsion angle values of these regular secondary structure elements. Filled squares of different sizes depict torsion angle restraints for X[1], depending on the number of allowed staggered rotamer positions. The bundle of the region 175-193 of the best 30 DYANA structures was obtained by best fitting of the backbone (RMSD = 1.13 ± 0.50 Å).

PrP[173-195]D178N. TOCSY experiments on the PrP[173-195]D178N analogue suggested that the replacement of Asp178 with Asn doesn't substantially affect the chemical shifts. Only 0.2 ppm protonic chemical shifts of HN and the CHβ of Asn178 as compared to Asp178 were recorded by superimposition of the two TOCSY experiments. Careful analysis of the NOESY spectrum highlighted effects typical of secondary structure essentially in the N-terminal region, even though the intensity of the $d_{NN(i,i+1)}$ ones was reduced. The $d_{\alpha N(i,i+1)}$ between the H-C$^\alpha$ and the HN-proton of Gln186 and His187, respectively, suggested the local presence of an extended conformation in the modified sequence, strongly perturbing the central core of the wild type helix motif. **Figure III.1.6** shows all diagnostic NOE effects and the superimposition of the region 175-193 of the best thirty structures obtained by DYANA calculations. However, the value of the backbone RMSD of 2.07±0.61 Å suggests the presence of several quite similar conformations. We argue that the negative charge of Asp178 plays a key role in forcing the entire 173-195 fragment to assume a full helical conformation, which would not be otherwise allowed.
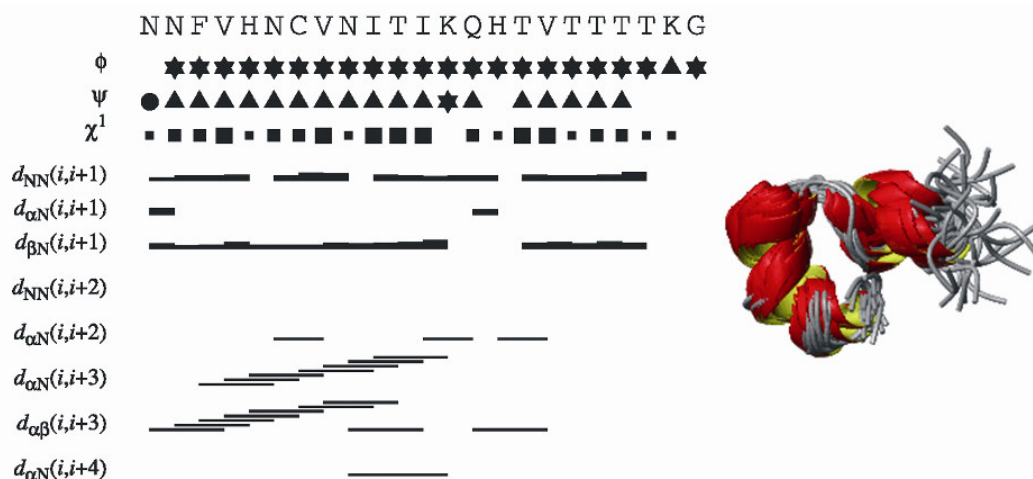
Figure III.1.6 NOE effects and DYANA backbone fitting of **PrP[173-195]D178N**. Connectivities were derived from NOESY spectra at 300 ms mixing time. Symbols used for connectivities are the same as reported in Figure III.1.5. The bundle of the region 175-193 of the best 30 DYANA structures was obtained by best fitting of the backbone (RMSD = 2.07 ± 0.61 Å).

PrP[180-195]. Figure III.1.7 shows the bar diagram of sequential and medium range NOE connectivities, as derived from the NOESY spectrum in TFE at 300 ms mixing time. Strong $d_{NN(i,i+1)}$ sequential and $d_{\alpha\beta(i,i+3)}$ medium range effects were typical of α-helical structure. **Figure III.1.7** also shows the superimposition of the region 182-191 of the best thirty DYANA structures with a backbone RMSD of 0.45 ± 0.25 Å.

Figure III.1.7 NOE effects and DYANA backbone fitting of **PrP[180-195]**. Connectivities were derived from NOESY spectra at 300 ms mixing time. Symbols used for connectivities are the same as reported in Figure III.1.5, but ▼ are used for torsion angles compatible with β-strand. The bundle of the region 182-191 of the best 30 DYANA structures was obtained by best fitting of the backbone (RMSD = 0.45 ± 0.25 Å).

Test of neurotoxicity

Neurotoxicity of the α-helix 2 derived peptides was assayed on B104 neuroblastoma cells derived from rat central nervous system [144]. The cells were cultured in Dulbecco's modified Eagle's minimal essential medium and exposed to increasing peptide concentration. Percent of cell survival was assessed by comparison with untreated cultures used as control. The FC_{50} µM value, defined as the 50% fatal concentration, was estimated after 48 h exposure by testing peptides over a broad range of concentrations from 0 to 240 µM. FC_{50} values were determined by Hill plot analysis. In **Table III.1.1** are summarized the FC_{50} values of the synthetic PrP fragments.

Table III.1.1 Neurotoxicity of α-helix 2 derived peptides

Peptide	FC_{50} value (µM)
PrP[173-195]	68
PrP[173-195]D178N	12
PrP[180-195]	11
PrP[173-179]	430

III.2. *Effect of salts and pH on PrP[180-195] and its H187A analogue*

As shown in **Figure III.2.1(A)**, in the absence of any added salt, the shape of the circular dichroism (CD) spectra of peptides **PrP[180-195]** and **PrP[180-195]H187A** was suggestive of an unordered structure. Neither the addition of NaCl or $NaClO_4$ nor the addition of small amounts of HCl or NaOH to adjust the pH caused any substantial modification. Spectra in sodium phosphate solution at pH 4.5, in which $H_2PO_4^-$ is the most populated anion, were also reminiscent of disordered conformation. By contrast, on addition of either sodium phosphate or sulfate at pH 7.0, where bivalent HPO_4^{2-} or SO_4^{2-} anions are dominant, the spectrum of PrP[180–195] was characterized by a pronounced negative maximum around 220 nm and a positive maximum around 200 nm, which are characteristic of β-sheet conformation (dashed lines in **Figure III.2.1(B)** and **(C)**, respectively), whereas PrP[180-195]H187A exhibited spectral features typical of the α-helix conformation, with a positive maximum around 195 nm and two negative maxima around 208 nm and 222 nm (bold lines in **Figure III.2.1(B)** and **(C)**, respectively). Finally, spectra of PrP[180-195]H187A and PrP[180-195] were modified to those typical of the β-sheet and disordered structure, respectively, by acidifying the Na_2SO_4 solution to pH 4.5 (**Figure III.2.1(D)**).
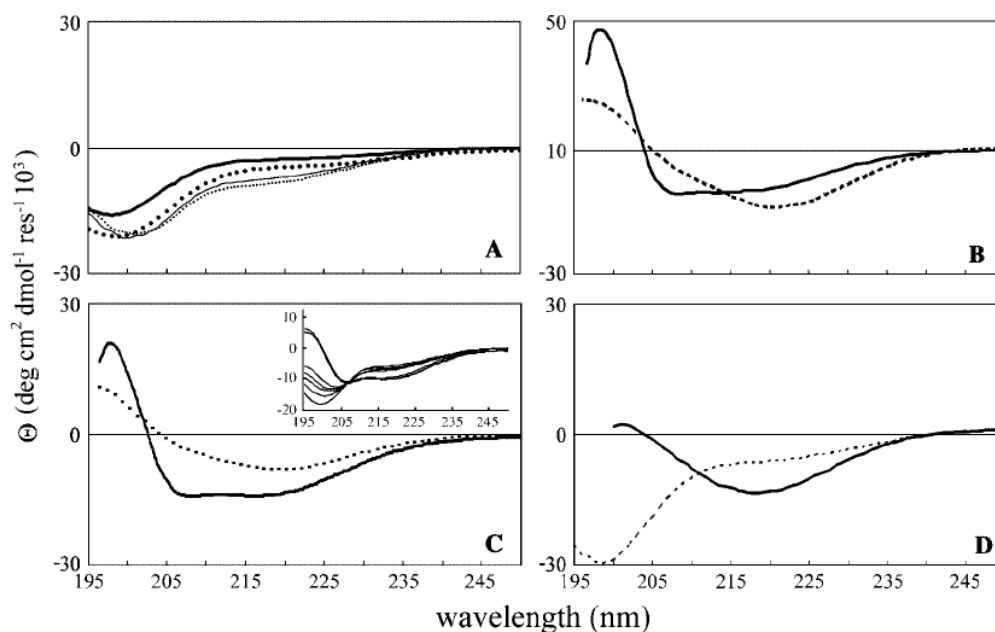
Figure III.2.1 Effect of salts on circular dichroism (CD) spectra of **PrP[180–195]** and **PrP[180-195]H187A.**
(A) PrP[180-195]H187A dissolved in H_2O (bold line), 100 mM NaCl (thin line), 100 mM $NaClO_4$ (dotted line), and 30 mM NaH_2PO_4 (dashed line). CD spectra of PrP[180–195] under the same conditions (not shown) were superimposable on those of PrP[180-195]H187A. **(B)** PrP[180–195] (dashed line) and PrP[180-195]H187A (bold line) dissolved in 30 mM NaH_2PO_4/Na_2HPO_4 (pH 7.0). **(C)** PrP[180–195] (dashed line) and PrP[180-195]H187A (bold line) dissolved in 50 mM Na_2SO_4 (pH 7.0); the inset shows spectra of PrP[180-195]H187A as obtained by titration with Na_2SO_4 up to 50 mM (pH 7.0). **(D)** PrP[180–195] (dashed line) and PrP[180-195]H187A (bold line) dissolved in 50 mM Na_2SO_4 (pH 4.5).

Table III.2.1 Effect of anions and pH on peptide conformation

Medium	C (mM)	pH	PrP[180-195]	PrP[180-195]H187A
water		4.5÷7.0		
Cl$^-$	0÷100	4.5÷7.0	disordered	
ClO$_4^-$	0÷100	4.5÷7.0		
H$_2$PO$_4^-$	0÷50	4.5		
HPO$_4^{2-}$/ H$_2$PO$_4^-$	0÷50	7.0	β-strand	α-helix
SO$_4^{2-}$	0÷50	7.0	β-strand	α-helix
SO$_4^{2-}$	0÷50	4.5	disordered	β-strand

Table III.2.1 summarizes the above described CD effects. It is worth noting that the thermodynamic processing of these salt-induced structural changes show features typical of most structural transitions and are therefore suited to be treated by some thermodynamic model that hinges on the structuring effect of the anion activity. For example, the isodichroic point that can be noticed around 207 nm in the spectra of PrP[180-195]H187A at neutral pH (see inset of **Figure III.2.1(C)**) suggests a two-state equilibrium between the unstructured peptide and the structured peptide, whose onset is accompanied by a sharp ellipticity change around 35–40 mM of salt (**Figure III.2.2**).
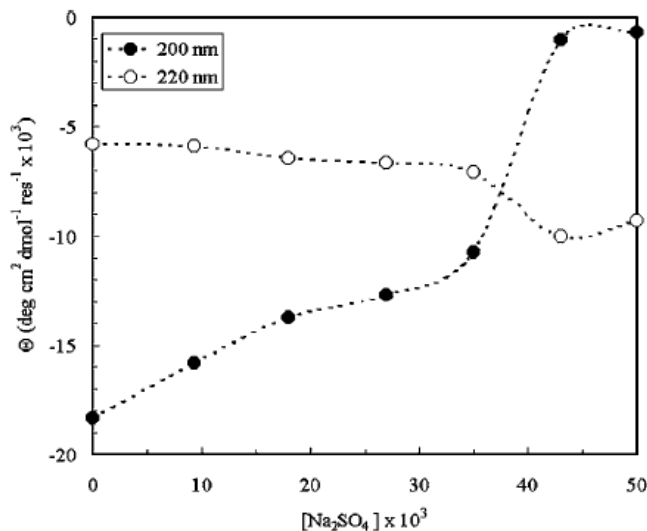
Figure III.2.2 Effect of Na$_2$SO$_4$ on the ellipticity values of **PrP[180-195]H187A** at pH 7.0.

Notably, PrP[180-195]H187A in Na_2SO_4 at acidic pH assumes a β-sheet-like conformation, which is irreversibly destroyed by heating, with an apparent midpoint temperature (Tm) of about 47 °C. Concentration-dependent experiments performed in the 6–300 µM range show that the peptide behaviour on salt addition is more complex than that described above. As can be appreciated from **Figure III.2.3**, the observed ellipticity shows a hyperbolic trend in 50 mM Na_2SO_4, whereas it is expected to depend linearly on the peptide concentration, according to the Lambert Beer's law. Such a deviation from linearity can be interpreted in terms of structural rearrangements that lead to self-association.
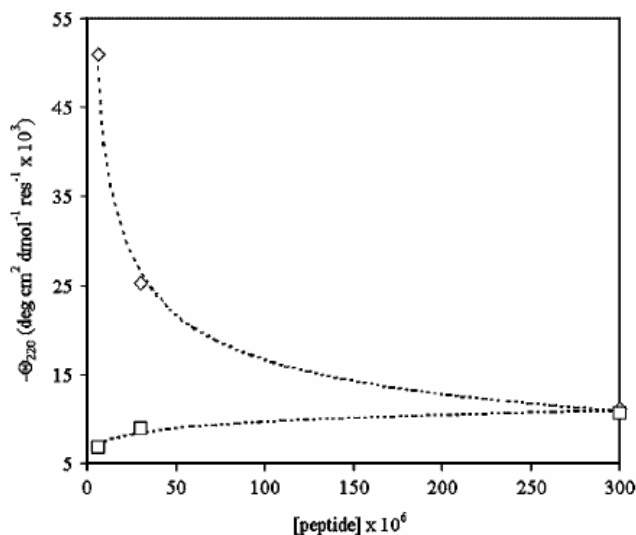
Figure III.2.3 Peptide self-association at pH 7.0. (◊) **PrP[180-195]** and (□) **PrP[180-195]H187A**. Concentration-dependent experiments were performed at 20 °C in 50 mM Na_2SO_4 maintaining the number of molecules in the optical path constant equimolecular condition. This was achieved by keeping the product of the protein concentration and optical path length constant.

Furthermore, pseudo first order rate constants show an anomalous increase with the peptide concentration. This suggests a kinetic behaviour different from the first order expected for a simple conformational rearrangement involving monomers (**Figure III.2.4**). We infer therefore that both peptides self-associate. At least in the case of PrP[180-195]H187A it is apparent that this follows secondary structure rearrangements because it occurs in the presence of 50 mM Na_2SO_4, which is higher than the salt concentration at which structural modifications were observed (**Figure III.2.2**). In general, it cannot be excluded that structural reorganization and self-association are to some extent concomitant.
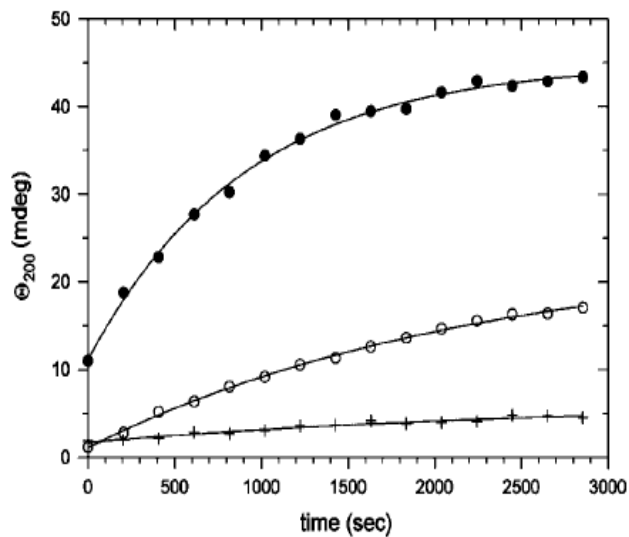
Figure III.2.4 Time-dependence of **PrP[180-195]H187A** reorganization at pH 7.0. Experiments were performed at 20 °C on 2.5 μM (+), 5.0 μM (○), and 10 μM (●) peptide dissolved in 50 mM Na_2SO_4, monitoring the dichroic signal at 200 nm. Rate constants were calculated by best fitting to a pseudo first order kinetic equation, which gave 3.8×10^{-4}, 4.5×10^{-4}, and 11.0×10^{-4} s for 2.5, 5.0, and 10×10^{-6} M peptide, respectively.

III.3. *NMR and CD titration of PrP[173-195] and its D178N analogue with metal cations*

As shown in **Figure III.3.1**, the far UV CD spectrum of **PrP[173-195]** in TFE solution shows features typical of α-helical conformation. The small spectral alterations that can be noticed on metal (Zn(II) and Cu(II)) titration are likely caused by modification of the dielectric properties of the solvent subsequent to salt addition and do not suggest any specific binding interaction between the peptide and the metal cation.

Figure III.3.2 depicts the amidic zone of the 1D spectra after Zn(II) addition. The addition of just one metal ion aliquot was sufficient to cause alteration of the imidazolic proton resonances. Concentration dependent peptide aggregation on further metal addition caused progressive broadening of all resonances, even causing them to disappear. Overall, this suggests non-specific metal-peptide interaction, a conclusion that is supported by the unchanged shape of CD spectra, where aggregation did not occur because of the lower peptide concentration.

The lower intensity of the far UV CD spectrum of **PrP[173-195]D178N**, run in the same condition as that of hPrP[173-195] (**Figure III.3.3**), suggests that the mutant peptide is less helical as compared to the wild type peptide. However, the conclusion that no specific binding interaction with the metal cation can be detected still holds for this peptide. The amidic zone of 1D NMR spectra of PrP[173-195]D178N in the presence of various amounts of Zn(II) is reported in **Figure III.3.4**. The protonic resonances of the His side chains exhibit the same behaviour as that observed for the wild type peptide fragment, but the progressive broadening of side-chain resonances is less relevant. As already observed for PrP[173-195], these data are not suggestive of well defined ion-peptide complex formation.
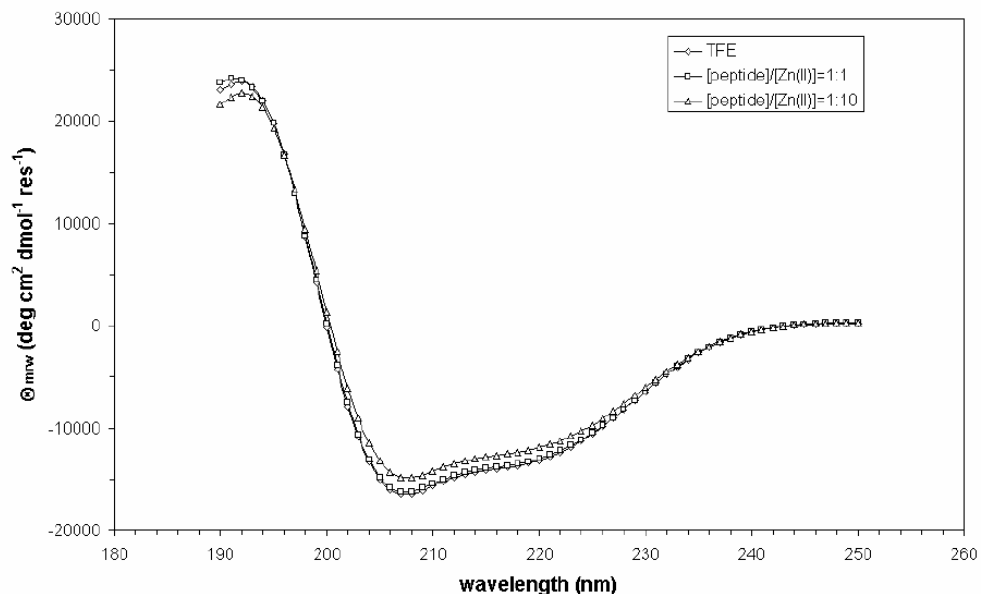
Figure III.3.1 Far UV CD spectra of **PrP[173-195]** dissolved in TFE before and after addition of $ZnCl_2$ solution. A similar spectral behaviour was observed after titration with $CuCl_2$ solution (spectra not shown).
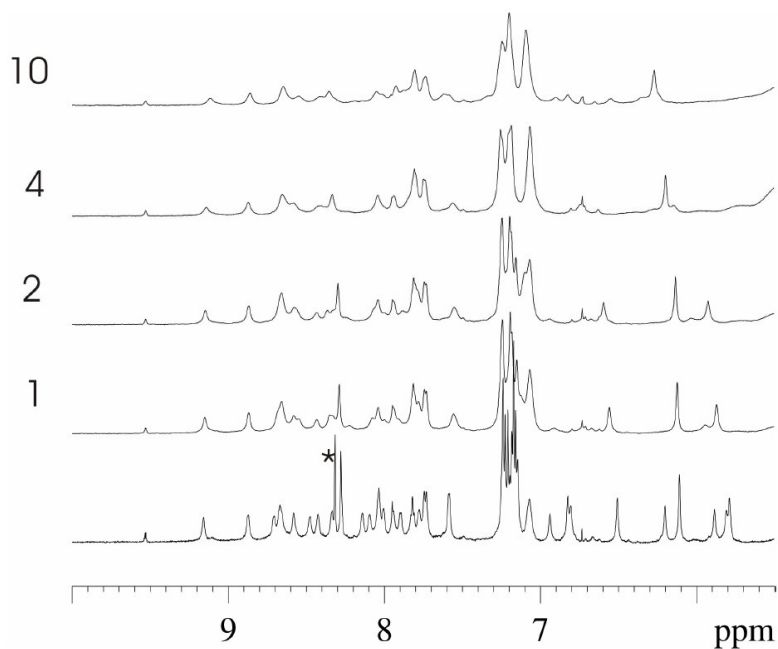
Figure III.3.2 1D NMR spectra of **PrP[173-195]** dissolved in TFE_{d2} before and after addition of $ZnCl_2$ solution. Labels 1, 2, 4 and 10 indicate the total volume (μL) of 0.5 M $ZnCl_2$ solution added to 500 μL of 0.6 mM peptide solution, corresponding to Zn(II)/peptide molar ratios of 1.7, 3.3, 6.7 and 16.7, respectively. Imidazolic proton resonances of His residues in metal absence are marked by an asterisk.

41
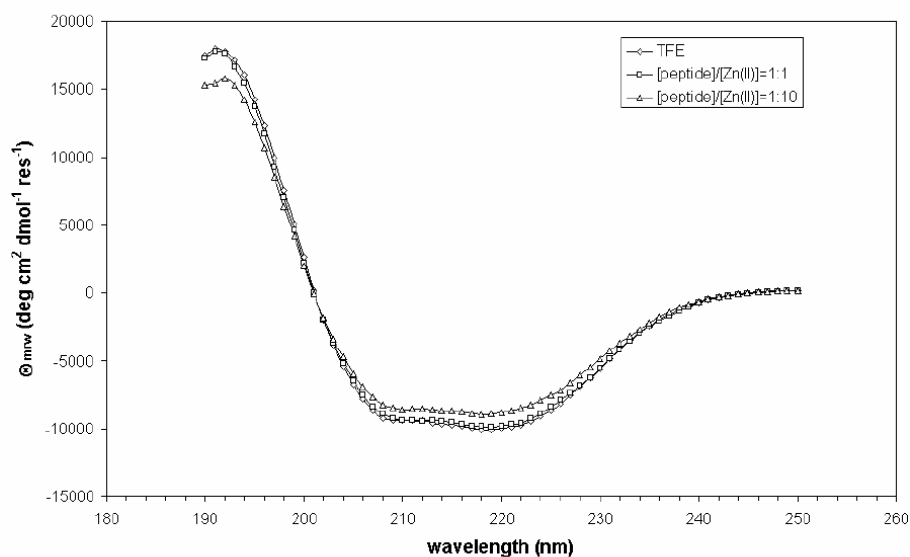
Figure III.3.3 Far UV CD spectra of **PrP[173-195]D178N** dissolved in TFE before and after addition of $ZnCl_2$ solution. A similar spectral behaviour was observed after titration with $CuCl_2$ solution (spectra not shown).
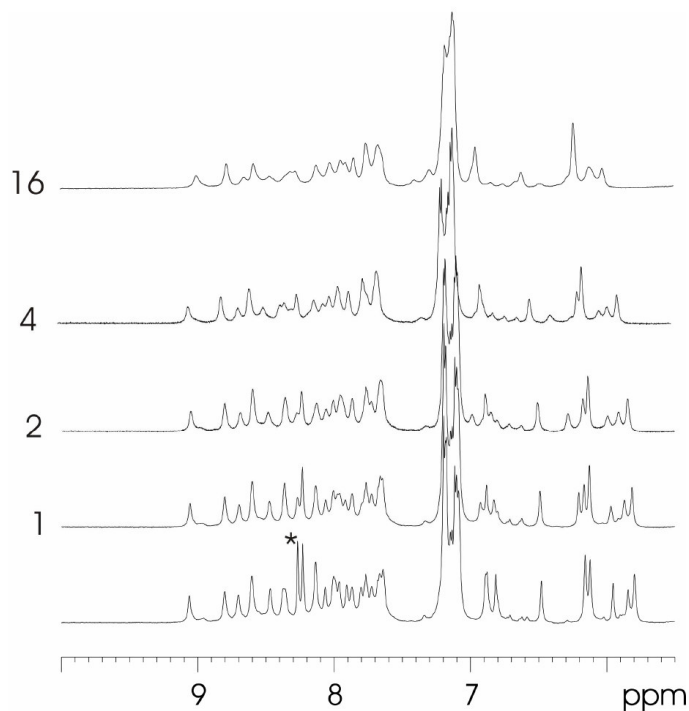
Figure III.3.4 1D NMR spectra of **PrP[173-195]D178N** dissolved in TFE_{d2} before and after addition of $ZnCl_2$ solution. Labels 1, 2, 4 and 16 indicate the total volume (μL) of 0.5 M $ZnCl_2$ solution added to 500 μL of 1.0 mM peptide solution, corresponding to Zn(II)/peptide molar ratios of 1.0, 2.0, 4.0 and 16.0, respectively. Imidazolic proton resonances of His residues in metal absence are marked by an asterisk.

III.4. *Integrated spectroscopical investigation and molecular dynamic simulation on tetracycline/α-helix 2 interaction*

CD investigation

An extensive investigation of the interaction of PrP peptides with TC has been conducted in water by using fluorescence spectroscopy. To this aim, at the N-*terminus* of each peptide was introduced fluorescein as fluorescent probe [145]. Before using any peptide in fluorescence studies, their conformation in water was evaluated by CD spectroscopy. In **Figure III.4.1**, an overlay of CD spectra of the fluoresceinated peptides Fluo-PrP[173-195], Fluo-PrP[180-195] and Fluo-βA[25-35] is reported. Unexpectedly, in water, the spectra of all peptides exhibited features typical of α-helix conformations, with a maximum at around 195 nm and two minima at around 208 and 222 nm. The CD spectrum of fluoresceinated Fluo-PrP[106-126], under the same conditions, shows that the polypeptide does not adopt canonical conformations; on the contrary, it is indicative of a random structure (**Figure III.4.2(D)**). Remarkably, the addition of increasing amounts of tetracycline (TC) to peptide solutions did not induce substantial structural changes (see **Figure III.4.2**), indicating that the effects produced by the antibiotic on peptide fluorescence emission (see later) were solely due to a direct interference with the fluorescein spectroscopic properties, and not to an alteration of peptide conformation.
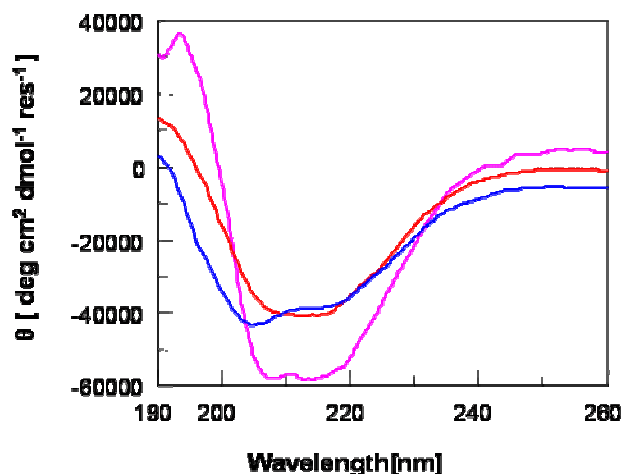
Figure III.4.1 CD spectra of the peptides Fluo-PrP[173-195] (red), Fluo-PrP[180-195] (magenta), and Fluo-βA[25-35] (blue) in water at 20 °C.
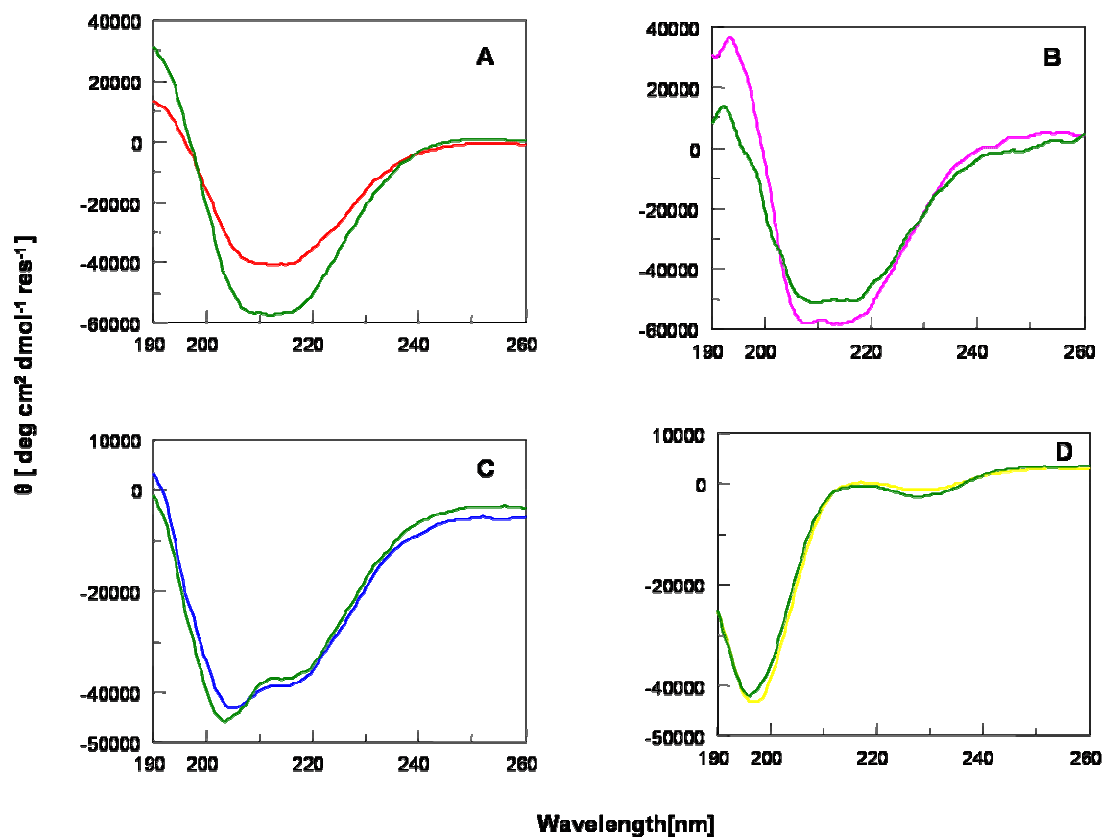
Figure III.4.2 Effect of tetracycline addition on CD spectra of fluoresceinated peptides dissolved in H_2O and in presence of 10 eq. of TC (green lines). **(A)** Fluo-PrP[173-195] (red line). **(B)** Fluo-PrP[180-195] (magenta line). **(C)** Fluo-βA[25-35] (blue line). **(D)** Fluo-PrP[106-126] dissolved in H_2O (yellow line).

Binding experiments

The fluorescence emission spectra of peptide Fluo-PrP[173-195] in the presence of increasing amounts of TC are reported in **Figure III.4.3(A)** The fluorescence intensity definitely decreases as a function of increasing TC concentration and this feature is much more evident in **Figure III.4.3(B)**, where intensity is plotted against the antibiotic concentration. The curve relative to Fluo-PrP[173-195] is superimposed to those of Fluo-PrP[180-195], Fluo-PrP[106-126], and Fluo-βA[25-35]. It is worth noting that, while curves of prion peptides corresponding to α-helix 2 show the hyperbolic trends expected by saturating dose-response effects, the Fluo-PrP[106-126] and the control Fluo-βA[25-35] exhibit a rather linear, nonsaturating dependence of fluorescence quenching on TC concentration, that is, typical for non-specific interactions. Non-linear regression analysis of curves relative to Fluo-PrP[173-195] and Fluo-PrP[180-195] provided an estimation of the apparent dissociation constants for the two peptide/TC complexes, which are 189 ± 7 and 483 ± 30 nM, respectively. Noteworthily, the dissociation constant of the shorter 180-195 fragment is about 2.5-fold higher than that of the full length α-helix 2, pointing out that, though a strong interaction with the polycyclic molecule is yet maintained, a contribution to binding between α-helix 2 and TC must derive from either the N-terminal residues or from a superior conformational stability of the longer peptide. Under the explored concentration range (nM), no quenching effects have been detected with the fluoresceinated, conformationally random, N-terminal 106-126 fragment. The absence of any effect of TC on the spectral properties of Fluo-PrP[106-126] rules out the occurrence of non-specific interactions of the antibiotic with fluorescein and, at the same time, the lack of interaction of the structured Fluo-βA[25-35] excludes a preferential interaction of the antibiotic with unrelated helical structures.
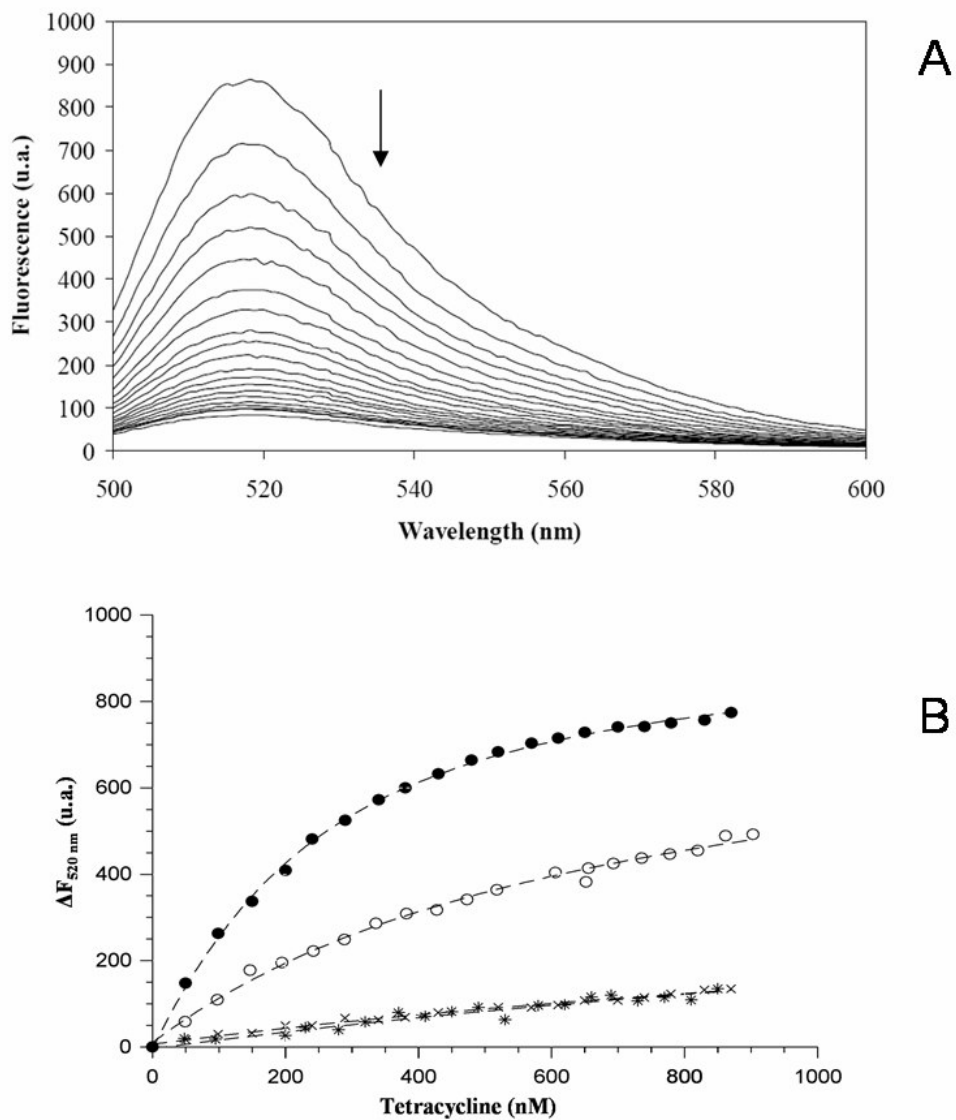
Figure III.4.3(A) Fluorescence emission spectra of Fluo-PrP[173-195] in presence of increasing amounts of tetracycline. Curve intensities decrease upon TC addition, as indicated by the arrow **(B)** Effect of tetracycline addition on fluorescence quenching of Fluo-PrP[173-195] (●), Fluo-PrP[180-195] (○), Fluo-βA[25-35] (×), and Fluo-PrP[106-126] (∗) in water at 20°C.
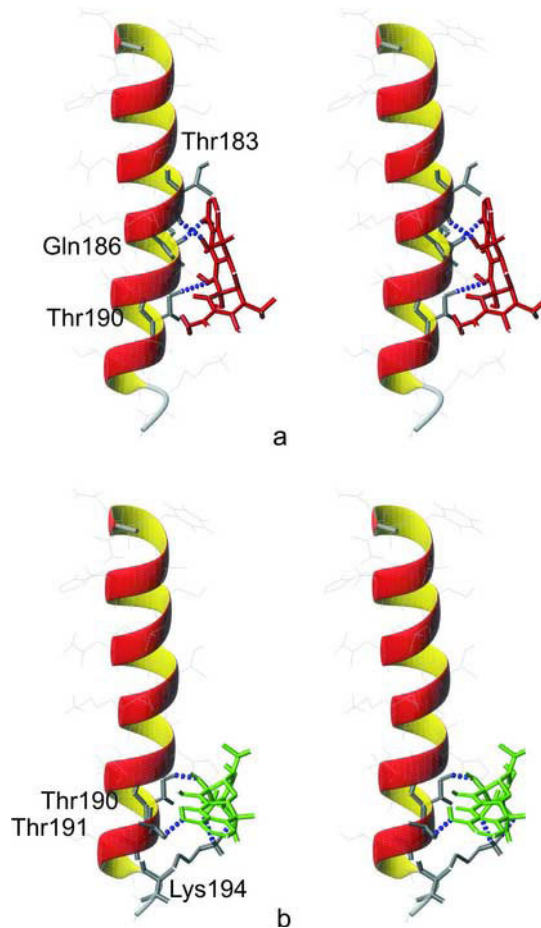
Docking calculations

Automated docking calculations predict that both neutral TC (TC^n) and zwitterionic TC (TC^{zw}) exhibit a strong preference for the coordination to the C-terminal part of PrP[173-195]. Furthermore, it emerges that the three energetically most favorite orientations for TC docked to PrP[173-195] are the same for both TC^{zw} and TC^n (**Table III.4.1** and **Figure III.4.4**). In both cases, the majority of the 100 lowest energy-docking structures belong to the same three clusters, which we label R1, R2 and R3 according to their energy rank. This result can be easily explained by the inspection of the most stable docked structures, showing that the groups involved into zwitterionic equilibrium are indeed not directly involved into the interaction with PrP[173-195]. It must be noticed that TC^n prefers R1 orientation (i.e., the lowest energy orientation), whereas the most populated cluster for TC^{zw} is the R3. However, it is important to remind that cluster orientations have very similar stability. Almost all of the 100 most stable docked structures of TC^{zw} belong to R1, R2, and R3, whereas, for TC^n, structures involving the coordination to the N-terminal portion of PrP[173-195] are also present. On the other hand, it is important to highlight that the average docking energy of these latter structures is significantly (more than 2 kcal/mol) lower than that of R1. Structures belonging to R1 are stabilized by hydrogen bonds involving both the polar side (carbonyl and hydroxyl groups) and the unique hydroxyl group of the apolar side of TC and residues Thr183, Gln186, His187, and Thr190 (**Figure III.4.5(a)**). R3 complexes, instead, are characterized by hydrogen bonds between the polar side (carbonyl, hydroxyl, and amidic groups) of TC and the aminoacids Gln186, His187, Thr190, Thr191, and Lys194 (**Figure III.4.5(b)**).

Table III.4.1 Docking Energy (in kcal/mol) and Percent Population on the 100 Lowest Energy-Docked Structures of the Three Preferred Orientations (see **Figure III.4.4**) for TC^{zw} and TC^n, according to AUTODOCK Calculations.

Cluster type	Percent Population		Lowest Docked Energy		Mean Docked Energy	
	TC^{zn}	TC^n	TC^{zn}	TC^n	TC^{zn}	TC^n
R1	12	35	-7.43	-7.42	-7.22	-7.05
R2	7	6	-7.14	-6.78	-6.97	-6.66
R3	70	7	-6.62	-6.28	-6.62	-6.18
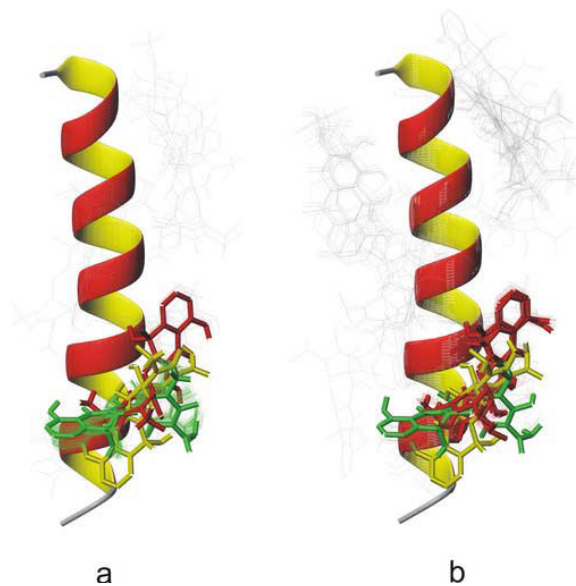
Figure III.4.4 Docked structures obtained by AutoDock calculations for (**a**) TC^{zw} and (**b**) TC^{n}. The three most stable clusters of docked structures are in color (red: R1, yellow: R2, green: R3).

Figure III.4.5 Docked The structure with the lowest docking energy in clusters (**a**) R1 and (**b**) R3.

Molecular dynamic simulations

As a first step of our MD analysis, we have performed three different MD runs labeled MD1, MD2, and MD3) of the isolated PrP[173-195] fragment. On the balance, the fragment is predicted to adopt preferentially α-helix structure, in agreement with the indication of CD experiments. However, the analysis of the RMSD on C^{α} carbon atoms confirms the flexibility of this region, as shown by previous MD studies of PrP and thereof fragments [37, 146-148] and in agreement with the previously described conformational ambivalence of the isolated peptide [48]. The comparison among the different simulations indicates that the region more susceptible to loose helix structure comprises some residues in the middle of the fragment (residues 185-187) and, most of all, the C-terminal residues 193-195. As a matter of fact, two of the three MD simulations predict that significant conformational changes take place in the C-terminal region (residues 189-194) during the second half of simulation, destructuring the initial helix conformation, and leading to the formation of a bend. The motion of Thr residues (190-193), especially that of side chains, critically influences the conformational behaviour of the C-terminal part of PrP[173-195]. When Thr residues (190-193) adopt an helix conformation, their side chains usually contribute to the stabilization of the helix, providing supplemental hydrogen bonds with the backbone. On the other hand, when Thr side chains of the C-terminal end freely fluctuate into the solvent, helix structures are much more unstable. Concerning the high flexibility of the C-terminal part of α-helix 2 and, in particular, the small tendency for Thr-rich regions to adopt helix conformations, our results agree with previous experimental and computational studies [14, 21, 37, 48].

- PrP[173-195]/TC^{zw} System

Although with some different details, the three simulations, labeled MD1zw, MD2zw, and MD3zw, agree in predicting that TC^{zw} strongly interacts with prion fragment. The analysis of the RMSD for the three simulations indicates that TC atoms rapidly reach the equilibrium, whereas PrP[173-195] fragment is more unstable. In two out of the three simulations, PrP[173-195] undergoes indeed significant conformational changes consisting in the loss of helical content at the C-*terminus* and in the middle of the fragment (around residues 183-185) (**Figure III.4.6**). However, it is important to highlight that, notwithstanding this distortion, PrP[173-195] still exhibits a predominant helical conformation, in agreement with CD experiments. In all the simulations, TC^{zw} interacts strongly with the prion fragment, being characterized by at least two stable hydrogen bonds between the polar side of TC and the C-terminal part of PrP[173-195]. In detail, MD1zw and MD3zw show a similar behaviour, exhibiting two stable intermolecular hydrogen bonds. The first one involves Thr190 and the polar side of TC, while the second one is formed by Ile182 (MD3zw) or Thr184 (MD1zw), respectively (**Figure III.4.6(a) and (c)**). In MD2zw, there is instead alternation between adducts stabilized by two and three hydrogen bonds, namely, between the polar side of TC and Thr191 and Lys194 and/or Gly195 (**Figure III.4.6(b)**).

- PrP[173-195]/TC^{n} System

On the balance, also when interacting with TC^{n}, helix conformation of PrP[173-195] is maintained. However, as found also in the absence of TC, the C-terminal region is very flexible. Depending on the simulation, between 2 and 6 C-terminal residues are indeed predicted to loose helix conformation (**Figure III.4.7**). Confirming the results

obtained on TC^{zw}, MD simulations, labeled MD1n, MD2n, and MD3n, predict the formation of a stable interaction between TC^n and PrP [173-195], stabilized by at least two persistent hydrogen bonds (**Figure III.4.7**).
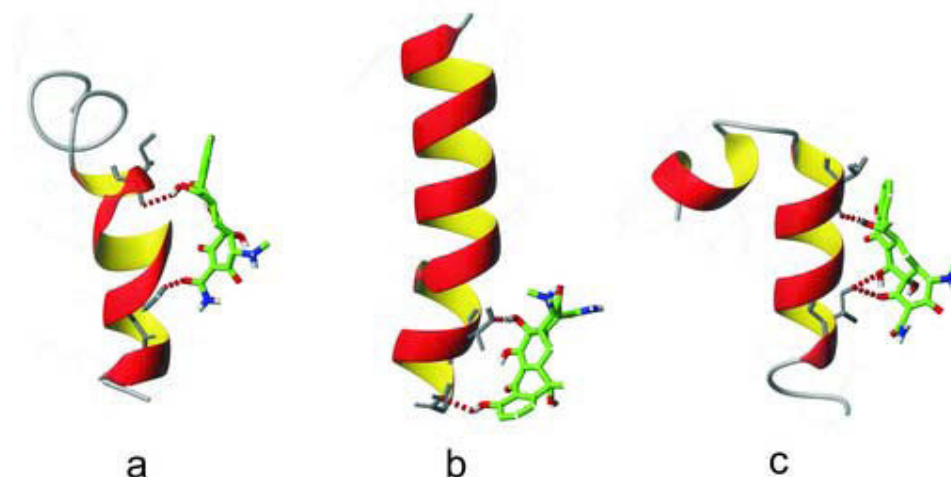
Figure III.4.6 Representative frames extracted during the MD1zw **(a)**, MD2zw **(b)**, and MD3zw **(c)** molecular dynamic simulations.
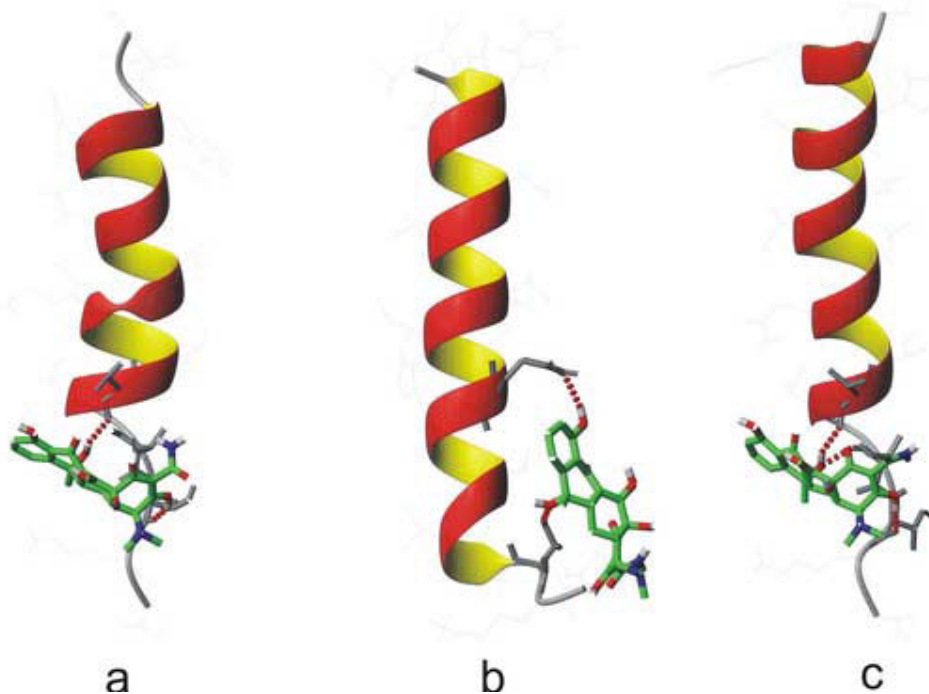
Figure III.4.7 Representative frames extracted during the MD1n **(a)**, MD2n **(b)** and MD3n **(c)** molecular dynamic simulations.

III.5. *Fluorimetric analysis of α-helix 2–binding synthetic peptide constructs*

The structure of the complex Fab-ovPrP shows that the epitope of the antibody consists mostly of PrP residues 188–199 (C-terminal part of α-helix 2 and N-terminal part of the α-helix 2/α-helix 3 loop) [127].

As shown in **Figure III.5.1**, we have identified the Fab[30-35] and Fab[46-53] fragments (TNYGMN and RLIYLVSR, respectively), which are able to form hydrogen bonds with the α-helix 2 C-terminal end in the Fab-ovPrP X-ray structure and designed peptide constructs putatively suitable to model the ovPrP-Fab interaction.
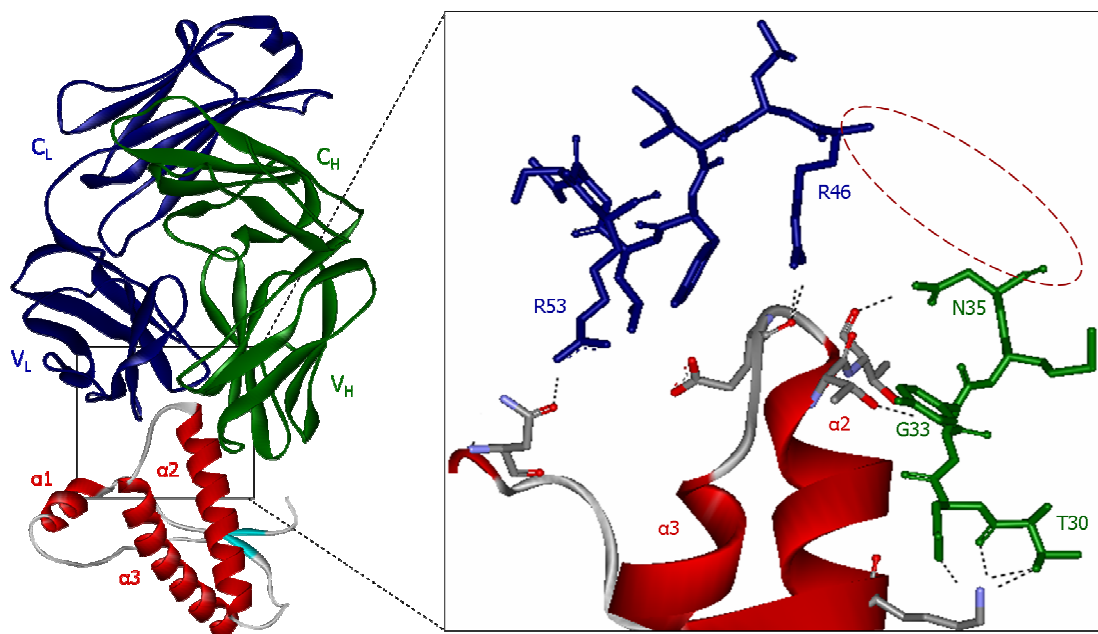
Figure III.5.1 (Left) Overview of the complex. **(Right)** Close-up view of the boxed region of the complex. For clarity, only atoms that establish an intermolecular hydrogen bond (dashed lines) are represented in the 'stick' format.

These peptide constructs, henceforth identified as JMV, were obtained linking the two identified peptide fragments by spacers of different size, rigidity and chemical nature; their general scheme of synthesis on SynPhase Lanterns is reported in **Figure III.5.2**.
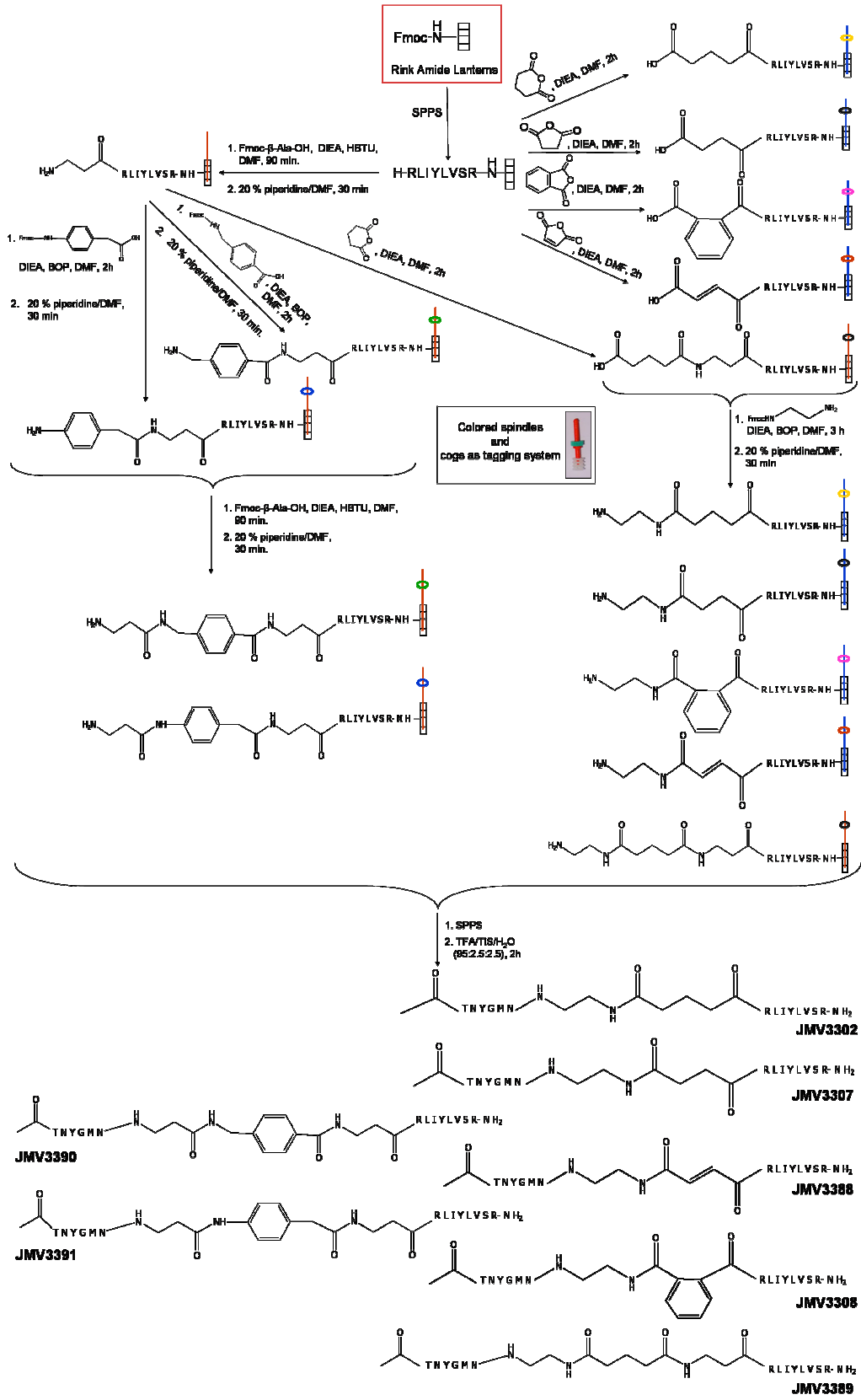
Figure III.5.2 Scheme of synthesis on SynPhase Lanterns of JMV peptide costructs.

Subsequently, in order to investigate the interaction between α-helix 2 and JMV compounds, we have recorded the emission spectra of fluorescein-modified PrP[173-195] in aqueous solution in presence of increasing amounts of JMV compounds. The fluorescence emission spectra of Fluo-PrP[173-195] in presence of increasing amount of JMV3391 are representatively reported in **Figure III.5.3(A)**. The fluorescence intensity decreases following JMV addition was appreciated by plotting modification of the emission intensity at 518 nm versus JMV concentration. All titration curves show the hyperbolic trend typical of saturating dose-response effects (**Figure III.5.3(B)**). Fluorescence intensities were then used to evaluate the fractions of Fluo-PrP[173-195] bound to each JMV construct and calculate the apparent dissociation constants (K_D') of the corresponding complexes according to 1:1 binding interaction (**Table III.5.1**).
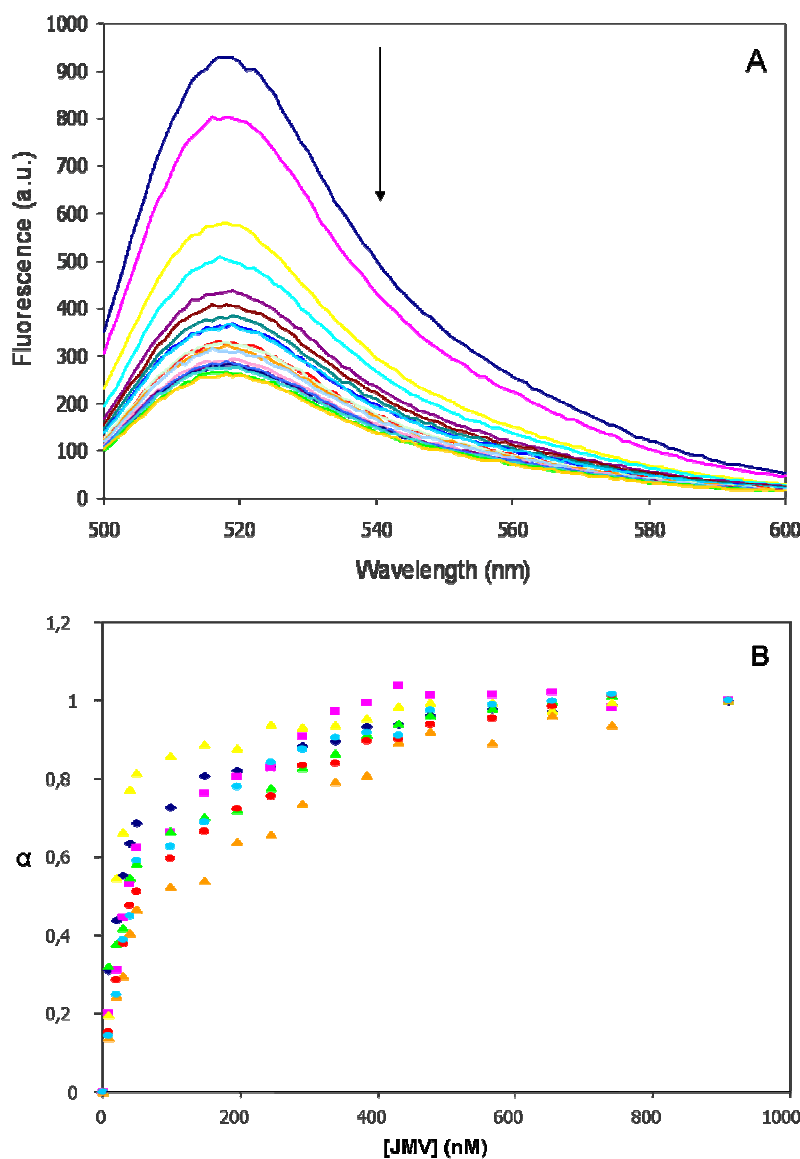
Figure III.5.3(A) Fluorescence emission spectra of Fluo-PrP[173-195] in presence of increasing amounts of JMV3391, curve intensities decrease upon JMV3391 addition, as indicated by the arrow. **(B)** Effect of JMV addition on fluorescence quenching of Fluo-PrP[173-195].

53

Table III.5.1 JMV compounds: apparent dissociation constants and corresponding structures and symbols.

Code	Structure	Symbol	K_D'(nM)
JMV3302		◆ (blue)	6 ± 5
JMV3307		▲ (green)	18 ± 7
JMV3388		■ (pink)	10 ± 6
JMV3308		▲ (orange)	51 ± 13
JMV3389		● (red)	27 ± 9
JMV3390		● (cyan)	18 ± 7
JMV3391		▲ (yellow)	1 ± 2

Finally, in order to analyze the potential correlation between the K_D' value and the conformation, a CD analysis of the JMV compounds was performed in aqueous solution. As shown in **Figure III.5.4**, the shape of the circular dichroism (CD) spectra of all JMV peptide constructs in water at pH 7.0 was suggestive of an unordered structure.
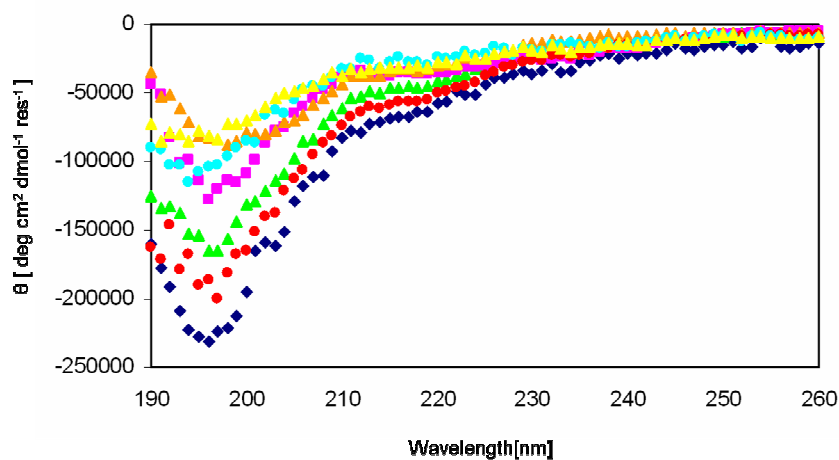
Figure III.5.4 CD spectra of JMV compounds in water at pH 7.0.

IV. DISCUSSION

IV.1. *Comparative CD, NMR and cellular toxicity study on PrP[173-195], its D178N analogue and the shorter PrP[180-195] segment*

We have performed comparative CD, NMR and cellular toxicity studies on the synthetic peptides PrP[173-195], PrP[173-195]D178N and PrP[180-195]. The first two peptides, corresponding to the full length α-helix 2 region, represent the wild type sequence and its D178N mutant, respectively. The shorter peptide includes the threonine-rich region and is therefore characterized by strong β-sheet forming propensity [133, 149, 150]. Furthermore, its structure is devoid of effects linked to the reactivity of the thiol moiety. Finally, it can be considered the peptide of maximal length that exhibits a regular structure different from the α-helix. This conclusion stems from the finding that the CD spectra of peptides derived from the N-terminal and the C-terminal part of the full length α-helix 2 (PrP[173-179] and PrP[180-195], respectively) are those typical of random and β-type organization, respectively (**Figure III.1.2** and **Figure III.1.1**). Thus, it seems reasonable to infer that the occurrence of disordered structure in the full length α-helix 2 peptides is associated with the N-terminal segment. As a matter of fact, CD spectra of PrP[173-195] and PrP[173-195]D178N, which both include the 173-179 segment, do not show the β-type peculiarities exhibited by PrP[180-195]. SDS titration of the D178N mutant goes to completion in a range of detergent concentration much narrower than that observed for the wild type peptide (see **Figure III.1.3**). Probably, the absence of the negative charge carried by the Asp178 side-chain permits stronger electrostatic interaction between SDS and the protonated His177 side-chain. Moreover, the higher β-inducing propensity of Asn may also contribute to favour reorganization of PrP[173-195]D178N into a β-type conformation. Overall, this suggests that the Asn side-chain renders the mutant peptide more prone to form β-structure. In agreement with that, the TFE-induced recovery of α-helical conformation is larger for the wild type peptide compared to the D178N mutant (see **Figure III.1.4**).

In addition, the fact that PrP[180-195] is able to assume β-arrangement at neutral pH even without SDS and that conformation doesn't dramatically change even in presence of TFE, suggests that the 180-195 parental region in PrP^C strongly contributes to the chameleon conformational behaviour of the segment corresponding to the full-length α-helix 2 [48] and could play a role in determining structural rearrangements of the entire PrP^C-globular domain.

Our CD spectra show that these α-helix 2 derived peptides do not possess the same α-helical conformation as that observed in the cellular prion protein. It is known that the lack of mutual interactions has dramatic effects on the integrity of the whole helical domain of the prion protein, and the stability of one single helical region strongly suffers from ablation of the other helical segments as well as of the disulphide bridge. However, native-like conditions can be to some extent restored choosing a medium that may help extract useful information using the peptide fragment approach. Thus, we have used TFE as the most suitable environment to investigate structural similarities between these synthetic peptides.

As a matter of fact, in NMR spectra, both PrP[173-195] and PrP[180-195] were found to be helices, whereas the PrP[173-195]D178N mutant was not even able to retain a fully helical arrangement in an α-inducing environment.

The major NMR result is that the conformation of the wild type peptide is significantly affected by replacing the negatively charged Asp178 with a neutral Asn residue. In the mutant peptide, increased conformational freedom characterizes all residues downstream Gln188, which ultimately causes unwinding and bending of the wild type fully helical structure. As a consequence, structural rearrangement leads to the formation of two short helices separated by a kink centred on Lys185 and Gln186. In this bent structure, His177 and His187 approach to each other as compared to the parent helical peptide, forming two major conformational families, characterized by proximal and distal imidazole rings, respectively. Moreover, the network of stabilizing H-bonds mainly involves the interaction between Asn174 and Thr188 (head-to-tail type) and between Asn181 and His187 or Gln186 (core type) (**Figure IV.1.1**). In conclusion, we argue that the negative charge of Asp178 plays a key role in forcing the entire 173-195 fragment to assume a full helical conformation.

Notably, the shorter 180-195 fragment still retains an almost fully helical structure, whether or not it is embedded in the 173-195 sequence, suggesting that helix unwinding in the region 180-187 is provoked by the D178N substitution. Indeed, though the sequence of the shorter peptide includes residues involved in the bending of the D178N analogue (Lys185 and Gln186), it does not show any kink in its structure, nor does the wild type peptide. This confirms that the D178N mutation destabilizes the region in which it is located, thus causing not only the unwinding of the wild type fully helical structure, but also its bending.
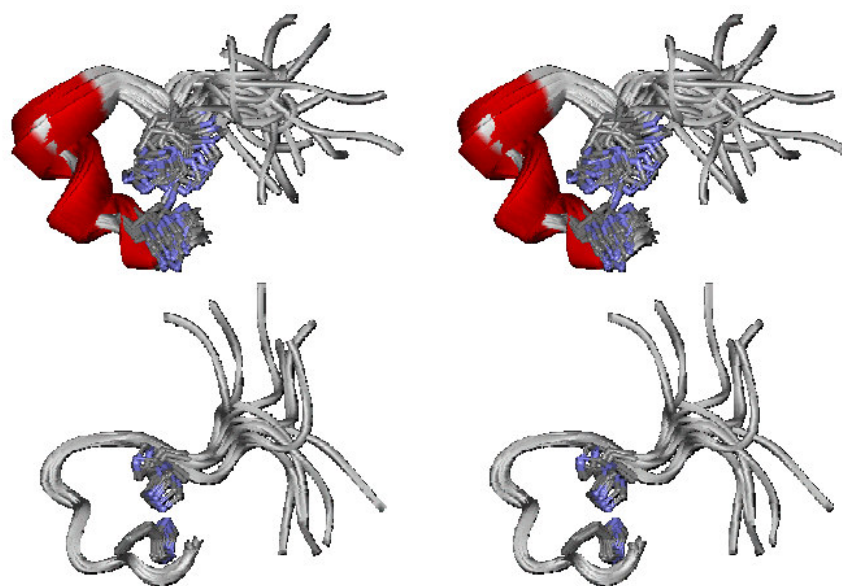
Figure IV.1.1 Stereo view of the backbone structure of **PrP[173-195]D178N**. Clusters identify two major conformational families, with proximal (top) and distal (bottom) histidine imidazolic rings.

Interestingly, comparing the FC_{50} value of **Table III.1.1** it is evident that the PrP[180-195] peptide and the complementary PrP[173-179] fragment possess the lowest and the highest FC_{50}, respectively, whereas the peptide derived from the full α-helix 2 (PrP[173-195]) displays an FC_{50} slightly higher than that of PrP[180-195]. This suggests that the intrinsic toxicity of PrP[173-195] can be totally ascribed to the segment 180-195. Furthermore, the peptide bearing the D178N mutation associated to the CJD displays a toxicity higher than that of the wild type peptide. This value is probably related to the structural destabilization caused by the Asp178 Asn replacement.

IV.2. *Effect of salts and pH on PrP[180-195] and its H187A analogue*

Environmental conditions, like pH, salts, and presence of nucleic acids or glycosaminoglycans, seem to affect the structural stability of prion proteins to a much larger extent than other proteins [151-158]. It was suggested that this unusual behaviour could be ascribed to the ability of PrP^C N-terminal region to interact with anions, which leads to destabilization of the prion core structure [155]. Also, in an extensive analysis on the interaction of anti-prion compounds and amyloid-binding dyes with a carboxy-terminal domain of prion protein, it has been found that sulfonates, like Congo red and phthalocyanine tetrasulfonate, bind with high affinity [159]. We have shown that the conformational properties of two PrP^C α-helix 2-derived analogues, PrP[180–195] and PrP[180-195]H187A, are affected by anion identity. Such large differences in the CD spectra of both peptides with anion identity can be rationalized via the ion charge density dependence that is typical of Hofmeister effects [134, 135] (**Figure IV.2.1**).
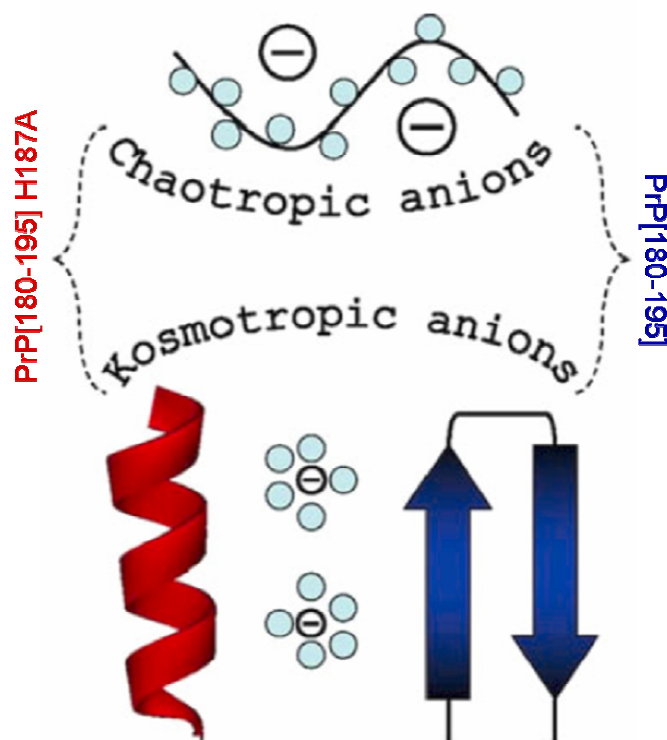
Figure IV.2.1 Weakly hydrated chaotropic anions (top) maximize the solvent accessible surface area and favor the unordered structure in both PrP[180–195] and PrP[180-195]H187A. Strongly hydrated kosmotropic anions (bottom) make bulk water a poorer solvent and cause PrP[180-195]H187A and PrP[180–195] to fold to α-helix and β-structure, respectively, to minimize their solvent accessible surface area.

Anions like Cl^-, ClO_4^-, and $H_2PO_4^-$ are weakly hydrated because of their low charge density, and their interaction with water molecules is weaker than that of water with itself. This causes them to behave as water structure breakers (chaotropes), which make the bulk solution a better solvent. As a consequence, both PrP[180–195] and

PrP[180-195]H187A maximize their solvent accessible surface area, favoring the formation of the unstructured conformation. On the other hand, multiply charged ions, like SO_4^{2-} and HPO_4^{2-}, exhibit stronger interactions with water molecules than water with itself because of their high charge density. These ions are water structure makers (kosmotropes) and make the bulk solution a poorer solvent. Thus, they encourage PrP[180–195] and PrP[180-195]H187A to minimize their solvent accessible surface area and assume β-sheet-like and α-helix-like conformations, respectively. It is likely that the compactness of these structures predisposes both peptides to self-association (**Figure III.2.3**), which may be a preliminary step toward fibril formation. This is also suggested by preliminary heat irreversible denaturation experiments on PrP[180-195]H187A, which assumes a β-sheet-like conformation when dissolved in Na_2SO_4 at acidic pH. The different conformational behaviour of the wild type peptide as compared to the mutant peptide in the presence of kosmotropic anions at neutral pH is likely caused by the His side chain, which displays an α-inducing ability lower than the Ala side chain. Nevertheless, in the prion protein, the segment containing the His187 residue is still able to retain an α-helical conformation owing to tertiary interactions [48]. Furthermore, in acidic solution, the His protonation and increased proton exchange [157] could play a role in causing PrP[180–195] and PrP[180-195]H187A to assume disordered structure and β-conformation, respectively. Also, our results confirm the chameleon like character of the helix 2 domain [48], suggesting that preferential binding with naturally occurring anions, rather than non specific interactions, such as ionic strength-dependent interactions, plays an important role in prion protein misfolding and amyloid fibril growth. Understanding ion-specific effects is a central theme of biology. Unfortunately, the complication of 'ion confounding' is extremely common in all disciplines concerned with ion-based research because ions are generally manipulated through the use of salts. It occurs because changing the concentration of a single cation or anion using a single salt results in a simultaneous change of the associated co-ion, which causes the main effect associated with that ion to be confounded with the effects caused by changing the concentration of the co-ion [160]. It is therefore worth stressing that, even in studies on prion and derived peptides, anion-bound effects may overlap the largely explored cation-bound effects. Unfortunately, experiments are not always designed so that the species that cause the modification can be unequivocally perceived. In conclusion, we highlight that the sensitivity of our peptides, as well as the entire prion proteins [47, 52, 53, 78] or other amyloidogenic systems [161], to environmental modifications suggests that the complication of anion involvement cannot be neglected anymore, either in investigating metal effects on peptide conformation [47, 52, 53, 78, 161] or in checking the inhibition of amyloid formation by unusual agents [162, 163].

IV.3. *NMR and CD titration of PrP[173-195] and its D178N analogue with metal cations*

We have performed CD and NMR titration of the synthetic peptides PrP[173-195] and PrP[173-195]D178N with metal cations. As can be judged from far UV CD spectra (**Figure III.3.1** and **Figure III.3.3**), the two negative bands at 222 and 208 nm, and a positive band at 192 nm indicate that both peptides exhibit α-helical arrangement. However, the lower intensity that characterizes the spectrum of the mutant peptide suggests some rearrangement as compared to the single helical structure exhibited by the wild type peptide.

For both peptides, addition of increasing metal cation aliquots did not perturb NMR spectra in any specific way. The chemical shifts of all resonances did not vary, as it could be expected in case of metal-peptide complex formation, and the overall effect was a progressive generalized broadening of all relevant resonances. In fact, addition of higher and higher metal aliquots caused irreversible aggregation, which always lies in wait when the peptide concentration is very high, possibly owing to ionic strength increase and/or to water addition on metal cation titration. However, that the interaction of the metal with the peptide backbone is non-specific was confirmed by the unaltered appearance of CD spectra after metal addition, where aggregation did not occur thanks to the lower peptide concentration. These analyses were performed in neat TFE in conformity to the NMR experimental conditions of the **III.1. Paragraph**, but further experiments in mixed water/TFE solvent suggested that water-induced effects largely dominate structural rearrangements, rendering metal-induced modifications, if any, hard to discriminate. Among studies that have been carried out on metal interaction with peptides derived from the PrP C-*terminus*, it is worth mentioning that recently Brown and co-authors [47] have characterized the formation of different Cu^{2+} complexes in blocked and free C- and N-*termini* analogues of the peptide fragment 180-193 (VNITKQHTVTTTT), which almost entirely encompasses the PrP^C α-helix 2. They suggested that the binding site of copper(II) in the structured region of the protein is located on the His187 residue, and that the anchoring imidazole residue drives the metal coordination environment towards a common binding motif in different regions of the prion protein. Other studies [4] showed that the PrP[178-193] peptide has both structural and bioactive properties in common with the amyloidogenic Alzheimer's disease βA[25-35] peptide and that the second putative helical region of PrP could be involved in modulation of Cu(II)-mediated toxicity in neurons during prion disease. However, our results suggest that the interaction of metal cations with peptide fragments derived from the C-terminal globular domain could be affected by experimental ambiguity caused by the fact that the structural organization of these peptides is different from that assumed in PrP^C. We believe that it is crucial to take this aspect into account when designing experiments aimed at investigating peptide-metal cation interaction. Furthermore, in the peptide fragment approach, it is unlikely that aqueous buffer is the most suitable environment to analyze metal interaction with peptide fragments, whose parent segments in the native protein experience different environmental conditions. We have shown that the use of the α-helix-inducer TFE to force peptides into a conformation close to the helical one that has been found in PrP^C may lead to conclusions different from those that can be obtained studying metal cation interaction with peptides in buffer solution. To embed our results in the body of data

on PrP structure and function, it is worth considering that the three-dimensional architecture of PrP^C consists of an unstructured leading tail encompassing residues 23-125 and a C-*terminus* globular domain, in which residues 126-231 are organized in three α-helices and a two-stranded β-sheet [14]. Although it is currently believed that the major structural modifications involved in PrP protein misfolding are located in the unstructured N-terminal region, the present results seem to provide further support to evidence accumulated in the literature that the two prion domains play a different role in the prion conversion, stressing that the N-terminal domain is likely the natural target of metal binding [53, 54].

IV.4. *Integrated spectroscopical investigation and molecular dynamic simulation on tetracycline/α-helix 2 interaction*

An integrated approach comprising fluorescence spectroscopy and calculations has been utilized to investigate the interaction between the α-helix 2 of prion protein and the antibiotic TC. To evaluate the meaningfulness of our results for understanding the interaction between TC and the entire structured core of human prion protein, a preliminary investigation of the conformational properties of isolated PrP[173-195] and PrP[180-195] peptides has been undertaken. In this respect, experimental and computational results are globally comforting and converge toward the indication that the general behaviour of the peptides is quite similar to that of α-helix 2 within the PrP protein. As a matter of fact, both Fluo-PrP[173-195] and Fluo-PrP[180-195] synthetic peptides tend to adopt a prevailingly helical structure, either when isolated and in the presence of TC. Consistently, MD simulations, performed with both the 173-195 fragment alone and in the presence of TC, strongly suggest that the N-terminal half of the fragment, though flexible, shows a clear-cut preference for helical conformations. On the other hand, the C-terminal end, encompassing residues 189-194, exhibits a much higher mobility. This result agrees with reported observations about the behaviour of α-helix 2 and further confirms the conclusions reached by Dima and Thirumalai [147] who have shown that the instability of α-helix 2 is independent of the protein intact structure. A further interesting feature emerged from the MD simulation on the isolated peptides regarding a modulation of the conformational behaviour of the C-terminal part of α-helix 2 exerted by the threonine side chains. Indeed, they can switch from a α-helix-stabilizing backbone interaction towards a solvent exposed conformation similar to that involved in the β-strand in the crystal dimer [21]. This outcome substantiates previous results based on X-ray [21] and NMR [14] studies that have demonstrated a high mobility of the Thr-rich region 190-193 region.

For what concerns the interaction with TC, experiments and calculations agree in predicting that TC has a strong affinity towards α-helix 2. As a matter of facts, fluorescence experiments indicates that the association constants of TC with Fluo-PrP[173-195] and Fluo-PrP[180-195] is in the nM range, whereas the Fluo-βA[25-35], though in a helical conformation, is unable to bind to the antibiotic in the explored concentration range. Anyhow, the experimental apparent association constant is smaller for the longer peptide, suggesting either a 'direct' interaction of those residues with TC and/or a smaller stability of the helix conformation in the shorter peptide. Furthermore, docking calculations and MD simulations do not predict that the 173-180 residues are significantly involved in TC interaction, whereas the C-terminal end, encompassing aminoacids 183-195, shows a strong affinity. Interestingly, MD simulations also suggest that the interaction between TC and prion peptides does not dramatically depend on the conformation adopted by the fragments, as stable hydrogen bonds can be formed with TC both in helix-like and in more extended conformations. In the C-terminal part of α-helix 2, there is indeed a hydrophilic patch in which several residue side chains potentially interacting with TC are gathered: Thr183, Gln186, His187, Thr190-193, Lys194. As a consequence, we can expect that, independently of the peptide conformation, two or three side chains can arrange in such a way to allow a strong interaction with the TC polar groups.

According to this hypothesis, the effect of TC on prion protein could be twofold: on one hand, a stabilization of the fluctuating helix conformation of the C-terminal part of α-helix 2 that prevents potentially dangerous transition to more extended conformations can be hypothesized. On the other hand, TC could interact with the peptide in the extended conformation, thus preventing protein association and the further aggregation into fibrils. Noticeably, among the C-terminal aminoacids of α-helix 2, threonine residues are significantly involved in the interaction with TC. Although previous studies by NMR have prompted a direct interaction of TC with the 106-126 peptide [113], these indications are not supported by our fluorescence experiments. In this regard, we suppose that affinity for this unstructured domain is much less intense being indeed detected at concentrations higher than those explorable by fluorescence (high micromolar range).

Besides the similarities between the conformational behaviour of the isolated fragments and that of α-helix 2 within the full length protein, a further distinctive element suggests that our findings can provide useful hints also on the interaction of TC with the entire protein. The region of the peptide PrP[173-195] involved into interaction with TC corresponds to a solvent-exposed region also in the entire protein PrP[125-228]. This tract can thus potentially interact with TC without significant conformational rearrangements. This conclusion is confirmed by a preliminary docking study carried out on both PrP[125-228] and on a model PrP[117-228] (with the addition of the 117-125 tail according to the X-ray human structure) with TC^n molecule. These results indicate that there is a strongly-preferred cleft for TC binding individuated by the region between the C-terminal end of α-helix 1 and the C-terminal end of α-helix 2.

We believe that the hypothesis on the TC binding suggested by our results has interesting, though indirect, implications for what concerns the conformational transition of the prion protein to the pathological isoform. As a matter of fact, experimental evidence indicates that TC interacts with PrP^{Sc} and slows down the onset of the illness [113, 164] and we have shown that the C-terminal region of α-helix 2, also in consideration of the high affinity, is one of the best candidate to be involved in the interaction with TC. These results, confirmed by preliminary docking calculations of TC and the entire PrP protein, could open interesting perspectives for the diagnosis and the use of TC derivatives for inactivating pathogenic form of PrP. From a complementary point of view, the experimental results concerning the capability of TC in retarding the onset of the illness, together with our observations, constitute an additional and significant, though indirect, hint for the involvement of the C-terminal part of α-helix 2 (especially, the threonine cluster) in the conformational transition, leading to the formation of the pathogenic form of PrP or at least in the formation of the recognition surfaces that hold together the misfolded monomers.

IV.5. *Fluorimetric analysis of α-helix 2–binding synthetic peptide constructs*

We have reported the spectroscopic studies on the interaction between the α-helix 2 derived peptide and peptide costructs putatively suitable to model the ovPrP-Fab interaction [127].

As can be judged from K_D' values listed in **Table III.5.1**, these preliminary experiments suggest that all Fab peptide constructs strongly interact with the α-helix 2-derived fragment, particularly the JMV 3391, which shows the highest affinity (K_D' = 2.3 nM). At the present these results have several different explanations. First, all of the spacers could be able to correctly orientate the peptide arms of the constructs. This hypothesis is supported by CD evidence that the JMV compounds assume an unordered structure and therefore no preferential organization has been identified for any of them. Second, only one peptide arm could be capable of interacting with the 173-195 peptide, and any affinity enhancement could be due to assembling of the second peptide arm through the spacers. Last, affinity could be poorly correlated to size, rigidity and/or chemical nature of the spacer and reasonably ascribed to sequence-specific features of the interaction between the 173-195 fragment and the JMV peptide constructs. Further studies are necessary to clarify structural details of this interaction. Whether or not spacer linking of the two Fab peptide sequences is advantageous could be clarified by fluorescence titration of the α-helix 2 derived peptide with the single Fab[30-35] or Fab[46-53] fragment. In addition, NMR experiments could be planned to identify residues involved in α-helix 2-JMV compound interaction.

Finally, experiments using more significant prion protein fragments could open interesting perspectives for the diagnostic or therapeutic use of these constructs in PrP-associated diseases.

V.   CONCLUSIONS

Prion diseases are a group of transmissible neurodegenerative disorders that enclose scrapie in sheep, spongiform encephalopathy in cattle (BSE), and Creutzfeldt–Jakob disease, fatal insomnia and Gerstmann–Sträussler–Scheinker disease in humans.

The pathogenic mechanism underlying these diseases is a conformational conversion of the cellular prion protein (PrP^C) into disease-specific species (PrP^{Sc}) that possess abnormal physicochemical properties, such as insolubility and protease resistance, and accumulate in the brain in the form of amorphous aggregates and amyloid fibrils [8].

Despite a large number of studies on PrP^C, possible causes of its pathogenic conversion and its role in cellular function still remain unclear. Moreover, the highly aggregated state of the abnormal form has hampered the elucidation of the PrP^{Sc} structure at the atomic level.

Importance attached to prion protein studies has remarkably increased following the BSE epidemic and appearance of a new variant of Creutzfeldt-Jakob disease that seems to be causally linked to it [165-167]. Although the number of CJD cases observed so far is limited, a future outbreak of this disease cannot be excluded.

Moreover, given that general features of prion diseases are common to other amyloid disorders [2], the prion protein could be used as a model to provide the bases for a comprehensive evaluation of the general protein misfolding mechanism.

It is therefore evident that a conformation based approach to the study of PrP can give useful hints both on the region/residues potentially important for the PrP^C→PrP^{Sc} conversion and on the identification or development of anti-prion compounds. Following the thread of these arguments we have investigated the conformational properties of the PrP[173-195] peptide, corresponding to hPrP α-helix 2, and its affinity towards potential PrP-binding compounds. The interest in the study of α-helix 2 comes from evidence that this segment possesses chameleon conformational behaviour [48], gathers several disease-promoting point mutations, and can be strongly fibrillogenic and toxic to neuronal cells [4], suggesting its involvement in the protein aggregation process and in the toxicity associated to the scrapie variant. Overall, all our data on the conformational landscape of α-helix 2 strongly suggest that the role played by the α-helix 2 domain is not to be considered neutral in the misfolding mechanism of the PrP^C to the scrapie isoform.

In particular, the CD and NMR analysis on the synthetic α-helix 2 derived peptides has shown that the 173-195 segment is characterized by unusually low α-helical content and high β-sheet propensies, in spite of the fact that this segment retains a helical conformation in the whole protein. This behaviour could be ascribed to the 180-195 fragment which includes the threonine-rich region and is able to assume a β-arrangement at neutral pH even without SDS or in presence of TFE.

Moreover, a single amino acid replacement in the α-helix 2 significantly affects the organization of the 173-195 peptide, enhancing the propension of this region for β-conformation and facilitating structural rearrangements. As a matter of fact, in the CJD-associated D178N mutant peptide, the substitution of a neutral Asn for an Asp residue weakens the helical arrangement of the 173-195 segment in TFE. In addition, the PrP[173-195]D178N peptide shows a higher β-type propensity in SDS compared to that exhibited by the wild type peptide in the same condition. Furthermore,

neurotoxicity assays have shown that the PrP[180-195] and PrP[173-195]D178N peptides display a toxicity higher than that of the wild type peptide, suggesting a linkage between β-conformation propensity and toxicity.

On the other side, enviromental conditions, such as pH and salts, can affect the conformational behaviour of the α-helix 2 domain. This confirms the chameleon-like character of this PrP fragment [48], suggesting that preferential binding with naturally occurring anions and pH changes play an important role in prion protein misfolding and amyloid fibril growth.

NMR and CD titrations with metal cations have shown that no specific interaction of Zn^{2+} or Cu^{2+} with α-helix 2 derived peptides occurs, providing further support to evidence accumulated in the literature that PrP N- and C-*termini* domains play a different role in the prion conversion and stressing that the N-terminal domain is likely the natural target of metal binding [53, 54].

Its intriguing structural properties make the α-helix 2 domain a primary target for therapeutic strategies and a suitable model to investigate rational structure-based drug design of compounds able to block or prevent prion diseases.

For what concerns the interaction with TC, experiments and calculations agree in predicting that TC has a strong affinity towards the α-helix 2 and that interaction mainly involves its C-terminal half, previously shown to be conformationally ambivalent [48] and suggested as a starting point of oligomerization [14].

TC could therefore stabilize the fluctuating conformation of the C-terminal part of the α-helix 2 preventing its structural transition and aggregation.

Moreover, we believe that the results on TC binding have interesting, though indirect, implications for the $PrP^C{\rightarrow}PrP^{Sc}$ conformational transition. Although previous NMR studies in the mM concentration range have demonstrated direct interaction of TC with the PrP[106-126] peptide [113], our fluorescence experiments in the sub-micromolar range suggest instead that the TC affinity toward this unstructured fragment is much lower than that displayed toward the PrP[173-195] peptide. These results, confirmed by preliminary docking calculations on the interaction between TC and the whole PrP, indicate that the α-helix 2 C-terminal part is one of the best candidates to be involved in the binding to TC. Therefore, the previously described ability of TC to reduce, block and revert effects produced by pathological forms of hPrP [113, 164] could be predominantly ascribed to the interaction of TC with the α-helix 2. These results can have important implications for the use of TC derivatives for inactivating pathogenic forms of PrP and constitute an additional and significant hint for the involvement of the C-terminal part of the α-helix 2 in the $PrP^C{\rightarrow}PrP^{Sc}$ conversion.

In order to shed further light on the importance of the α-helix 2 domain as target for therapeutic and diagnostic approaches in prion diseases, we have designed and synthesized peptide costructs able to interact with the 173-195 peptide. Although this aspect needs further investigation, our results open interesting perspectives for the use of these constructs as therapeutic and diagnostic tools in PrP-associated misfolding.

VI. EXPERIMENTAL SECTION

VI.1. *Materials*

All solvents were peptide synthesis grade. HPLC chemicals and other organic reagents were purchased from Sigma-Aldrich (Milan, Italy). N-αFmoc-protected aminoacids, the activating agents and the resin were purchased from Novabiochem (Läufelfingen, CH). SDS and TFE were obtained from Sigma-Aldrich (Milano, Italia) and Romil LTD (Dublin, Ireland), respectively. Dulbecco's modified Eagle's medium was from Euroclone Life Science (Milan, Italy). MTT was from SIGMA-Aldrich (St. Louis, MO, USA). Lanterns, cogs and spindles were purchased from Mimotopes.

VI.2. *Solid Phase Peptide Synthesis*

Peptide of Table II.1

The peptides reported in **Table II.1** were synthesized by Fmoc standard chemistry protocol on Rink-amide 4-methylbenzhydrylamine (MBHA) resins 0,63 mmol/g. The Fmoc-amino acid side chain were selected as follows: tBu (Asp, Glu, Ser, Thr, Tyr), Boc (Lys), Pbf (Arg), Trt (Cys, Asn, Gln, His). Generally, the peptide chains were assembled by the sequential coupling of activated N-αFmoc-protected aminoacids (3 eq) in DMF in the presence of HBTU (3 eq) and DIEA (6 eq) with a reaction time of 1 h at room temperature. The resins were than washed with DMF (x 3), MeOH (x 1) and DCM (x 3). The completeness of each coupling was verified by the Kaiser test [168]. N-αFmoc deprotection was carried out by treatment with piperidine (20% v/v in DMF) for 30 min followed by washing with DMF (x 3), MeOH (x 1) and DCM (x 3). If necessary, the coupling and deprotection cycles were repeated. After the assembling of peptides reported in **Table II.1(A)**, acetylation was carried out by treatment with acetic anhydride (50% v/v in DCM). At the N-*terminus* of peptides reported in **Table II.1(B)**, a β-Alanine was linked and, after Fmoc removal, fluorescein was added using fluorescein isothiocyanate (2 eq) and DIEA (2 eq) for 2 h at room temperature. The β-Alanine residue was introduced as spacer and to avoid fluorescein elimination by the Edman degradation mechanism.

The peptides were then cleaved from the resin with TFA in the presence of TIS and distilled water (90 : 5 : 5, v/v/v) for 2 h at room temperature, concentrated *in vacuo*, and precipitated with diethyl ether at 0 °C followed by centrifugation at 3000 rpm for 5 min (x3). The resultant peptides were dissolved or suspended in water/acetonitrile (1:1, v/v) mixture and lyophilized.

In **Figure VI.2.1** and **VI.2.2** are representatively reported the LC-MS profiles of PrP[180-195] and Fluo-PrP[180-195]. In **Table VI.2.1** are listed, per peptide: the molecular formula and the exact mass, the retention time (t_R) and the masses (derived from the LC-MS analyses) and the yield of peptide after purification.
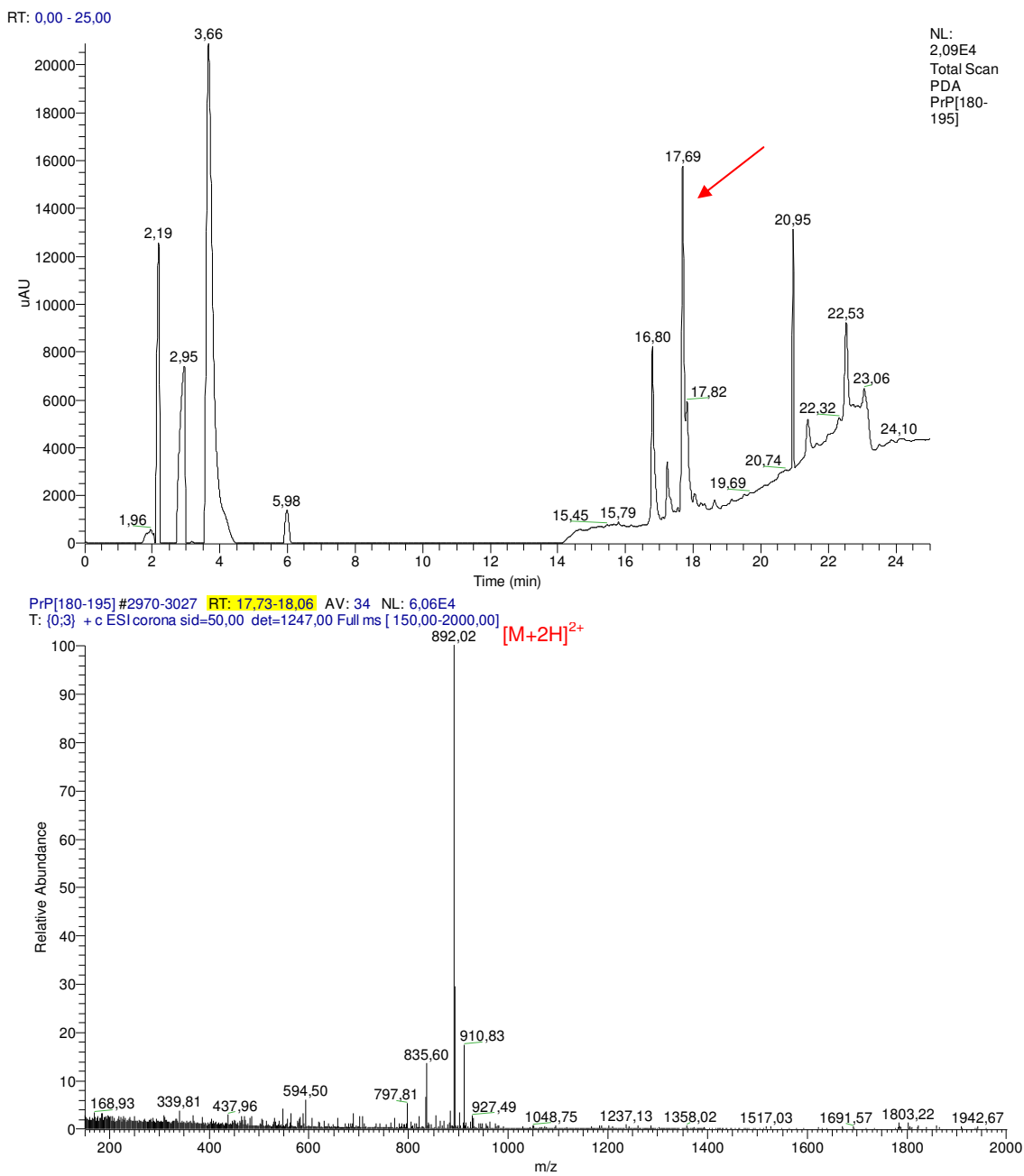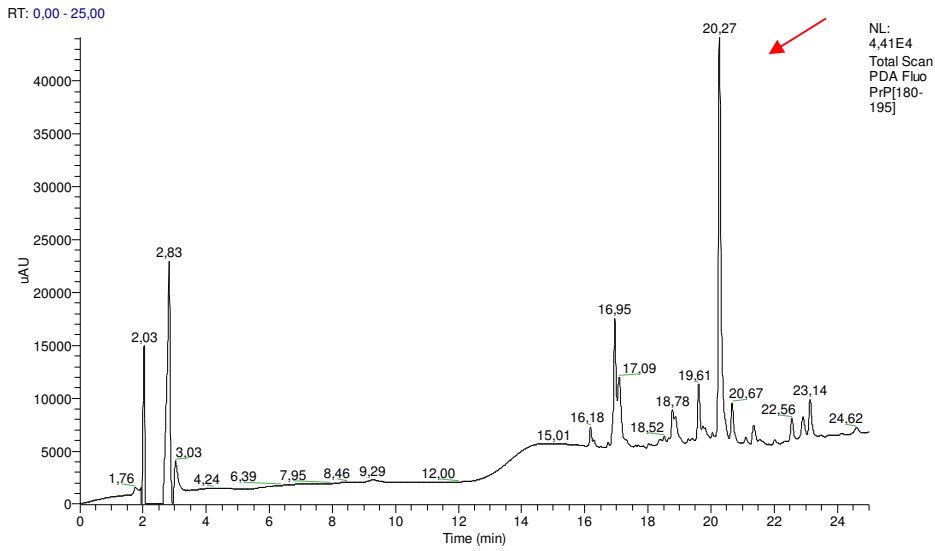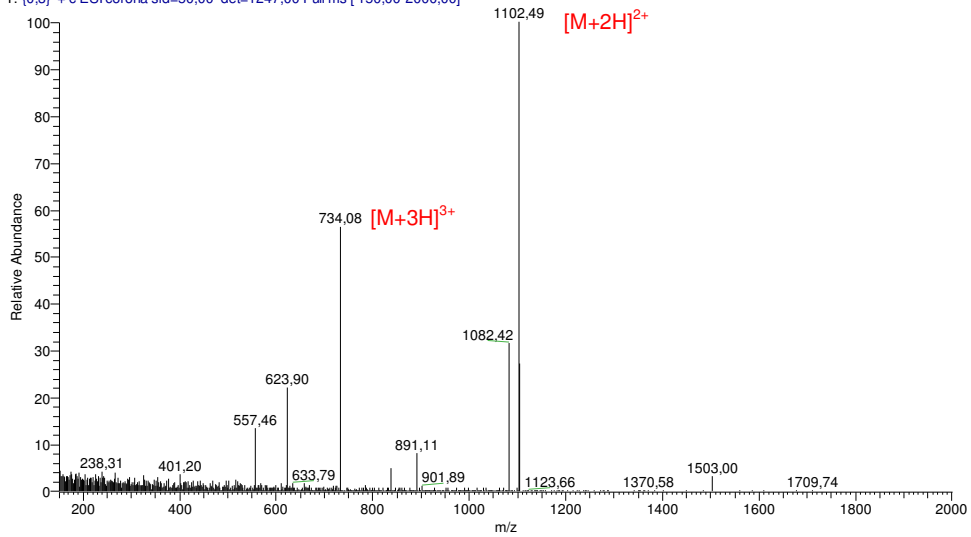
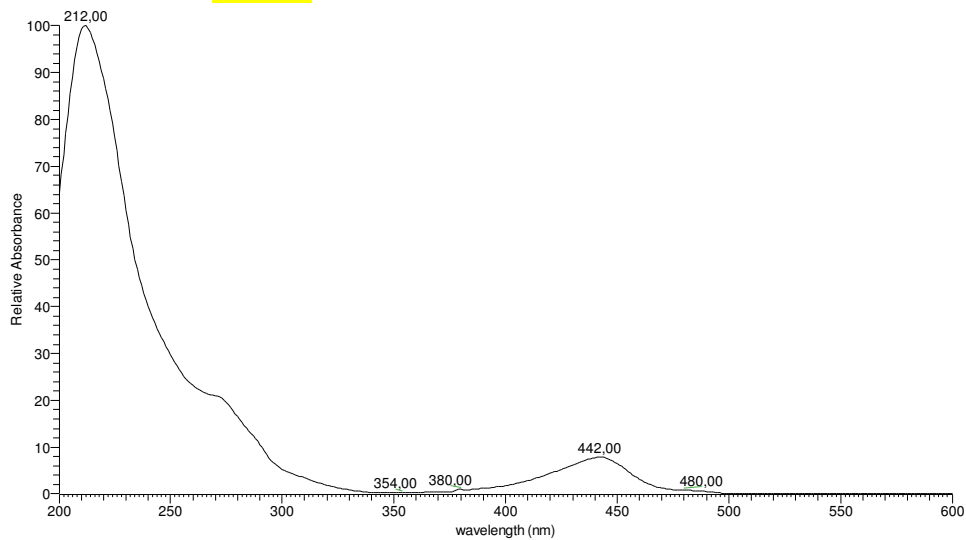**Figure VI.2.1** LC-MS profile of PrP[180-195].

Figure VI.2.2 LC-MS profile of Fluo-PrP[180-195].

Table VI.2.1 Analytical parameters of synthetic PrP peptides.

Peptide	Molecular formula	Exact mass	t_R	$[M+H]^+$	$[M+2H]^{2+}$	$[M+3H]^{3+}$	yield
PrP[173-195]	$C_{112}H_{182}N_{34}O_{36}S$	2611.32	18.8	n.d.	1306.8	871.5	14%
PrP[173-195]D178N	$C_{112}H_{183}N_{35}O_{35}S$	2610.33	18.7	n.d.	1306.2	870.9	12%
PrP[180-195]	$C_{77}H_{135}N_{23}O_{25}$	1782.0	17.7	n.d.	892.0	n.d.	13%
PrP[180-195]H187A	$C_{74}H_{133}N_{21}O_{25}$	1715.98	18.4	1717.3	858.8	n.d.	10%
PrP[173-179]	$C_{37}H_{52}N_{12}O_{12}S$	888.35	17.6	888.9	n.d.	n.d.	9%
Fluo-PrP[173-195]	$C_{135}H_{198}N_{36}O_{41}S_2$	3043.4	20.6	n.d.	1523.4	1016.3	16%
Fluo-PrP[180-195]	$C_{99}H_{149}N_{25}O_{30}S$	2200.06	20.3	n.d.	1102.5	734.1	15%
Fluo-PrP[106-126]	$C_{104}H_{155}N_{29}O_{29}S_3$	2370.07	21.7	n.d.	1185.8	790.9	8%
Fluo-βA[25-35]	$C_{69}H_{98}N_{16}O_{19}S_2$	1518.66	22.6	1518.9	760.2	n.d.	12%

Peptide constructs of Table III.5.1

The JMV compounds reported in **Table III.5.1** were synthesized by Fmoc standard chemistry on D-sized polystyrene Rink-Amide lanterns with a 35 µmol loading as schematized in **Figure III.5.2**.

Mimotope Synphase Lanterns are well adapted for combinatorial chemistry and multiple parallel synthesis. They are constituted of a rigid unreactive polymeric support grafted with a mobile phase which can be a polystyrene or polyamide copolymer. Lanterns are available with a variety of linkers (the same than conventional resin). The reaction was tracked by a visual tagging system using colored cogs and spindles.

The Fmoc deprotection step was carried out by immersing lanterns in piperidine (20% v/v in DMF) for 30 min at room temperature. One single flask with a driller topped was used. The solution was removed simply reversing the flask.

Coupling step was performed by immersing the lanterns for 90 min at room temperature in a solution containing, per lantern, 420 µL of a 0.4 M Fmoc-AA-OH solution in DMF, 420 µL of a 0.8 M DIEA solution in DMF and 420 µL of a 0.4 M HBTU solution in DMF.

Washing step after coupling or deprotection was performed by dipping the lanterns in DMF (3 x 3 min) and DCM (3 x 3 min), successively. The lanterns were allowed to air-dry for 15 min after the last DCM washing.

After the first peptide fragment assembling, different spacers were linked before continuing the second peptide fragment assembling.

On JMV3302, JMV3307, JMV3388, JMV3308 and JMV3389 were coupled different anhydrides: glutaric anhydride, succinic anhydride, phthalic anhydride, maleic anhydride and glutaric anhydride, respectively.

The anhydride coupling was performed by immersing each lantern for 2 h at room temperature in a solution containing: 420 µL of a 0.4 M anhydride solution in DMF and 420 µL of a 0.4 M DIEA solution in DMF. After the anhydride coupling, ethylenediamine was linked by dipping the lanterns for 3 h at room temperature in a solution containing, per lantern: 350 µL of a 0.1 M N-Fmoc-ethylenediamine solution in DMF, 350 µL of a 0.2 M DIEA solution in DMF and 350 µL of a 0.1 M BOP solution in DMF.

On JMV3390 and JMV3391 were coupled N-Fmoc protected 4-(Aminomethyl)benzoic acid and 4-(Aminophenyl)acetic acid, respectively. This coupling was performed by immersing each lantern for 2 h at room temperature in a

solution containing: 420 µL of a 0.2 M N-Fmoc protected acid solution in DMF, 420 µL of a 0.4 M DIEA solution in DMF and 420 µL of a 0.2 M BOP solution in DMF.

After the second peptide fragment assembling, acetylation was carried out by immersing the lanterns in acetic anhydride (50% v/v in DCM). The JMV peptide constructs were then cleaved from the lanterns using 2.5 mL per lantern of a solution of TFA/TIS/H_2O (90:5:5, v/v/v) for 2 h. The TFA solution was reduced under nitrogen flow and the cleaved compound was precipitated in cold diethyl ether, washed with cold diethyl ether and then air dried. In **Figure VI.2.3** and **VI.2.4** are representatively reported the LC-MS profiles of JMV3389 and JMV3391. In **Table VI.2.2** are listed, per peptide: the molecular formula and the exact mass, the retention time (t_R) and the masses (derived from the LC-MS analyses) and the yield of peptide after purification.
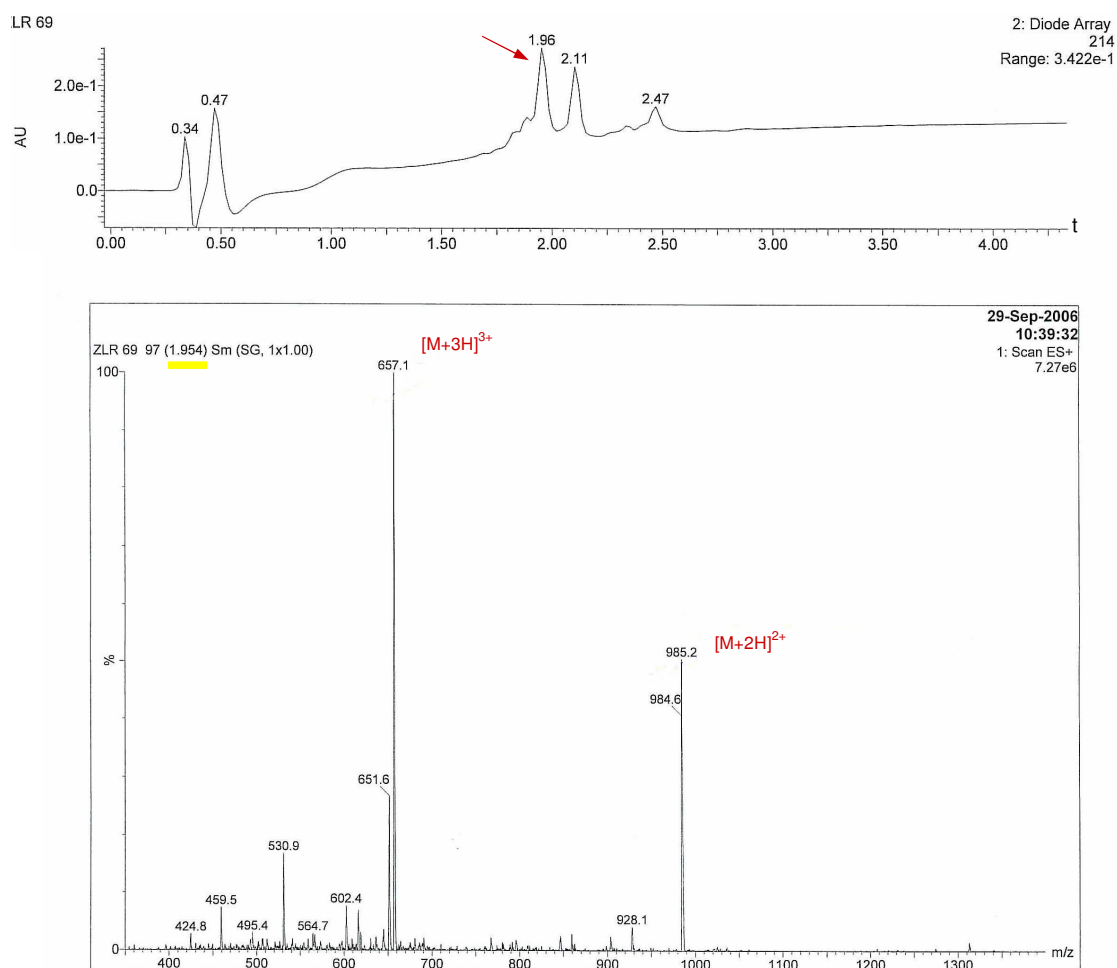
Figure VI.2.3. LC-MS profile of JMV3389.
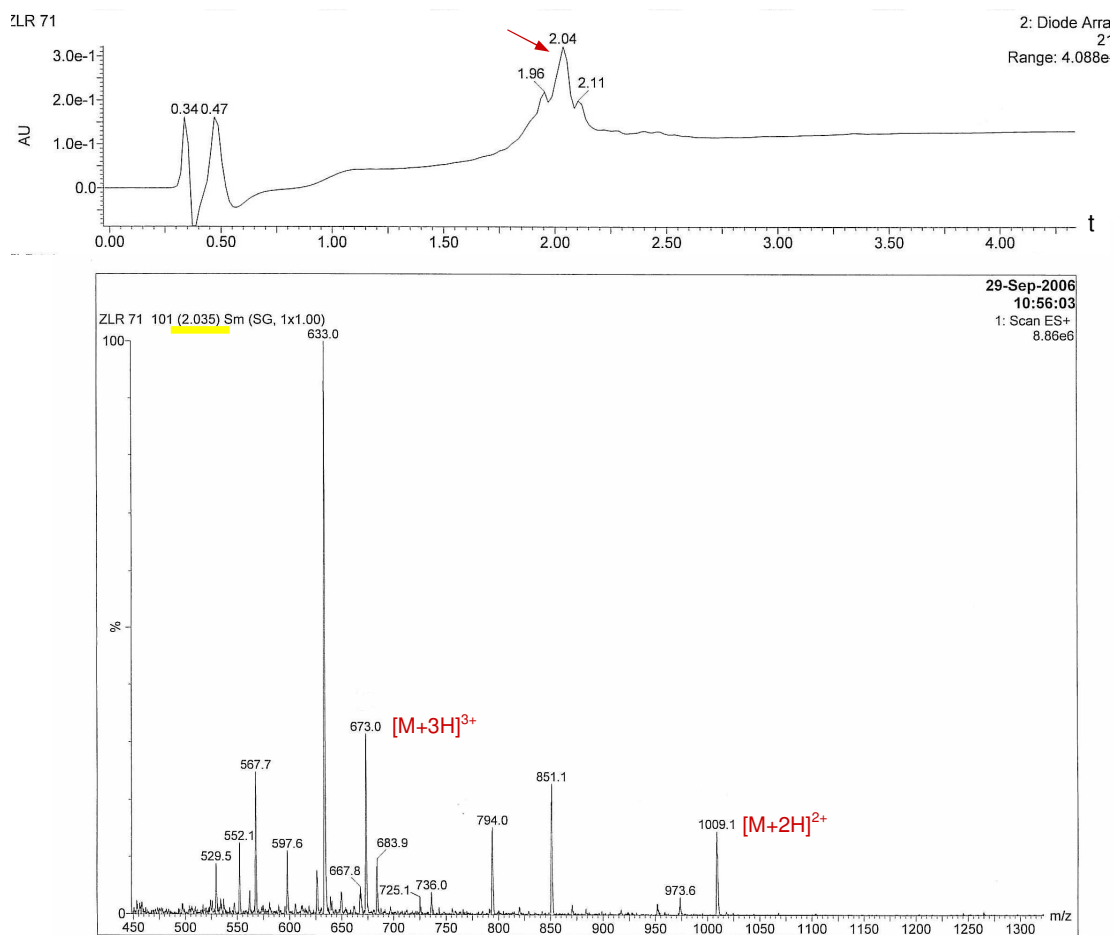
Figure VI.2.4 LC-MS profile of JMV3391.

Table VI.2.2 Analytical parameters of JMV synthetic peptide constructs.

Peptide constructs	Molecular formula	Exact mass	t_R	$[M+2H]^{2+}$	$[M+3H]^{3+}$	yield
JMV3302	$C_{84}H_{137}N_{25}O_{23}S$	1896.00	1.99	949.58	633.34	10%
JMV3307	$C_{83}H_{135}N_{25}O_{23}S$	1881.99	2.02	942.6	628.5	13%
JMV3388	$C_{87}H_{135}N_{25}O_{23}S$	1929.99	2.17	966.5	644.6	12%
JMV3308	$C_{83}H_{133}N_{25}O_{23}S$	1879.97	2.07	941.46	628.01	9%
JMV3389	$C_{87}H_{142}N_{26}O_{24}S$	1967.04	1.96	985.2	657.1	14%
JMV3390	$C_{91}H_{142}N_{26}O_{24}S$	2015.04	2.02	1009.1	673.1	11%
JMV3391	$C_{91}H_{142}N_{26}O_{24}S$	2015.04	2.04	1009.1	673.0	13%

VI.3. *RP-HPLC Peptide Purification*

The crude peptides were purified by a Shimadzu LC system equipped with a LC-8A pumps model and a SPD-10AV diode array detector, using a Phenomenex Jupiter C18 column (250 X 21.2 mm, 15 µm, 300 Å). A flow rate of 20 mL/min and a linear gradient from 5% to 70% of B over 30 min were used. Eluent A, water (0.1% TFA); eluent B, acetonitrile (0.1% TFA).

VI.4. *LC-MS characterization*

The identity and purity of peptides reported in **Table II.1** were confirmed by LC-MS mass analysis using a Finnigan Mass spectrometer system equipped with an electrospray ionization source and a Single Quadrupole detector. All analyses were carried out using a Phenomenex Jupiter Proteo column (150 X 2.0 mm, 4 µm, 90 Å). A flow rate of 0.2 mL/min and a linear gradient from 5% to 70% of B over 20 min were used. Eluent A, water (0.05% TFA); eluent B, acetonitrile (0.05 % TFA).
The identity and purity of JMV compounds reported in **Table III.5.1** were confirmed by LC-MS mass analysis using a Water Alliance 2690 HPLC coupled to a Micromass Platform II spectrometer equipped with an electrospray ionization source and a Triple Quadrupole detector. All analyses were carried out using a C18 column (30 X 2.1 mm, 3.5 µm, 90 Å). A flow rate of 0.6 mL/min and a gradient from 0% to 100% of B over 5 min were used. Eluent A, water (0.1% TFA); eluent B, acetonitrile (0.1% TFA).

VI.5. *UV characterization*

The concentration of peptide solutions used for CD and Fluorescence experiments were determined by UV spectroscopy by using a JASCO UV-Vis spectrophotometer V550 and a 1.0 cm pathlength quartz cell. The experimental settings were: 40 nm/min, scanning speed; 0.2 nm, data pitch; medium, response and 1.0 nm, band width.
The concentration of PrP[173-195], PrP[173-195]D178N and PrP[173-179] solutions were measured by absorbance at 257.5 nm, assuming a molar extinction coefficient of 195 M^{-1} cm^{-1} for phenylalanine [169]. The concentration of fluoresceinated peptide solutions were measured by absorbance at 482.5 nm, assuming a molar extinction coefficient of 92300 M^{-1} cm^{-1} for fluorescein [170]. The concentrations of JMV compound solutions were measured by absorbance at 275 nm, assuming a molar extinction coefficient of 1405 M^{-1} cm^{-1} for tyrosine [169].

VI.6. *CD characterization*

All CD spectra were recorded on a Jasco J-810 spectropolarimeter equipped with a thermostated water bath using 1.0 or 0.10 cm pathlength quartz cells. Each spectrum was obtained averaging three scans and converting the signal to mean residue ellipticity in units of deg cm^2 dmol^{-1} res^{-1}. The experimental settings were: 20 nm/min, scanning speed; 2.0 nm, band width; 0.2 nm, resolution; 50 mdeg, sensitivity and 4 s, response.

III.1. Paragraph

Far UV CD spectra of PrP[173-195], PrP[173-195]D178N and PrP[180-195] were recorded at room temperature, using 1.0 cm pathlength quartz cell containing 20 µM peptide dissolved in 10 mM phosphate buffer at pH 7.0.
SDS titration experiments were carried out adding to these peptide solutions small aliquots from a 12 mM SDS solution in 10 mM phosphate buffer at pH 7.0.
TFE titration experiments were performed adding to 20 µM peptide solution, at neutral pH, pure TFE (up to 50%, v/v).

III.2. Paragraph

All working solutions were prepared in Milli-Q water, adjusting the pH value by using small amounts of 0.1 M HCl or NaOH. Spectropolarimetric titrations as a function of salt concentration were carried out at 20 °C, adding small aliquots from a 200 mM salt solution to 3 µM PrP[180-195] and PrP[180-195]H187A aqueous samples in 1.0 cm pathlength quartz cells. Concentration-dependent experiments were performed at 20 °C by keeping the product of protein concentration and optical pathlength constant, which ensured that the number of molecules in the optical path was constant. In thermal experiments, PrP[180-195]H187A dissolved in 20 mM Na$_2$SO$_4$ at pH 4.5 was heated from 20 to 80 °C at the rate of 1 °C min^{-1} and recooled at the same rate. In time-dependent experiments, different amounts of PrP[180-195]H187A were dissolved in 50 mM Na$_2$SO$_4$ at pH 7.0.

III.3. Paragraph

Far UV CD spectra of PrP[173-195] and PrP[173-195]D178N were recorded at room temperature, using 1.0 cm pathlength quartz cell containing 20 µM peptide dissolved in TFE. Spectra were also collected after addition of increasing amounts of metal cations (Zn(II) and Cu(II)) up to a 10:1 metal/peptide molar ratio.

III.4. Paragraph

Far UV CD spectra of Fluo-PrP[173-195], Fluo-PrP[180-195], Fluo-PrP[106-126] and βA[25-35] were recorded at room temperature, using 1.0 cm pathlength quartz cell

containing 10 μM peptide dissolved in Milli-Q water. Spectra were also collected after addition of increasing amounts of a 0.5 mM TC solution up to a 10:1 TC/peptide molar ratio.

III.5. Paragraph

Far UV CD spectra of JMV compunds were recorded at room temperature, using 0.1 cm pathlength quartz cell containing 0.1 mM peptide dissolved in Milli-Q water.

VI.7. *NMR experiments*

All samples were prepared by dissolving each peptide at a final concentration of 2 mM in TFE_{d2}-OH (99%). NMR spectra were acquired at 300 K on a 600 MHz Bruker DRX spectrometer. ^{1}H-^{13}C HSQC [171], ^{1}H TOCSY [172], NOESY [173], double quantum filtered COSY [174] and ^{1}H-^{15}N HSQC spectra were used for resonance assignments. The H_2O solvent resonance was suppressed using the WATERGATE pulse sequence [175]. NOESY mixing times were set at 200, 300 and 400 ms to follow the NOE build-up rates. 2D-TOCSY experiments were recorded with mixing times of 30 and 70 ms. Data were typically apodized with a Gaussian window function and zero-filled to 1 K in f1 prior to Fourier transform. NMRPipe [176] and NMRView [177] programs were used for data processing and spectral analysis, respectively. Spin system identification and assignment of individual resonances were carried out by using a combination of TOCSY and DQF-COSY spectra. The TOCSY spectra of all peptide solutions showed well resolved resonances for almost all residues, and sequence specific assignment was obtained by the combined use of TOCSY and NOESY experiments, according to the standard procedure [178]. One-dimensional NMR spectra were also collected after the addition of small aliquots of a 0.5 M $ZnCl_2$ aqueous stock solution to the peptide solution.

VI.8. *Structure calculations*

NOESY spectra at 300 ms mixing time were used for the integration of NOE cross-peaks. Peak integrals were evaluated by NMRView, transferred to the program package DYANA 1.0.6 [179], and converted to upper distance limits by using the CALIBA [180] module of DYANA. Distance constraints were then worked out by the GRIDSEARCH module to generate a set of allowed dihedral angles. Structure calculation was carried out with the macro ANNEAL module by torsion angle dynamics. Eighty structures were calculated by TSSA, starting with a total of 10,000 MD steps and a default value of maximum temperature. The thirty best structures in terms of target functions were considered. A total of 193, 150 and 118 distance restraints were used for structure calculation of PrP[173-195], PrP[173-195]D178N, and PrP[180-195], respectively. These restraints, derived from inter-residue, sequential and medium range NOEs, were introduced in SA torsion space calculation

performed by DYANA package. The best thirty structures in terms of root mean square deviation (RMSD) were selected from 80 structures sampled in TSSA calculations.

VI.9. *Neurotoxicity tests*

B104 neuroblastoma cells derived from rat central nervous system [144] were grown at 37°C, 5% CO_2, in Dulbecco's modified Eagle's medium, 1 g/L glucose, supplemented with 10% fetal bovine serum (FBS), 1.0 mM Na-piruvate, 2.0 mM glutamine and antibiotics (penicillin/streptomycin 5000 U/ 5 mg mL) [181].
Neuroblastoma cells were plated into 96-well trays and, after a day, peptides were added to the culture medium with increasing concentrations from 0 to 55 µM. Cell survival was determined after 18, 24, 48 h of incubation. MTT (5mg/mL) was added to cell culture for 3 h at 37°C. The MTT formazan product was released from cells by addition of dymethilsulfoxide and measured spectrophotometrically at 570 nm [182]. Percent of survival was assessed by comparison with untreated cultures (control). The FC_{50} (defined as the 50% fatal concentration) after 48 h exposure were estimated by testing peptides over a broad range of concentrations from 0 to 240 µM. FC_{50} values were determined by Hill plot analysis. Results of MTT tests were reported as means of three experiments with three replicates for each one and analysed by GraphPad Prism 4 software. Comparison of treated cultures versus control condition was performed by means of one way-ANOVA (Tukey's multiple comparison).

VI.10. *Fluorescence spectroscopy*

The fluorimetric titrations relating to the peptides reported in **Table II.1(B)** were carried out at room temperature using a Varian Cary Eclipse fluorescence spectrophotometer and 482 nm exciting wavelenght, with 5-nm excitation and emission bandwidths. All titrations were carried out at least thrice and the obtained values averaged before using them in calculations. Then, modifications of the fluorescein emission intensity were recorded at 520 nm and best fitted to a hyperbolic curve.

III.4. Paragraph

TC (10 µM) was added to a fixed volume of 100 nM aqueous solutions of Fluo-PrP[173-195] or Fluo-PrP[180-195]. TC, in the same conditions, was also added to 100 nM solutions of the peptides Fluo-βA[25-35] and Fluo-PrP[106-126], used as negative control. The fluorescence intensities were used to evaluate the fraction of TC bound by α=ΔF/ΔF$_{max}$, where ΔF is the fluorescence change observed after each

addition and ΔF_{max} refers to 100% binding. Then, the apparent dissociation constant (K_D') was evaluated by the equation:

$$\alpha=\{K_D'+P_0+T_0-[(K_D'+P_0+T_0)^2-4P_0T_0]^{1/2}\}/2P_0.$$

Here, P_0 and T_0 stand for the initial concentration of peptide and the concentration of added TC, respectively. This equation describes one-site binding equilibrium [183,184] and we assume this hold true for all our systems.

III.5. Paragraph

JMV compounds (10 µM) were added to a fixed volume of 100 nM aqueous solution of Fluo-PrP[173-195]. To evaluate the K_D' of each Fluo-PrP[173-195]/JMV complex was followed the same procedure previously described.

VI.11.   *Computational analyses*

TC can exist in different tautomeric forms differing in their protonation state [185]. In **Figure VI.11.1**, a schematic structure of the antibiotic is reported in its neutral form. Thus, it is important to verify that our computational results do not depend on the selected protonation state of TC. We, therefore, performed all our computational analyses (docking calculations and MD simulations) for two different TC tautomers: the zwitterionic form (TC^{zw}), which according to the existing experimental indications [185] should be predominant at pH ~7, and the 'neutral' one (i.e., not exhibiting any formal charge separation, TC^n), which according to a very recent quantum mechanical study has similar stability to TC^{zw} [186].
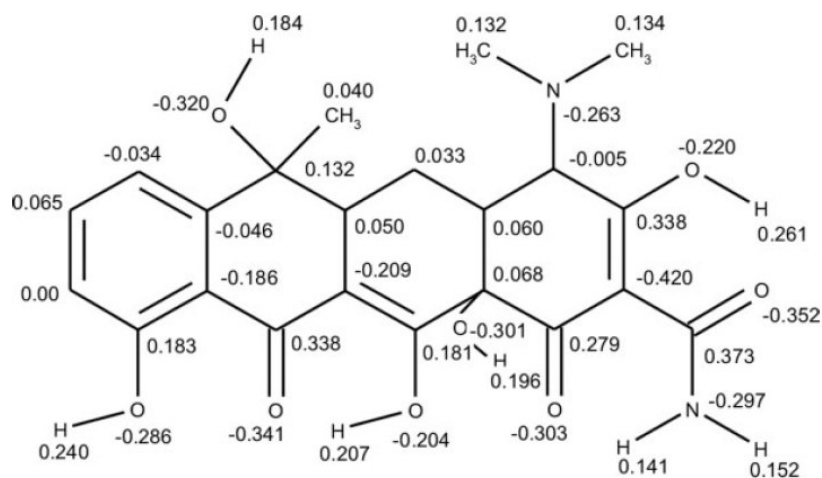
Figure VI.11.1 The chemical structure of tetracycline in the non-zwitterionic form TC^n. Partial MNDO atomic charges (in a.u.) are also reported.

Docking analysis

The AutoDock 3.0 program package [187] was employed for the generation of complexes between the prion fragment and the TC ligand in both its zwitterionic (TC^{zw}) and neutral (TC^n) forms. TC coordinates were extracted from X-ray structure of the complex with the Tet-repressor [188] hydrogens and charges were added using InsightII (semi-empirical MNDO calculations were used to compute charges) (INSIGHTII, 1998), whereas its active torsions were defined by the Auto- Tors tool of the AutoDock package. Affinity grids were generated with 0.55 Å spacing by the AutoGrid program for the whole protein target using the Lennard–Jones parameters supplied with the program. The Lamarckian genetic algorithm and the pseudo- Solis and Wets methods were used for the conformational search. One-hundred runs were performed with a maximum number of generations of 10 million per run. The parameters used were chosen according to the study by Hetényi and van der Spoel [189] proposing a docking procedure without prior knowledge of the binding site. The resultant docked conformations of the ligand were clustered and ranked according to the default AutoDock scoring function.

MD simulations

Both the PrP[173-195] fragment alone and the PrP [173-195] docked to TC^{zw} and to TC^n tautomers were studied by means of MD simulations. The starting structures of MD simulations on the PrP[173-195]/TC complexes were chosen according to Auto-Dock results: TC^{zw} is placed like in Rank 3 and TC^n like in Rank 1, since they represent the most populated clusters of complexes for TC^{zw} and TC^n, respectively (see **Table III.4.1**). However, the distances between TC and PrP[173-195] have been slightly increased (translation of about 2.5 Å in the direction perpendicular to the helix axis) with respect to the AutoDock results to decrease the bias on the MD results due to the choice of the starting structure. Coordinates of the prion fragment PrP[173-195] were extracted from the NMR [14] structure of human PrP[125-228] (PDB entry 1QLX). TC coordinates were extracted from X-ray structure of the complex [188] whereas topological parameters required to undertake the MD study were generated by PRODRG program [190] that uses the GROMOS87 force field. Simulations were performed at constant temperature within a fixed-volume box filled with SPC [191] water molecules by using periodic boundary conditions. The net charges of the three systems were compensated by adding 1 Cl^- ion. Simulations include around 4800 (box size 50 x 34 x 34) and 5300 (box size 51 x 35 x 32) atoms in the case of the fragment alone or the complexes, respectively. The temperature was kept constant at 300 K using the isothermal Gaussian temperature coupling [192]. LINCS [193] was used to constrain bond lengths, allowing a time step of 2 fs. The particle mesh Ewald method [194, 195] (grid spacing of 0.12 nm) was used for electrostatic calculations, thus properly accounting for long-range interactions. A nonbonded cutoff of 0.9 nm for Lennard–Jones potential was used. For all the systems, the solvent was relaxed by energy minimization, followed by 15 ps of MD at 300 K, while restraining protein atomic positions with a harmonic potential. The systems were then minimized without restraints and their temperature brought to 300 K in a stepwise manner: 15-ps-long MD runs were carried out at 50, 100, 200, 250, and 300 K before the production runs

were started at 300 K. Subsequently all the systems were simulated for 10 ns. For each one of the systems, other two independent MD simulations were performed by using different random seed generator numbers during the free dynamic. GROMACS simulation package [196] was employed to perform the MD simulations, and a modification of gromos87 force field [197-199] was used. INSIGHTII (Accelrys) and MOLMOL [200] programs were used for model manipulation, visual analysis, and figure production.

VII. REFERENCES

[1]   Carrel, R.W. and Lomas, D.A. (1997) Lancet, 350, 134-138.
[2]   Temussi, P.A., Masino, L. and Pastore, A. (2003) EMBO J., 22, 355-361.
[3]   Blake, C. and Serpell, L. (1996) Structure, 4, 989-998.
[4]   Thompson, A., White, A.R., McLean, C., Masters, C.L., Cappai, R. and Barrow, C.J. (2000) J. Neurosci. Res., 62, 293-301.
[5]   Booth, D.R., Sunde, M., Bellotti, V., Robinson, C.V., Hutchinson, W.L., Fraser, P.E., Hawkins, P.N., Dobson, C.M., Radford, S.E., Blake, C.C. and Pepys, M.B. (1997) Nature, 385, 787-793.
[6]   Tan, S.Y. and Pepys, M.B. (1994) Histopathology, 25, 403-414.
[7]   Sunde, M., Serpell, L.C., Bartlam, M., Fraser, P.E., Pepys, M.B. and Blake, C.C. (1997) J. Mol. Biol., 273, 729-739.
[8]   Prusiner, S.B. (1998) Proc. Natl. Acad. Sci. USA, 95, 13363-13383.
[9]   Collinge, J. and Rossor, M. (1996) Lancet, 347, 916-917.
[10] Collee, J.G. (1996) Lancet, 347, 917-918.
[11] Stahl, N., Borchelt, D.R., Hsiao, K. and Prusiner, S.B. (1987) Cell, 51, 229-240.
[12] Chesebro, B., Trifilo, M., Race, R., Meade-White, K., Teng, C., LaCasse, R., Raymond, L., Favara, C., Baron, G., Priola, S., Caughey, B., Maslian, E. and Oldstone, M. (2005) Science, 308, 1435-1439.
[13] Bosques, C.J. and Imperiali, B. (2003) Proc. Natl. Acad. Sci. USA, 100, 7593-7598.
[14] Zahn, R., Liu, A., Lührs, T., Riek, R., von Schroetter, C., Garcia, F.L., Billeter, M., Calzolai, L., Wider, G. and Wüthrich, K. (2000) Proc. Natl. Acad. Sci. USA, 97, 145-150.
[15] Garcia, F.L., Zahn, R., Riek, R. and Wüthrich, K. (2000) Proc. Natl. Acad. Sci. USA, 97, 8334-8339.
[16] Perez, D.R. and Wüthrich, K. (2005) J. Biomol. NMR, 31, 259-260.
[17] Calzolai, L., Lysek, D.A., Perez, D.R., Güntert, P. and Wüthrich, K. (2005) Proc. Natl. Acad. Sci. USA, 102, 651-655.
[18] Lysek, D.A., Schorn, C., Nivon, L.G., Esteve-Moya, V., Christen, B., Calzolai, L., von Schroetter, C., Fiorito, F., Herrmann, T., Güntert, P. and Wüthrich, K. (2005) Proc. Natl. Acad. Sci. USA, 102, 640-645.
[19] Gossert, A.D., Bonjour, S., Lysek, D.A., Fiorito, F. and Wüthrich, K. (2005) Proc. Natl. Acad. Sci. USA, 102, 646-650.
[20] Riek, R., Hornemann, S., Wider, G., Billeter, M., Glockshuber, R. and Wüthrich, K. (1996) Nature, 382, 180-182.
[21] Knaus, K.J., Morillas, M., Swietnicki, W., Malone, M., Surewicz, W.K. and Yee, V.C. (2001) Nat. Struct. Biol., 8, 770–774.
[22] Jackson, G.S., Hosszu, L.L.P., Power, A., Hill, A.F., Kenney, J., Saibil, H., Craven, C.J., Waltho, J.P., Clarke, A.R. and Collinge, J. (1999) Science, 283, 1935-1937.
[23] Shaked, G.M., Shaked, Y., Kariv-Inbal, Z., Halimi, M., Avraham, I. and Gabizon, R. (2001) J. Biol. Chem., 276, 31479-31482.
[24] Pan, K.-H., Baldwin, M., Nguyen, J., Gasset, M., Serban, A., Groth, D., Mehlhorn, I., Huang, Z., Fletterick, R.J., Cohen, F.E. and Prusiner, S.B. (1993) Proc. Natl. Acad. Sci. USA, 90, 10962-10966.
[25] Huang, Z., Prusiner, S.B. and Cohen, F.E (1996) Fold. Des., 1, 13-19.

[26] Frankenfield K.N., Powers E.T., Kelly J.W. (2005) Protein. Sci., 14, 2154–2166.

[27] Cordeiro Y., Kraineva J., Gomes M.P., Lopes M.H., Martins V.R., Lima L.M., Foguel D., Winter R., Silva J.L. (2005) Biophys. J., 89, 2667–2676.

[28] Forloni G., Angeretti N., Chiesa R., Monzani E., Salmona M., Bugiani O., Tagliavini F. (1993) Nature, 362, 543–546.

[29] Fioriti, L., Quaglio, E., Massignan, T., Colombo, L., Stewart, R.S., Salmona, M., Harris, D.A., Forloni, G. and Chiesa, R. (2005) Mol. Cell. Neurosci., 28, 165-176.

[30] Jobling, M.F., Stewart, L.R., White, A.R., McLean, C., Friedhuber, A., Maher, F., Beyreuther, K., Master, C.L., Barrow, J., Collins, S.J. and Cappai, R. (1999) J. Neurochem., 73, 1557-1565.

[31] Gu Y., Fujioka H., Mishra R.S., Li R., Singh N. (2002) J. Biol. Chem., 277, 2275–2286.

[32] Haire, L.F., Whyte, S.M., Vasisht, N., Gill, A.C., Verma, C., Dodson, E.J., Dodson, G.G. and Bayley, P.M. (2004) J. Mol. Biol., 336,1175-1183.

[33] Swietnicki, W., Petersen, R., Gambetti, P. and Surewicz, W.K. (1997) J. Biol. Chem., 272, 27517-27520.

[34] Hornemann, S. and Glockshuber, R. (1998) Proc. Natl. Acad. Sci. USA, 95, 6010-6014.

[35] Swietnicki, W., Morillas, M., Chen, S.G., Gambetti, P. and Surewicz, W.K. (2000) Biochemistry, 39, 424-431.

[36] Zou, W.-Q. and Cashman, N.R. (2002) J. Biol. Chem., 277, 43942-43947.

[37] Langella, E., Improta, R. and Barone, V. (2004) Biophys. J., 87, 3623-3632.

[38] Borchelt, D.R., Taraboulos, A. and Prusiner, S.B. (1992) J. Biol. Chem., 267, 16188-16199.

[39] Wopfner, F., Weidenhöfer, G., Schneider, R., von Brunn, A., Gilch, S., Schwarz, T.F., Werner, T. and Schätz, H.M. (1999) J. Mol.Biol., 289, 1163-1178.

[40] Minor, D.L. Jr. and Kim, P.S. (1994) Nature, 367, 660-663.

[41] Welker, E., Raymond, L.D., Scheraga, H.A. and Caughey, B. (2002) J. Biol. Chem., 277, 33477-33481.

[42] Liu, A., Riek, R., Zahn, R., Hornemann, S., Glockshuber, R. and Wutrich, K. (1999) Biopolymers, 51, 145-152.

[43] Ziegler, J., Sticht, H., Marx, U.C., Muller, W., Rosch, P. and Schwarzinger, S. (2003) J. Biol. Chem., 278, 50175-50181.

[44] Gallo, M., Paludi, D., Cicero, D.O., Chiovitti, K., Millo, E., Salis, A., Damonte, G., Corsaro, A., Thellung, S., Schettini, G., Melino, S., Florio, T., Paci, M. and Aceto, A. (2005) Int. J. Immunopathol. Pharmacol., 18, 95-112.

[45] Winklhofer, K.F., Heske, J., Heller, U., Reintjes, A., Muranyi, I.M. and Tatzelt, J. (2003) J. Biol. Chem., 278, 14961-14970.

[46] Hirschberger, T., Stork, M., Schropp, B., Winklhofer, K.F., Tatzelt, J. and Tavan, P. (2006) Biophys. J., 90, 3908-3918.

[47] Brown, D.R., Guantieri, V., Grasso, G., Impellizzeri, G., Pappalardo, G. and Rizzarelli, E. (2004) J. Inorg. Biochem., 98, 133-143.

[48] Tizzano, B., Palladino, P., De Capua, A., Marasco, D., Rossi, F., Benedetti, E., Pedone, C., Ragone, R. and Ruvo, M. (2005) Proteins, 59, 72-79.

[49] Ikeda, K. and Higo, J. (2003) Protein Sci., 12, 2542-2548.

[50] Riek, R., Wider, G., Billeter, M., Hornemann, S., Glockshuber, R. and Wütrich, K. (1998) Proc. Natl. Acad. Sci. USA, 95, 11667–11672.

[51] Salmona, M., Morbin, M., Massignan, T., Colombo, L., Mazzoleni, G., Capobianco, R., Diomede, L., Thaler, F., Mollica, L., Musco, G., Kourie, J.J., Bugiani,

O., Sharma, D., Inouye, H., Kirshner, D.A., Forloni, G. and Tagliavini, F. (2003) J. Biol. Chem., 278, 48146-48153.

[52] Brown, D.R., Qin, K., Herms, J.W., Madlung, A., Manson, J., Strome, R., Fraser, P.E., Kruck, T., von Bohlen, A., Schulz- Schaeffer, W., Giese, A., Westaway, D. and Kretzschmar, H. (1997) Nature, 390, 684-687.

[53] Millhauser, G.L. (2004) Acc. Chem. Res., 37, 79-85.

[54] Millhauser, G.L. (2007) Annual Review of Physical Chemistry, 58, 299–320.

[55] Jackson, G.S., Murray, I., Hosszu, L.L.P., Gibbs, N., Waltho, J.P., Clarke, A.R. and Collinge, J. (2001) Proc. Natl. Acad. Sci. USA, 98, 8531-8535.

[56] Stöckel, J., Safar, J., Wallace, AC., Cohen, FE. and Prusiner, SB. (1998) Biochemistry, 37, 7185-7193.

[57] Miura, T., Hori-I, A., Mototani, H. and Takeuchi, H. (1999) Biochemistry, 38, 11560-11569.

[58] Bonomo, R.P., Impellizzeri, G., Pappalardo, G., Rizzarelli, E. and Tabbì, G. (2000) Chemistry, 6, 4195-4202.

[59] Cereghetti, G.M., Schweiger, A., Glockshuber, R. and Van Doorslaer, S. (2001) Biophys. J., 81, 516-525.

[60] Luczkowski, M., Kozlowski, H., Stawikowski, M., Rolka, K., Gaggelli, E., Valensin, D. and Valensin, G. (2002) J. Chem. Soc. Dalton Trans., 2269-2274.

[61] Hasnain, S.S., Murphy, L.M., Strange, R.W., Grossmann, J.G., Clarke, A.R., Jackson, G.S. and Collinge, J. (2001) J. Mol. Biol., 311, 467-473.

[62] Pushie, M.J. and Rauk, A. (2003) J. Biol. Inorg. Chem., 8, 53-65.

[63] Van Doorslaer, S., Cereghetti, G.M., Glockshuber, R. and Schweiger, A. (2001) J. Phys. Chem. B, 105, 1631-1639.

[64] Jobling, M.F., Huang, X., Stewart, L.R., Barnham, K.J., Curtain, C., Volitakis, I., Perugini, M., White, A.R., Cherny, R.A., Masters, C.L., Barrow, C.J., Collins, S.J., Bush, A.I. and Cappai R. (2001) Biochemistry, 40, 8073-8084.

[65] Hornshaw, M.P., McDermott, J.R. and Candy, J.M. (1995) Biochem. Biophys. Res. Commun., 214, 621-629.

[66] Hornshaw, M.P., McDermott, J.R., Candy, J.M. and Lakey, J.H. (1995) Biochem. Biophys. Res. Commun., 214, 993-999.

[67] Aronoff-Spencer, E., Burns, C.S., Avdievich, N.I., Gerfen, G.J., Peisach, J., Antholine, W.E., Ball, H.L., Cohen, F.E., Prusiner, S.B. and Millhauser, G.L. (2000) Biochemistry, 39, 13760-13771.

[68] Burns, C.S., Aronoff-Spencer, E., Dunham, C.M., Lario, P., Avdievich, N.I., Antholine, W.E., Olmstead, M.M., Vrielink, A., Gerfen, G.J., Peisach, J., Scott, W.G. and Millhauser, G.L. (2002) Biochemistry, 41, 3991-4001.

[69] Lippard, S.J. and Berg, J.M. (1994) Principles of Bioinorganic Chemistry, University Science Books, Mill Valley, CA.

[70] Freeman H.C. (1966) in The Biochemistry of Copper (Peisach, J., Aisen, P., Blumberg, W.E., Eds.). pp. 77-113. Academic Press, New York.

[71] Bryce, G.F. and Gurd, F.R.N. (1966) J. Biol. Chem., 241, 122-129.

[72] Sundberg, R.J. and Martin, R.B. (1974) Chem. Rev., 74, 471-517.

[73] Kramer, M.L., Kratzin, H.D., Schmidt, B., Römer, A., Windl, O., Liemann, S., Hornemann, S. and Kretzschmar, H. (2001) J. Biol. Chem., 276, 16711-16719.

[74] Qin, K., Yang, Y., Mastrangelo, P. and Westaway, D. (2002) J. Biol. Chem., 277, 1981-1990.

[75] Burns, C.S., Aronoff-Spencer, E., Legname, G., Prusiner, S.B., Antholine, W.E., Gerfen, G.J., Peisach, J. and Millhauser, G.L. (2003) Biochemistry, 42, 6794-6803.

[76] Quaglio, E., Chiesa, R. and Harris, D.A. (2001) J. Biol. Chem., 276, 11432-11438.

[77] Ricchelli, F., Buggio, R., Drago, D., Salmona, M., Forloni, G., Negro, A., Tognon, G. and Zatta, P. (2006) Biochemistry, 45, 6724-6732.

[78] Cereghetti, G.M., Schweiger, A., Glockshuber, R. and van Doorslaer, S. (2003) Biophys. J., 84, 1985-1997.

[79] Cervenakova, L., Buetefisch, C., Lee, H.S., Taller, I., Stone, G., Gibbs, C.J. Jr., Brown, P., Hallett, M. and Goldfarb, L.G. (1999) Am. J. Med. Genet., 88, 653-665.

[80] Bütefisch, C.M., Gambetti, P., Cervenakova, L., Park, K.-Y., Hallett, M. and Goldfarb, L.G. (2000) Neurology, 55, 517-522.

[81] Harris, D.A.(2003) Br. Med. Bull., 66, 71-85.

[82] Campana, V., Sarnataro, D. and Zurzolo, C. (2005) Trends Cell Biol., 15, 102-111.

[83] Collins, J.S., Lawson, V.A. and Masters, C.L. (2004) The Lancet, 363, 51-61.

[84] Peters, P.J., Mironov, A.Jr., Peretz, D., van Donselaar, E., Leclerc, E., Erpel, S., DeArmond, S.J., Burton, D.R., Williamson, R.A., Vey, M. and Prusiner, S.B. (2003) J. Cell. Biol., 162, 703–717.

[85] Harris, D.A. (1998) Bull. Inst. Pasteur, 96, 207–210.

[86] Shyng S.L., Heuser, J.E. and Harris, D.A. (1994) J. Cell. Biol., 125, 1239–1250.

[87] Caughey, B., Raymond, G.J., Ernst, D. and Race, R.R. (1991) J. Virol., 65, 6597–6603.

[88] Ivanova, L., Barmada, S., Kummer, T. and Harris, D.A. (2001) J. Biol. Chem., 276, 42409–42421.

[89] Baron, G.S., Wehrly, K., Dorward, D.W., Chesebro, B. and Caughey, B. (2002) Embo J., 21, 1031–1040.

[90] Yedidia, Y., Horonchik, L., Tzaban, S., Yanai, A. and Taraboulos, A. (2001) EMBO J., 20, 5383–5391.

[91] Drisaldi, B., Stewart, R.S., Adles, C., Stewart, L.R., Quaglio, E., Biasini, E., Fioriti, L., Chiesa, R. and Harris, D.A. (2003) J. Biol. Chem., 278, 21732–21743.

[92] Ma, J., Wollmann, R. and Lindquist, S. (2002) Science, 298, 1781–1785.

[93] Ma, J. and Lindquist, S. (2002) Science, 298, 1785–1788.

[94] Kocisko, D.A., Come, J.H., Priola, S.A., Chesebro, B., Raymond, G.J., Lansbury, P.T., and Caughey, B. (1994) Nature, 370, 471–474.

[95] Farquhar, C.F. and Dickinson, A.G. (1986) J. Gen. Virol., 67, 463–473.

[96] Kimberlin, R.H. and Walker, C.A. (1986) Antimicrob. Agents Chemother., 30, 409–413.

[97] Caughey, B. and Raymond, G.J. (1993) J. Virol., 67, 643–650.

[98] May, B.C.H., Fafarman, A.T., Hong, S.B., Rogers, M., Deady, L.W., Prusiner, S.B. and Cohen, F.E. (2003) Proc. Natl. Acad. Sci. USA, 100, 3416–3421.

[99] Barret, A., Tagliavini, F., Forloni, G., Bate, C., Salmona, M., Colombo, L., DeLuigi, A., Limido, L., Suardi, S., Rossi, G., Auvré, F., Adjou, K.T., Salès, N. Williams, A., Lasmézas, C. and Deslys, J.P. (2003) J. Virol., 77, 8462–8469.

[100] Caughey, W.S., Raymond, L.D., Motohiro, H. and Caughey, B. (1998) Proc. Natl. Acad. Sci. USA, 95, 12117–12122.

[101] Lorenzo, A. and Yankner, B.A (1994) Proc. Natl. Acad. Sci. USA, 91, 12243–12247.

[102] Poli, G., Ponti, W., Carcassola, G., Ceciliani, F., Colombo, L., Dall'Ara, P., Gervasoni, M., Giannino, M.L., Martino, P.A., Pollera, C., Villa, S. and Salmona, M. (2003) Arzneimittelforschung, 53, 875–888.

[103] Adjou, K.T., Privat, N., Demart, S., Deslys, J.P., Seman, M., Hauw, J.J. and Dormont, D. (2003) J. Comp. Pathol., 122, 3–8.

[104] Supattapone, S., Nguyen, H.O., Cohen, F.E., Prusiner, S.B. and Scott, M.R. (1999) Proc. Natl. Acad. Sci. USA, 96, 14529–14534.

[105] Supattapone, S., Wille, H., Uyechi, L., Safar, J., Tremblay, P., Szoka, F.C., Cohen, F.E., Prusiner, S.B. and Scott, M.R. (2001) J. Virol., 75, 3453–3461.

[106] Soto, C., Saborio, G.P.and Permanne, B. (2000) Acta Neurol. Scand. Suppl., 176, 90–95.

[107] Forloni, G., Varí, M.R., Colombo, L., Bugiani, O., Tagliavini, F. and Salmona, M. (2003) Curr. Med. Chem.-Imun., Endoc. and Metab. Agents, 3: 185-197.

[108] Chopra, I. and Roberts, M. (2001) Microbiol. Mol. Biol. Rev., 65, 232-260.

[109] Mitscher, L.A. (1978) Medicinal Research Series, vol. 9. The chemistry of antibiotics. Marcel Dekker, New York.

[110] de Leenheer, A.P. and Nelis, H.J.C.F. (1979) J. Pharma. Sci., 68, 999-1002.

[111] Tavares, M.F.M. and McGuffin, V.L. (1994.) J. Chromatogr. A., 686, 129–142.

[112] Sande, M.A. and Mandell, G.L. (1990) Tetracyclines, chloramphenicol, erythromicin and miscellaneous antibacterial agents. In Goodman Gilman A., Rall, T.W., Nies, A.S., Taylor, P. (eds) The pharmacological basis of therapeutics, 8th edn. Pergamon Press, New York, 1117-1145.

[113] Tagliavini, F., Forloni, G., Colombo, L., Rossi, G., Girala, L., Canciani, B., Angeretti, N., Giampaolo, L., Peressini, E., Awan, T., De Gioia, L., Ragg, E., Bugiani, O. and Salmona, M. (2000) J. Mol. Biol., 300, 1309–1322.

[114] Forloni, G., Del Bo, R., Angeretti, N., Chiesa, R., Smiroldo, S., Doni, R., Ghigaudi, E., Salmona, M., Porro, M., Verga, L., Giccone, G., Bugiani, O., Tagliavini, F. (1994) Eur. J. Neurosi., 6, 1415–1422.

[115] Selvaggini, C., Del Gioia, L., Cantù, L., Ghibaudi, E., Diomede, L., Passerini, F., Forloni, G., Bugiani, O., Tagliavini, F. and Salmona, M. (1993) Biochem. Biophys. Res., 194, 1380–1386.

[116] Tagliavini, F., Prelli, F., Verga, L., Giaccone, G., Sarma, R., Gorevic, P., Ghetti, B., Passerini, F., Ghibaudi, E., Forloni, G., Salmona, M., Baggiani, O. and Frangione, B. (1993) Proc. Natl. Acad. Sci. USA, 90, 9678–9682.

[117] Brown, D., Schmidt, B. and Kretzschmar, H.A. (1996) Nature, 380, 345–347.

[118] Polymenidou, M., Heppner, F.L., Pellicioli, E.C., Urich, E., Miele, G., Braun, N., Wopfner, F., Schatzl, H.M., Becher, B. and Aguzzi, A. (2004) Proc. Natl. Acad. Sci. USA, 101, Suppl. 2, 14670–14676.

[119] Gilch, S., Wopfner, F., Renner-Muller, I., Kremmer, E., Bauer, C., Wolf, E., Brem, G., Groschup, M.H. and Schatzl, H.M. (2003) J. Biol. Chem., 278, 18524–18531.

[120] Sigurdsson, E.M., Brown, D.R., Daniels, M., Kascsak, R.J., Kascsak, R., Carp, R., Meeker, H.C., Frangione, B. and Wisniewski, T. (2002) Am. J. Pathol., 161, 13–17.

[121] Horiuchi, M. and Caughey, B. (1999) EMBO J., 18, 3193–3203.

[122] Enari, M., Flechsig, E. and Weissmann, C. (2001) Proc. Natl. Acad. Sci. USA, 98, 9295–9299.

[123] Peretz, D., Williamson, R.A., Kaneko, K., Vergara, J., Leclerc, E., Schmitt-Ulms, G., Mehlhorn, I.R., Legname, G., Wormald, M.R., Rudd, P.M., Dwek, R.A., Burton, D.R. and Prusiner, S.B. (2001) Nature, 412, 739–743.

[124] Perrier, V., Solassol, J., Crozet, C., Frobert, Y., Mourton-Gilles, C., Grassi, J. and Lehmann, S. (2004) J. Neurochem., 89, 454–463.

[125] Kim, C.L., Karino, A., Ishiguro, N., Shinagawa, M., Sato, M. and Horiuchi, M. (2004) J. Gen. Virol., 85, 3473–3482.

[126] Heppner, F.L., Musahl, C., Arrighi, I., Klein, M.A., Rulicke, T., Oesch, B., Zinkernagel, R.M., Kalinke, U. and Aguzzi, A. (2001) Science, 294, 178–182.

[127] Eghiaian, F., Grosclaude, J., Lesceu, S., Debey P., Doublet, B., Tréguer, E., Rezaei, H. and Knossow, M. (2004) Proc. Natl. Acad. Sci. USA, 101, 10254-10259.

[128] Kuznetsov, I.B. and Rackovsky, S. (2004) Protein Sci., 13, 3230-3244.

[129] Barducci, A., Chelli, R., Procacci, P. and Schettino, V. (2005) Biophys. J., 88, 1334-1343.

[130] Kiachopoulos, S., Bracher, A., Winklhofer, K.F. and Tatzelt, J. (2005) J. Biol. Chem., 280, 9320-9329.

[131] Gasset, M., Baldwin, M.A., Lloyd, D.H., Gabriel, J.-M., Holtzman, D.M., Cohen, F., Fletterick, R. and Prusiner, S.B. (1992) Proc. Natl. Acad. Sci. USA., 89, 10940-10944.

[132] Gsponer, J., Ferrara, P. and Caflisch, A. (2001) J. Mol. Graph. Model., 20, 169-182.

[133] Chou, P.Y. and Fasman, G.D. (1974) Biochemistry 13, 211-222.

[134] Collins, K.D. (1997) Biophys. J., 72, 65–76.

[135] Collins, K.D. (2004) Methods, 34, 300–311.

[136] D'Ursi, A.M., Armenante, M.R., Guerrini, R., Salvadori,S., Sorrentino, G. and Picone, D. (2004) J. Med. Chem., 47, 4231-4238.

[137] Wu, C.S., Ikeda, K. and Yang, J.T. (1981) Biochemistry, 20, 566-570.

[138] Wu, C.S. and Yang, J.T. (1981) Mol. Cell. Biochem., 40, 109-122.

[139] Zhong, L. and Johnson, W.C., Jr. (1992) Proc. Natl. Acad. Sci. USA, 89, 4462-4465.

[140] Yang, J.T., Wu, C.S.C. and Martinez, H.M. (1986) Meth. Enzymol., 130, 208-269.

[141] Nelson, J.W. and Kallenbach, N.R. (1986) Proteins, 1, 211–217.

[142] Nelson, J.W. and Kallenbach, N.R. (1989) Biochemistry, 28, 5256–5261.

[143] Merutka, G. and Stellwagen, E. (1989) Biochemistry, 28, 352–357.

[144] Schubert, D., Heinemann, S., Carlisle, W., Tarikas, H., Kimes, B., Patrick, J., Steinbach, J.H., Culp, W. and Brandt, B.L. (1974) Nature, 249, 224-227.

[145] Fülöp, L., Penke, B. and Zarándi, M. (2001) J. Pept. Sci., 7, 397-401.

[146] Langella, E., Improta, R., Crescenzi, O. and Barone, V. (2006) Proteins: Struct. Funct. Bioinform., 64, 167–177.

[147] Dima, R.I. and Thirumalai, D. (2004) Proc. Natl. Acad. Sci. USA, 101, 15335–15340.

[148] Pappalardo, M., Miliardi, D., La Rosa, C., Zannoni, C., Rizzarelli, E. and Grasso, D. (2004) Chem. Phys. Lett., 390, 511–516.

[149] Jones, D.T. (1999) J. Mol. Biol., 292, 195-202.

[150] Costantini, S., Colonna, G. and Facchiano, A.M. (2006) Biochem. Biophys. Res. Comm., 342, 441-451.

[151] Nandi, P.K. and Nicole, J.C. (2004) J. Mol. Biol., 344, 827-837.

[152] Zanusso, G., Farinazzo, A., Fiorini, M., Gelati, M., Castagna, A., Righetti, P.G., Rizzuto, N. and Monaco, S. (2001) J. Biol. Chem., 276, 377–380.

[153] Nandi, P.K., Leclerc, E. and Marc, D. (2002) Biochemistry, 41, 17–24.

[154] Zuegg, J. and Gready, J.E. (1999) Biochemistry, 38, 862–876.

[155] Wong, C., Xiong, L.W., Horiuchi, M., Raymond, L., Wehrly, K., Chesebro, B. and Caughey, B. (2001) EMBO J., 20: 377–386.

[156]   Cordeiro, Y., Machado, F., Juliano Neto, L., Juliano, M.A., Brentani, R.R., Foguel, D. and Silva, J.L. (2001) J. Biol. Chem., 276, 400-409.

[157]   Calzolai, L. and Zahn, R. (2003) J. Biol. Chem., 278, 592–596.

[158]   De Simone, A., Dodson, G.G., Verma, C.S., Zagari, A. and Fraternali, F. (2005) Proc. Natl. Acad. Sci. U.S.A., 102, 7535–7540.

[159]   Kawatake, S., Nishimura, Y., Sakaguchi, S., Iwaki, T. and Doh-ura, K. (2006) Biol. Pharm. Bull., 29, 927–932.

[160]   Niedz, R.P. and Evens, T.J. (2006) Nat. Methods, 3, 417.

[161]   Chen, Y.R., Huang, H.B., Chyan, C.L., Shiao, M.S., Lin, T.H. and Chen, Y.C. (2006) J. Biochem. (Tokyo), 139, 733–740.

[162]   Roberts, M.F. (2005) Saline Syst., 1, 1–30.

[163]   Arora, A., Ha, C. and Park, C.B. (2004) FEBS Lett., 564, 121–125.

[164]   Forloni, G., Iussich, S., Awan, T., Colombo, L., Angeretti, N., Girala, L., Bertani, I., Poli, G., Caramelli, M., Buzzone, M.G., Farina, L., Limido, L., Rossi, G., Giaccone, G., Ironside, J.W., Bugiani, O., Salmona, M. and Tagliavini, F. (2002) Proc. Natl. Acad. Sci. USA, 99, 10849–10854.

[165]   Will, R.G., Ironside, J.W., Zeidler, M., Cousens, S.N., Estibeiro, K., Alperovitch, A., Poser, S., Pocchiari, M., Hoffmann, A. and Smith, P.J. (1996) Lancet, 347, 921–925.

[166]   Collinge, J., Sidle, K.C.L., Meads, J., Ironside, J. and Hill, A.F. (1996) Nature, 383, 685–690.

[167]   Bruce, M.E., Will, R.G., Ironside, J.W., McConnell, I., Drummond, D., Suttie, A., McCardle, L., Chree, H., Hope, J., Birkett, C., Cousens, S., Fraser, H. and Bostock, C.J. (1997) Nature, 389, 498–501.

[168]   Kaiser, E., Colescott, R.L., Bossinger, C.D. and Cook, P.I. (1970) Anal. Biochem., 34, 595-598.

[169]   Fasman, G.D. (1976) Handbook of Biochem. and Mol. Biol., Proteins, 1, 183-203.

[170]   Seybold, P.G, Gouterman, M. and Callis, J. (1969) Photochem. Photobiol., 9, 229-242.

[171]   Bodenhausen, G. and Ruben, D.J. (1980) Chem. Phys. Lett., 69, 185-189.

[172]   Bax, A. and Davis, D.G. (1985) J. Magn. Res., 65, 355-360.

[173]   Jeener, J., Meyer, B.H., Bachman, P. and Ernst, R.R. (1979) J. Chem. Phys., 71, 4546-4553.

[174]   Rance, M, Sørensen, O.W., Bodenhausen, G., Wagner, G., Ernst, R.R. and Wüthrich., K. (1983) Biochem. Biophys. Res. Commun., 117, 479-485.

[175]   Piotto, M., Saudek, V., and Sklenar, V. (1992) J. Biomol. NMR, 2, 661-665.

[176]   Delaglio, F., Grzesiek, S., Vuister, G.W., Zhu, G., Pfeifer, J. and Bax, A. (1995) J. Biomol. NMR, 6, 277-293.

[177]   Johnson, B.A. and Blevins, R.A. (1994) J. Biomol. NMR, 4, 603-614.

[178]   Wüthrich, K. (1986). NMR of Proteins and Nucleic Acids. Wiley and Sons, New York.

[179]   Güntert, P., Braun, W. and Wüthrich, K. (1991) J. Mol. Biol., 217, 517-530.

[180]   Güntert, P., Mumenthaler, C. and Wüthrich, K. (1997) J. Mol. Biol., 273, 283-298.

[181]   Luo, J. and Miller, M.W. (1997) Brain Research, 770, 139-150.

[182]   Mosmann, T. (1983) J. Immunol. Meth., 65, 55-63.

[183]   Palladino, P., Pedone, C., Ragone, R., Rossi, F., Saviano, M. and Benedetti, E. (2003) Protein Pept. Lett., 10, 133–138.

[184] Ragone, R., De Luca, S., Tesauro, D., Pedone, C. and Morelli, G. (2000) Biopolymers, 56, 47–53.

[185] Pinsuwan, S., Alvarez-Nunez, F.A., Tabibi, S.E. and Yalkowsky, S.H. (1999) J. Pharm. Sci., 88, 535–537.

[186] Othersen, O.G., Beierlein, F., Lanig, H. and Clark, T. (2003) J. Phys. Chem. B., 107, 13743–13749.

[187] Morris, G.M., Goodsell, D.S., Halliday, R.S., Huey, R., Hart, W.E., Belew, R.K. and Olson, A.J. (1998) J. Comput. Chem., 19, 1639–1662.

[188] Kisker, C., Hinrichs, W., Tovar, K., Hillen, H. and Saenger, W. (1995) J. Mol. Biol., 247, 260–280.

[189] Hetenyi, C. and van der Spoel, D. (2002) Protein Sci., 11, 1729–1737.

[190] Schuettelkopf, W. and van Aalten, D.M.F. (2004) Acta Crystallogr D., 60, 1355–1363.

[191] Berendsen, H.J.C., Postma, J.P.M., van Gunsteren, W.F. and Hermans, J. (1981) Intermolecular Forces. Pullman, B, editor. Dordrecht, The Netherlands: Reidel.

[192] Brown, D. and Clarke, J.H.R. (1984) Mol. Phys. 51, 1243–1252.

[193] Hess, B., Bekker, H., Berendsen, H.J.C., Fraaije, J.G.E.M. (1997) J. Comput. Chem., 18, 1463–1472.

[194] Darden, T., York, D. and Pedersen, L., (1993) J. Chem. Phys., 98, 10089–10092.

[195] Darden, T., Perera, L., Li, L. and Pedersen, L. (1999) Structure, 7, R55–R60.

[196] van der Spoel, D., van Drunen, R. and Berendsen, H.J.C. (1994) GROningen MAchine for chemical simulation. Department of Biophysical Chemistry, BIOSON Research Institute. Nijenborgh, Groningen.

[197] van Gunsteren, W.F., and Berendsen, H.J.C. (1986) Groningen: Laboratory of Physical Chemistry, University of Groningen.

[198] van Buuren, A.R.S, Marrink, J. and Berendsen, H.J.C. (1993) J. Phys. Chem., 97, 9206–9212.

[199] van Gunsteren, W.F., Billeter, S., Eising, A., Hunenberger, P.H., Kruger, P., Mark, A.E., Scott, W.R.P. and Tironi, I.G. (1996) Biomolecular simulation: the GROMOS96 manual and user guide. Zurich/Gronigen: VdF Hochschulverlag AG an der ETH Zurich and BIOMOS.

[200] Koradi, R., Billeter, M. and Wüthrich, K. (1996) J. Mol. Graphics, 14, 51–55.

SCIENTIFIC PRODUCTION LIST

PUBLICATIONS:

1. **Ronga L.**, Palladino P., Tizzano B., Marasco D., Benedetti E., Ragone R. and Rossi F. "Effect of Salts on the Structural Behaviour of hPrP α2-Helix-Derived Analogues: the Counterion Perspective". *Journal of Peptide Sciences* (2006) **12**: 790-5.
2. **Ronga L.**, Langella E., Palladino P., Marasco D., Tizzano B., Saviano M., Pedone C., Improta R. and Ruvo M. "Does Tetracycline Bind Helix 2 of Prion? An Integrated Spectroscopical and Computational Study of The Interaction Between the Antibiotic and alpha helix 2 Human Prion Protein Fragments". *Proteins* (2007) **66**: 707-15.
3. **Ronga L.**, Tizzano B., Palladino P., Ragone R., Urso E., Maffia M., Ruvo M., Benedetti E. and Rossi F. "The Prion Protein: Structural Features and Related Toxic Peptides". *Chemical Biology & Drug Design* (2006) **68**: 139-147.
4. **Ronga L.**, Palladino P., Costantini S., Facchiano A., Ruvo M., Benedetti E., Ragone R. and Rossi F. "Conformational diseases and structure-toxicity relationships: lessons from prion-derived peptides". *Current Protein & Peptide Science* (2007) **8**: 83-90.
5. **Ronga L**., Palladino P., Saviano G., Tancredi T., Benedetti E., Ragone R. and Rossi F. "NMR structure and CD titration with metal cations of human prion a2-helix-related peptides". *Bioinorganic Chemistry and Applications* (2007)*, in press*.

PROCEEDINGS :

1. Palladino P., **Ronga L.**, Tizzano B., Rossi F., Ragone R., Tancredi T., Saviano G., Facchiano A., Costantini S. and Benedetti E. "Prion Protein Misfolding: Conformational stability of the alpha-2 helix", 19th APS Symposium: Understanding Biology Using Peptides, San Diego (USA), June 18-23, 2005. *Peptide Science* (2005) **80** (4): 575.
2. **Ronga L.**, Palladino P., Tizzano B., Marasco D., Ragone R., Ruvo M., Saviano G., Tancredi T., Constantini S., Facchiano A., Benedetti E., Pedone C. and Rossi F. "Prion Protein helix-2 conformational properties: implications for full length protein folding and stability". *Proceedings of 29th European Peptide Symposium*. Gdansk (Poland) September 3-8, 2006, in press.
3. Ruvo M., **Ronga L.**, Langella E., Improta R., Tizzano B., Palladino P., Marasco D., Pedone C. and Benedetti E. "Fluorimetric investigation and Molecular Dynamics simulation on interaction between Prion Protein helix 2 and tetracycline". *Proceedings of 29th European Peptide Symposium*. Gdansk (Poland) September 3-8, 2006, in press.
4. **Ronga L.**, Palladino P., Ragone R., Martinez J., Benedetti E., Rossi F. and Amblard M. "Spectroscopic analysis of synthetic PrP helix 2–binding peptide constructs". *Proceedings of 20th American Peptide Society Symposium: Peptides for Youth.* Montreal (Canada) June 26-30, 2007, submitted.

COMMUNICATIONS:

1. **Ronga L.,** Tizzano B., Rossi F., Benedetti E., Ruvo M., Ragone R., Urso E., Maffia M. and Palladino P. "Role of the α2 helix in prion protein misfolding: conformational preferences of hPrP[180-195] analogues". **Poster presentation**: *1st International Symposium on Biomolecules and Related Compounds*. Montpellier (France) March 20-25, 2005.

2. Tizzano B., **Ronga L.**, Palladino P., Saviano G., Tancredi T., Urso E., Benedetti E., Ragone R., Ruvo M. and Rossi F. "Conformational preferences and biological activity of prion protein fragments". **Poster presentation**: *1st International Symposium on Biomolecules and Related Compounds.* Montpellier (France) March 20-25, 2005.

3. Palladino P., **Ronga L.**, Tizzano B., Rossi F., Ragone R., Tancredi T., Saviano G., Facchiano A., Costantini S., Benedetti E. "Prion protein Misfolding: Conformational Stability of α2-Helix". **Poster presentation**: *19th American Peptide Society Symposium: Understanding Biology Using Peptides.* San Diego (USA) June 18-26, 2005.

4. Urso E., Tizzano B., **Ronga L.**, Maffia M. "Effects of Prion Protein fragments on the proliferation of B104 Neuroblastoma cells". **Poster presentation**: *Joint Symposium SIF-Physiological Society.* Palermo (Italy) September 27-30, 2005.

5. **Ronga L.**, Palladino P., Tizzano B., Ragone R., Saviano G., Tancredi T., Ruvo M., Constantini S., Facchiano A., Benedetti E. and Rossi F. "Involvement of the human prion protein helix 2-like fragment PrP[173-195] in fibril formation". **Poster presentation**: *10th Naples workshop on bioactives peptides*. Napoli (Italy) June 11-14, 2006.

6. Urso E., Rizzello M., Lionetto M.G., Palladino P., **Ronga L.**, Giordano M., Schettino T. and Maffia M. "Confocal microscopy analysis of Prion Protein fragment PrP[173-195]C179Me internalization in rat B104 neuroblastoma cell line". **Poster presentation**: *10th Naples workshop on bioactives peptides*. Napoli (Italy) June 11-14, 2006.

7. **Ronga L.**, Palladino P., Tizzano B., Marasco D., Ragone R., Ruvo M., Saviano G., Tancredi T., Constantini S., Facchiano A., Benedetti E., Pedone C. and Rossi F. "Prion Protein helix-2 conformational properties: implications for full length protein folding and stability". **Poster presentation**: *29th European Peptide Symposium*. Gdansk (Poland) September 3-8, 2006.

8. **Ronga L.**, Langella E., Improta R., Tizzano B., Palladino P., Marasco D., Ruvo M., Pedone C. and Benedetti E. "Fluorimetric investigation and Molecular Dynamics simulation on interaction between Prion Protein helix 2 and tetracycline". **Poster presentation**: *29th European Peptide Symposium*. Gdansk (Poland) September 3-8, 2006.

9. **Ronga L.** "Conformational diseases: the structural landscape of the human Prion protein helix 2 domain". **Oral communication**: *SAJEC 2006 7ème Symposium Sigma-Aldrich.* Balaruc-les-Bains (France) October 16-18, 2006.

10. **Ronga L.** "Prion protein helix 2 domain: locus of conformational flexibility and potential target for therapeutic approach". **Oral communication**: Seminar invitation by the *Ecole Doctorale de Chimie des Biomolécules.* Montpellier (France) October 19th, 2006.

11. **Ronga L.** "Equilibri di formazione tra cationi metallici e proteina prionica: studio dell'elica-2 del dominio C-globulare". **Oral communication**: *6° Pharmaco-Bio-Metallics.* Napoli (Italy) December 1th, 2006.

12. **Ronga L.**, Palladino P., Ragone R., Saviano G., Tancredi T., Ruvo M., Benedetti E. and Rossi F. "The conformational landscape of the human prion protein C-globular α2-helix: role of metal cations". **Poster presentation**: *9th International Symposium on Applied Bioinorganic Chemistry.* Napoli (Italy) December 2-8, 2006.

13. Sandomenico A., Monti S.M., Tornatore L., Dathan N., Doti N., Viparelli F., Marasco D., **Ronga L.**, Saporito A., Sabatella M., Pedone C., Benedetti E. and Ruvo M. "Synthetic peptide ligands for α1AT". **Poster presentation**: *9th International Symposium on Applied Bioinorganic Chemistry.* Napoli (Italy) December 2-8, 2006.

14. **Ronga L.**, Amblard M., Palladino P., Ragone R., Martinez J., Benedetti E. and Rossi F. "Spectroscopic analysis of synthetic PrP helix 2–binding peptide constructs". **Poster presentation**: *15ème Réunion Peptides et Protéines.* Dinard (France) May 20-25, 2007.

15. **Ronga L.**, Amblard M., Palladino P., Ragone R., Martinez J., Benedetti E. and Rossi F. "Spectroscopic analysis of synthetic PrP helix 2–binding peptide constructs". **Poster presentation**: *20th American Peptide Society Symposium: Peptides for Youth.* Montreal (Canada) June 26-30, 2007.

16. **Ronga L.**, Palladino P., Perretta G., Ragone R., Saviano G., Tancredi T., Benedetti E. and Rossi F. "Human prion α2-helix-related peptides: have metal cations a role in the misfunction of the whole protein?". **Poster presentation**: *BioMet7.* Palermo (Italy) October 26-28, 2007.